Rapid Melt
Dynamic Nuclear Polarization

Proefschrift

ter verkrijging van de graad van doctor
aan de Radboud Universiteit Nijmegen
op gezag van de rector magnificus prof. dr. J.H.J.M. van Krieken,
volgens besluit van het college van decanen
in het openbaar te verdedigen op dinsdag 10 oktober 2017
om 12.30 uur precies

door
Manvendra Sharma
geboren op 13 december 1987
te Kota, India

Promotor:	Prof. dr. A.P.M. Kentgens
Copromotor:	Dr. P.J.M. van Bentum
Manuscriptcommissie:	Prof. dr. S.Y.T. van de Meerakker Prof. dr. J. Oomens Dr. W. Köckenberger (University of Nottingham, Verenigd Koninkrijk)

Rapid Melt Dynamic Nuclear Polarization

Doctoral Thesis

to obtain the degree of doctor
from Radboud University Nijmegen
on the authority of the Rector Magnificus prof. dr. J.H.J.M. van Krieken,
according to the decision of the Council of Deans
to be defended in public on Tuesday, October 10, 2017
at 12.30 hours

by
Manvendra Sharma
Born on December 13, 1987
in Kota, India

Supervisor:	Prof. dr. A.P.M. Kentgens
Co-supervisor:	Dr. P.J.M. van Bentum
Doctoral Thesis Committee:	Prof. dr. S.Y.T. van de Meerakker Prof. dr. J. Oomens Dr. W. Köckenberger (University of Nottingham, United Kingdom)

Contents

Chapter 1

NMR and DNP

"That is the study of nuclear magnetism for the light it can throw on problems of molecular structure and molecular motion, problems rather close to physical chemistry. Indeed certain branches of this work are now being pursued in chemical laboratories."

Nobel Lecture, December 11, 1952
EDWARD M. PURCELL

1.1 Introduction

Samuel Goudsmit and George Uhlenbeck were the first to describe the concept of spin in 1925 [1]. Nuclear magnetic resonance (NMR) is based on the interaction of the nuclear spin with magnetic fields. NMR was first observed in molecular beams [2] by Isodor Rabi, for which he was awarded the Nobel prize in 1944. Felix Bloch and Edward Mills Purcell observed NMR on liquids and solids in independent experiments [3, 4]. They shared the Nobel prize in Physics in 1952. Richard R. Ernst received the Noble prize for his contributions to the development of high resolution NMR spectroscopy [5, 6]. Kurt Wüthrich shared the Noble prize in chemistry in 2002 for his development of nuclear magnetic resonance spectroscopy for determining the three-dimensional structure of biological macromolecules in solution [7]. Peter Mansfield and Paul C. Lauterbur shared the Noble prize in 2003 in physiology or medicine for the usage of a gradient in magnetic field to create two dimensional images [8, 9]. These days, NMR is a well established technique which is regularly used in various fields including medicine, chemistry and industry to investigate the

structural and dynamical properties of molecules.

1.2 The Boltzmann law and the problem of NMR sensitivity

When spins are placed in a magnetic field ($\vec{B_0}$) the spin Hamiltonian is given by

$$\begin{aligned} \hat{H_z} &= -\vec{\mu}.\vec{B_0} \\ &= -\gamma\hbar I_z B_0 \end{aligned} \tag{1.1}$$

Where γ is the gyromagnetic ratio, $\hbar$ is Planck's constant devided by 2 π, I_z is the spin angular momentum in the direction of $\vec{B_0}$, and $\vec{\mu}$ is the magnetic moment. When spins are placed in the magnetic field the degeneracy on the angular momentum is lifted and 2 states are obtained for a spin 1/2, $|I, m_I\rangle$=$|1/2, 1/2\rangle$ (α) and $|1/2, -1/2\rangle$ (β). The difference in energy between these two states can be given by Equation 1.2

$$\begin{aligned} \Delta E &= \hbar\gamma B_0 \\ &= \hbar\omega_0 \end{aligned} \tag{1.2}$$

where, ω_0 is the Larmor frequency.

The energy difference given in Equation 1.2 is much smaller than the thermal energy (kT) at ambient temperatures even up to the highest available NMR magnetic field of 24 Tesla. k is the Boltzmann constant and T is the temperature. At a given temperature and magnetic field, the ratio of populations of the two spin levels is given by the Boltzmann distribution Equation 1.3.

$$\frac{N_\beta}{N_\alpha} = e^{-\Delta E/kT} = e^{\hbar\gamma B_0/kT} \tag{1.3}$$

The polarization is then given by Equation 1.4, also given in [10]

$$P = \frac{N_\beta - N_\alpha}{N_\beta + N_\alpha} = tanh\frac{\gamma\hbar B_0}{2kT} \tag{1.4}$$

The polarization is dependent on the gyromagnetic ratio of the spin (γ), the strength of the external magnetic field (B_0) and the temperature (T). To obtain higher polarization, as can be seen in Equation 1.4, one can increase the external magnetic field or decrease the temperature. Figure 1.1 shows the polarization of different spin species versus temperature at a magnetic field of 3.4 Tesla. At this field and a temperature of 300 K the proton polarization is only .001 %. Even at the current highest available NMR magnetic field of 24 Tesla the proton polarization only increases to

0.008 %. In other words, the NMR signal corresponds to a net polarization of only 1 spin in 12000.

The polarization depends on the gyromagnetic ratio, which is a constant for any given spin. Gyromagnetic ratios of the different spins are given in Table 1.1 [11].

Table 1.1: Gyromagnetic ratio and natural abundance of common spins in the field of dynamic nuclear polarization (DNP) and NMR

Spin	$\gamma(10^6\ rad\ s^{-1}\ T^{-1})$	Natural abundance %
^{1}H	267.522	~100
^{13}C	67.283	1.1
^{15}N	-27.126	0.37
^{19}F	251.815	~100
^{29}Si	-53.190	4.7
^{31}P	108.394	~100
electron	1.76 x 10^5	100

The gyromagnetic ratio of an electron is 660 times higher than that of a proton. Carbon has a gyromagnetic ratio four times smaller than that of a proton hence it has four times less polarization under similar experimental conditions[1]. The polarization versus temperature for electron, proton and carbon spins is shown in Figure 1.1. At identical experimental conditions electrons have ~660 times higher polarization than protons and ~2640 times more polarization than carbons. In the next section we will see how can we use this large electron polarization to increase the polarization of the nuclear spins.

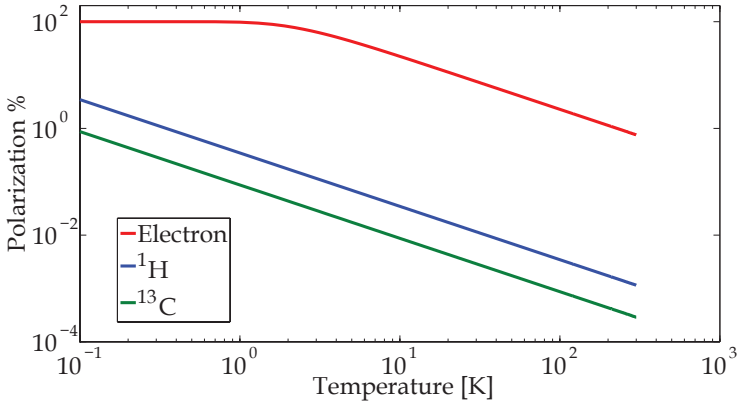

Figure 1.1: The polarization of different spin species as function of temperature at 3.4 T.

[1]Although the gyromagnetic ratio of ^{13}C is only 4 times small than ^{1}H, it's natural abundance is only 1.1 % which results in very low NMR signals.

1.3 Sensitivity enhancement by Dynamic Nuclear Polarization

In 1953 Albert Overhauser predicted the DNP (Dynamic Nuclear Polarization) effect in his seminal paper [12]. For metals, he predicted that "*if the electron spin resonance of the conducting electrons is saturated, the nuclei will be polarized to the same degree they would if their gyromagnetic ratio were that of the electron spin*". The ratio of the gyromagnetic constants for electron and proton is ∼660. According to Overhauser, for coupled nuclear and electron spin systems we can increase the proton polarization by a factor 660 compared to their Boltzmann polarization. This idea of Overhauser was much debated until Carver and Slichter demonstrated it experimentally in metallic lithium dispersed in mineral oil, in 1953 [13], as shown in Figure 1.2. In further experiments Carver and Slichter also observed DNP of protons in a solution of sodium in anhydrous liquid NH_3 [14].

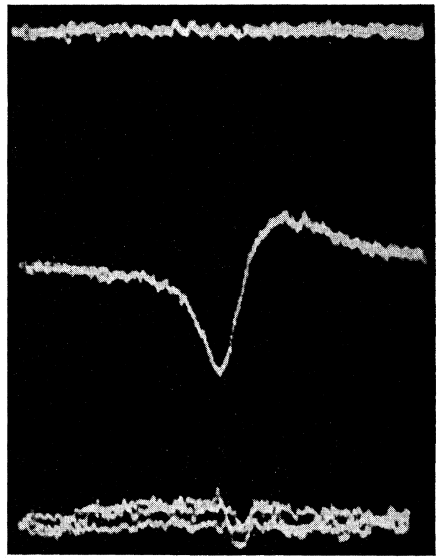

Figure 1.2: The first experimental demonstration of DNP in lithium. Top: The noisy ^{7}Li resonance. Middle: The ^{7}Li resonance enhanced by DNP. Bottom: Proton resonance of a glycerin sample.

Different DNP mechanisms have been observed in the solid state and the liquid state. After the discovery made by Overhauser, the idea was extended by Abragam [15], to other systems having mobile electron spins like dielectric solids and electron-nuclear spin systems in the liquid state. In the solid state there are four known DNP mechanisms namely the Solid Effect, the Cross Effect, Thermal Mixing and the Solid Overhauser Effect. The Solid Effect DNP was described by

Abragam and Jeffries for the case of paramagnetic substances [15, 16]. In the Solid Effect DNP an electron-nuclear spin pair is dipolar coupled and DNP occurs through the saturation of pseudo forbidden transitions. The Cross Effect was reported and experimentally verified in the 1960's [17, 18]. For the Cross Effect three dipolar coupled spins (2 electron spins and 1 nuclecar spin) are involved while DNP is carried out by saturating an allowed transition of one of the electrons. The thermodynamic description of Thermal Mixing was given by Abragam and Goldman [19, 20]. Thermal Mixing is the principle mechanism for the spin systems consisting of many dipolar coupled electron spins. DNP in the case of Thermal mixing also occurs via saturation of an allowed electron spin transition. The Solid Overhauser Effect was recently reported by Griffin and co-workers for insulating solids [21]. They suggested that high frequency modulations of the strong electron-nuclear hyperfine coupling is the reason for this effect.

1.4 Other hyperpolarization methods

As the polarization given by Equation 1.4 is proportional to the magnetic field strength and inversely proportional to the temperature, higher polarization can be obtained by increasing the magnetic field and/or lowering the temperature. Over time, the field strength of the NMR magnets have increased to 1 GHz proton Larmor frequency (24 T). Even at this high field the polarization of proton spins is less than 1 % at room temperature. Performing the experiment at lower temperature can provide a higher polarization level. Recently, James Kempf and co-workers reported enhancement factors of >1500 for ^{13}C spins, using the so called brute-force approach. They polarized the spins at a field of 14 T and at low temperature of 2.3 K. For measurement, the sample was transferred to a field of 1 T and rapidly dissolved and measured at 40 °C [22]. Although higher polarization can be obtained at higher fields and lower temperatures, there are also limitations to these approaches. Technologically one is limited to make NMR magnets of even higher fields. Furthermore, at very lower temperatures (liquid helium) the longitudinal relaxation times of spins can become very long (several hours or more) hence the buildup of the nuclear polarization will be very slow.

Rather than using the electron polarization, one can use the spin order in diatomic hydrogen to produce molecules with hyperpolarized nuclear spins. This hyperpolarization method is called para-hydrogen induced polarization (PHIP). The hydrogen atoms of a molecule can be in triplet ($\alpha\alpha, \beta\beta, \alpha\beta+\beta\alpha$) or singlet ($\alpha\beta-\beta\alpha$) nuclear states. The anti-symmetric singlet state is called para-hydrogen. At lower

temperatures the percentage of para-hydrogen in molecular hydrogen increases. The addition of para-hydrogen to a target molecule through a hydrogenation reaction will result in breaking the symmetry of para-hydrogen molecule and highly polarized nuclear spin state on the target molecule [23, 24]. PHIP was restricted to unsaturated molecules due to the essential requirement of hydrogenation reaction, until in 2009 Duckett demonstrated the reversible exchange of para-hydrogen using a metal catalyst to hyperpolarize nuclear spins without any chemical modification to the target molecule [25]. The approach of hyperpolarization with reversible exchange of para-hydrogen is called signal amplification by reversible exchange (SABRE)

In noble gases hyperpolarization can be obtained by the spin exchange optical pumping (SEOP) method. In the first step (of SEOP), an alkali metal vapor is polarized by optically pumping with circularly polarized light. In the next step the noble gas is polarized by spin exchange with the polarized metal [26, 27, 28]. These hyperpolarized noble gases are mainly used for gas phase imaging [29].

For molecules having hindered methyl rotors e.g. acetone, ethanol, isopropanol, DMSO, and acetic acid; hyperpolarization can be induced by Quantum rotor polarization (QRP) by employing a rapid temperature jump from very low temperatures (few K) [30]. A negative enhancement is observed on protons, and also on carbons, through cross relaxation from protons [31, 30]. No radicals or microwaves are required for this effect. The origin of this enhancement is the quantum tunneling due to rotational hindrance in methyl groups [30, 26]. This effect was first observed by Haupt in 1972 [31]. A combination of other DNP mechanisms with QRP at low temperatures can result in improved or worse results.

1.5 DNP theory

DNP mechanisms describe the transfer of polarization from unpaired electron spins to nuclear spins. The dominant DNP mechanism in any system depends on many experimental parameters e.g. the phase of the sample, temperature, the concentration of the spins, the frequency of microwave irradiation etc. The transfer of polarization is facilitated by irradiation of microwaves at or close to the electron Larmor frequency. The Hamiltonian for a coupled electron-nucleus spin system can be written as ([26]):

$$H = \omega_e S_Z - \omega_n I_Z + H_{ee} + H_{en} + H_{nn} \tag{1.5}$$

Here, S and I are the spin operators, and ω_e and ω_n are the Larmor frequencies of electrons and nuclei respectively. In Equation 1.5, the first two terms are the Zeeman interaction of the electron and nucleus respectively. The last three terms H_{ee}, H_{en}, H_{nn} represent the spin-spin interactions of electron-electron, electron-nucleus, and nucleus-nucleus respectively. The term H_{ee} can be neglected for systems with dilute electron spins like liquids and solids with low free electron spin concentration. However this is not the case for solids with higher free electron spin concentrations where electron-electron spin interaction can dominate the DNP process e.g. in the Cross Effect and Thermal Mixing.

Details of DNP mechanisms are presented in the following sections.

1.5.1 Overhauser effect

The Overhauser effect is based on the cross-relaxation of electron and nuclear spins where both the electron and nuclear spins flip simultaneously [26, 32, 33]. The cross relaxation is caused by the modulation of the electron-nuclear interaction. In liquids this modulation is provided by the translational and rotational motions and in solids e.g. by the motion of conduction electrons. The efficiency of the Overhauser effect depends on the condition $\omega_e\tau < 1$, where ω_e is the electron Larmor frequency and τ being the correlation time. In general, at higher fields and for liquids with slower dynamics this condition is difficult to satisfy.

For a coupled electron nucleus system, the equilibrium spin population can be seen in Figure 1.3(a). W^0, W_S, W_0, W_2, W_1 are the nuclear relaxation rate in the absence of electron spins, the electron relaxation rate, the zero quantum transition rate, the rate of double quantum transitions and the nuclear relaxation rate induced by electron respectively. For the Overhauser effect the electron spin is saturated by irradiating microwaves at the electron Larmor frequency. Saturation of the population in the electronic levels leads to Figure 1.3(b). The cross relaxation between electronic and nuclear spins is induced by zero (W_0) and double (W_2) quantum transitions. If the rates of zero quantum (W_0) and double quantum (W_2) transitions are not equal, a higher population difference can be obtained between the nuclear spin levels as is shown in Figure 1.3(c).

The polarization enhancement by the Overhauser effect can be calculated by solving the rate equations for the electron and nuclear polarizations. The enhancement after solving the rate equations can be written as [33]

$$\epsilon = 1 - \frac{W_2 - W_0}{W_0 + 2W_1 + W_2 + W^0} \cdot \frac{S_0 - \langle S_z \rangle}{S_0} \cdot \frac{\gamma_e}{\gamma_n} \tag{1.6}$$

The term $\frac{W_2-W_0}{W_0+2W_1+W_2+W^0}$ is actually the ratio of the net cross relaxation to the total relaxation. The important parameters for Overhauser DNP are the coupling factor (ρ), the leakage factor (f) and the saturation factor (s), which are defined as

$$\rho = \frac{W_2 - W_0}{W_0 + 2W_1 + W_2} \tag{1.7}$$

$$f = \frac{W_0 + 2W_1 + W_2}{W_0 + 2W_1 + W_2 + W^0} \tag{1.8}$$

$$s = \frac{S_0 - \langle S_z \rangle}{S_0} \tag{1.9}$$

The enhancement in terms of ρ, f and s can be written as

$$\epsilon = 1 - \rho f s \frac{\gamma_e}{\gamma_n} \tag{1.10}$$

The coupling factor is defined as the ratio of the difference of zero and double quantum transition rates and all other nuclear transition rates. The coupling factor can assume value of -1 to 0.5 for cross relaxation being completely scalar to completely dipolar. It depends on the correlation time of electron-nuclear spin complex and can be improved by facilitating fast dynamics. The leakage factor is defined as the ratio of the relaxation of the nuclear spin induced by the electron spin to the total relaxation of the nuclear spin. The leakage factor can have values from 1 to 0, for fully dominated to zero nuclear relaxation induced by electron-nuclear relaxation. It depends on the radical concentration. As the name suggests the saturation factor is the level of saturation of the free radical spins by microwaves. The saturation factor can also take values from 0 to 1 for no saturation to complete saturation of the electron spin transition.

1.5.2 Solid Effect

The Solid Effect is a two spin process, where one spin is an electron spin and the other spin is a nuclear spin. The Solid Effect occurs because of the mixing of the spin states by the non secular part of the hyperfine coupling H_{en}. This results in finite probabilities for otherwise forbidden transitions ($W_\pm$) [34]. The probabilities for the forbidden transitions are given by [26]

$$W_\pm = 2|q_{ij}|^2 \pi \omega_e^2 f(\omega_e \pm \omega_n) \tag{1.11}$$

Here q_{ij} is the coefficient for the mixing of states i and j and is given by

$$q_{ij} = -\frac{3}{4}\frac{\gamma_e \gamma_n \hbar}{\omega_n} \cdot \frac{1}{r_{ij}^3} \cdot sin\theta_{ij} cos\theta_{ij} e^{-i\phi_{ij}} \tag{1.12}$$

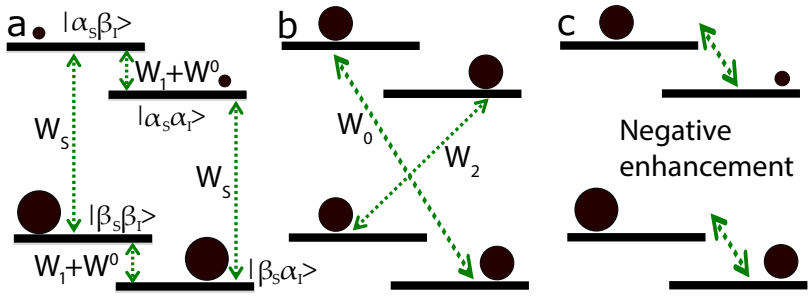

Figure 1.3: The energy diagram for a coupled electron and nuclear spin to understand the Overhauser effect. The size of sphere indicates the population of the level. a) The equilibrium population distribution for an electron-nuclear spin system. W^0, W_S, W_1 are the nuclear relaxation rate, the electron relaxation rate, and the nuclear relaxation rate induced by electron-nuclear interactions respectively. The microwaves are irradiated at the electron Larmor frequency to saturate the electron spins. b) Zero quantum and/or double quantum cross relaxation occurs at the rates W_0 and W_2 depending on the interaction of nuclear and electron spins. c) A bigger population difference for nuclear population is obtained assuming a faster double quantum relaxation.

where (r, θ, ϕ) are the polar coordinates of the electron-nuclear vector and $f(\omega_e \pm \omega_n)$ is the normalized EPR lineshape function. The efficiency of Solid Effect DNP is expected to go down at higher fields as $W_\pm$ is proportional to B_0^{-2}.

The energy diagrams for the Solid Effect can be seen in Figure 1.4. The populations of the different energy levels are shown by the size of the spheres in the diagram. At equilibrium the population difference of electronic energy levels is much higher than that of the nuclear energy levels due to the difference in their gyromagnetic ratios. If microwaves are applied at the sum or the difference of the nuclear Larmor frequency and the electron Larmor frequency($\omega_n \pm \omega_e$), zero and double quantum transitions can occur through $(\omega_e - \omega_n)$ (flip-flip) and $(\omega_e + \omega_n)$ (flip-flop) respectively. In Figure 1.4, the microwaves are applied at $(\omega_n + \omega_e)$. The rate of these transitions is much slower than the electronic flips. The electronic levels reach equilibrium populations because of fast electronic relaxation. The resulting populations of the coupled levels have a higher population difference for the nuclear levels as shown in Figure 1.4(c) and therefore a negative enhancement is obtained.

This effect is most efficient when the width of the electron paramagnetic resonance (EPR) line is smaller than the nuclear Larmor frequency (ω_n), meaning there is no overlap of zero, electronic and double quantum transitions. If the EPR line width is broader than ω_n, both ($W_\pm$) transitions may be excited at the same time and complete or partial cancellation of polarization is the result. This is also known as the Differential Solid Effect [35].

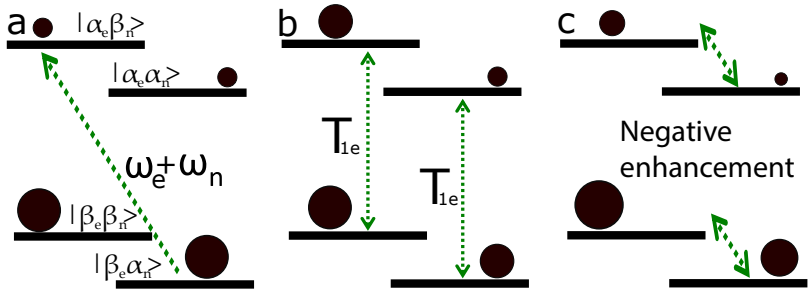

Figure 1.4: The energy diagram for a coupled electron and nuclear spin to understand Solid Effect DNP. The size of sphere indicates the population of the level. a) The equilibrium population distribution. Microwaves are irradiated at $(\omega_e + \omega_n)$ or $(\omega_e - \omega_n)$, here at $(\omega_e + \omega_n)$. b) As the electron's longitudinal relaxation T_{1e} is very fast w.r.t. the rate of zero and double quantum transitions, the electronic levels attain equilibrium much faster than zero or double quantum transitions. c) The final state shows higher population difference for nuclear levels.

1.5.3 Cross Effect

The Cross Effect (CE) is a three spin process in which two electrons and one nucleus are coupled by a dipolar interaction [34]. The CE becomes dominant in case $\Delta > \omega_n > \delta$ where, Δ is the inhomogeneous line width of the EPR lineshape, ω_n is the nuclear Larmor frequency, and δ is the homogeneous line width of the EPR resonance. The CE is based on an allowed transition of the electron spins. The condition for CE is

$$\omega_{e1} - \omega_{e2} = \pm\omega_n \tag{1.13}$$

meaning that the difference in Larmor frequency of the two electrons should be equal to the nuclear Larmor frequency. The equilibrium energy diagram for a 3-spin system is shown in Figure 1.5(a). If the CE condition (Equation 1.13) is matched, the energy levels 4 and 5 or 6 and 3 become degenerate for $\omega_{e1} > \omega_{e2}$ and $\omega_{e1} < \omega_{e2}$ respectively. We have assumed $\omega_{e1} > \omega_{e2}$ in the Figure 1.5(b) and 1.5(c). Saturation of the first electron by microwave irradiation at ω_{e1} results in a negative enhancement of the nuclear spin polarization (1.5(b)). The reason for this enhancement is the degeneracy of the energy levels 4 and 5, which allows for an energy conserving flop-flip-flop transition of the electron-electron-nucleus spin system. In a similar way microwave irradiation at ω_{e2} results in positive enhancement of nuclear spin polarization (1.5(c)).

CE is inversely proportional to B_0 as the linewidth of the EPR spectra scales with B_0 [34].

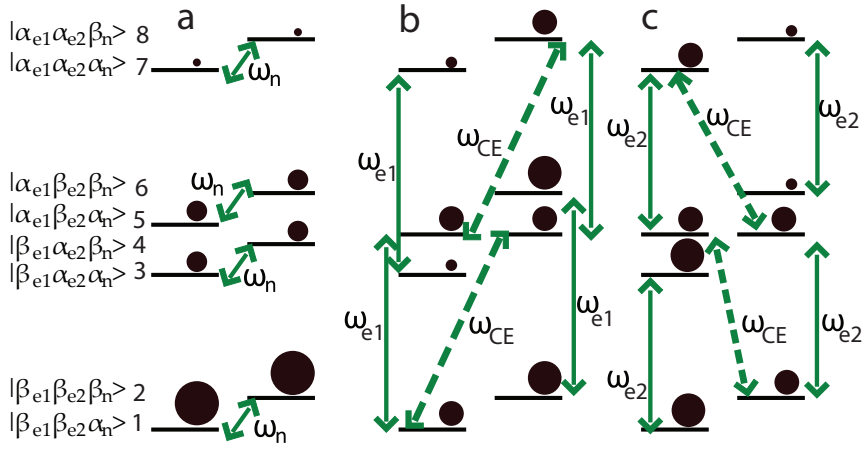

Figure 1.5: (a) The energy level diagram of an electron-electron-nucleus spin system. The size of sphere indicates the population of the level. Levels 4 and 5 become degenerate when $\omega_{e1} - \omega_{e2} = \omega_n$. Irradiation at ω_{e1} (shown in b) results in negative enhancement of nuclear spin by flop-flip-flop transition of electron-electron-nucleus system allowed by degeneracy. Irradiation at ω_{e2} (shown in c) produces negative enhancement by flip-flop-flip transition. Figure adapted from [34].

1.5.4 Thermal Mixing

Thermal Mixing (TM) occurs for spin systems consisting of many dipole coupled electrons and nuclei [34]. TM becomes dominant for $\delta > \omega_n$ where ω_n is the nuclear Larmor frequency, and δ is the homogeneous line width of the EPR line. TM is based on allowed transitions of the electron spins. TM is inversely proportional to B_0 as the line width of the EPR spectra scales with B_0 [34].

TM is based on the spin temperature of different "baths", and is described by Provotov theory [20]. The Hamiltonian for many spins is not easy to solve and the spin system is assumed to involve the interaction of three thermodynamic baths: the electron Zeeman system (EZS), the electron dipolar system (EDS) and the nuclear Zeeman system (NZS). Each of these thermodynamic systems have populations defined by their respective temperatures T_e, T_d and T_n given by the Boltzmann distribution. At thermal equilibrium all of these temperatures are equal to the lattice temperature (T_l). The electron Zeeman levels can be approximated by a quasi continuous band due to the splitting by the electronic dipolar interaction as shown in Figure 1.6(a). When microwaves are irradiated at $\omega_e \mp \delta$, the populations of inner or outer (shown in Figure 1.6(b) and 1.6(c) respectively) parts of the electron Zeeman bands become equal. These new population distributions are defined by the Boltzmann distribution at a decreased or negative T_d, in other words the EDS is

cooled (shown in Figure 1.6(b)) or heated (for negative T_d shown in Figure 1.6(c)). The EDS can further cool down the NZS ($T_n = T_d$) as they are in thermal contact, resulting in DNP enhancement. The thermal contact between EDS and NZS can be be provided by an energy conserving electron-electron-nuclear transition [36, 37].

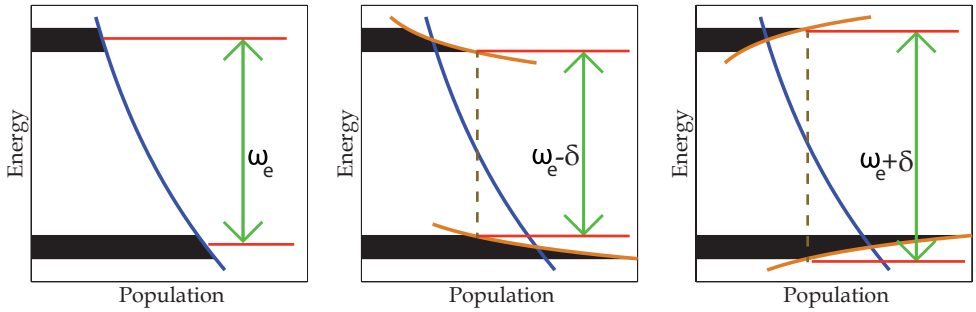

Figure 1.6: (a) Thermal equilibrium distribution of populations for many dipolar coupled electrons. (b) If microwaves are irradiated at $\omega_e - \delta$ inner parts of the electron Zeeman bands become equal and a new population distribution characterized by a low temperature T_d ($T_d < T_e$) is obtained. (c) If microwaves are irradiated at $\omega_e + \delta$ outer parts of the electron Zeeman bands become equal and the population distribution can be defined by a negative T_d ($|T_d| < T_e$). Low temperature T_d results in nuclear spin polarization through a energy conserving electron-electron-nuclear transition. Figure adapted from [37].

1.6 Experimental DNP setups

Although DNP was predicted and experimentally verified in 1953, it was limited to lower magnetic fields and microwave frequencies until the last decade. The limitation to perform DNP at higher fields was mainly caused by the experimental restrictions, like the availability of high power microwave sources, and optimal radicals etc. Developments of gyrotron technology by Griffin and co-workers enabled high power and high frequency microwave irradiation [38, 39, 34]. Now a days, both DNP and NMR are performed in the solid state as well as in the liquid state.

The experimental DNP setups can be divided into two categories: 1. DNP is performed in the liquid state, 2. DNP is performed in the solid state. When DNP is performed in the liquid state, in the current setups, NMR is also acquired in the liquid state. If DNP is performed in solid state, NMR signal is acquired either in the solid state using a magic angle spinning (MAS) setup or in the liquid state after changing the phase of sample either by dissolution or melting.

1.6.1 Magic angle spinning DNP

MAS-DNP was initially used for radical doped polymers in the 1990s [40]. In the present form of MAS-DNP the sample is irradiated with continuous high power microwave irradiation followed by NMR-detection in a cryogenic MAS setup. The high power microwaves are generated by gyrotron oscillators and transferred to the probe through corrugated wave guides. Optimized biradicals are used in MAS-DNP to profit from CE polarization transfer. MAS-DNP is mainly employed in the studies of surface chemistry [41] and proteins [42, 43].

Although MAS-DNP is used widely and commercially available, it has some drawbacks. The use of a high concentration of radicals may result in broadening of NMR lines. Furthermore, detection at low temperature can also have a negative effect on the resolution if the frozen glassy state leads to variation in local conformations. This method also requires substantial investment by adding another magnet to house the gyrotron source and high operating costs, due to the cryogenic liquids required for the cryo-MAS.

1.6.2 Overhauser DNP

The Overhauser Effect is the only known DNP mechanism in liquids. For Overhauser DNP, there are mainly two kinds of setups: One for static samples, where DNP and NMR take place in the same spectrometer, and another so-called sample-transfer setups, where DNP is usually performed at lower fields and the NMR signal is acquired at a higher field.

Low field Overhauser DNP and high field NMR detection

In low field Overhauser DNP and high field NMR detection, the sample is polarized at a lower field under favorable conditions (discussed in 1.5.1) to attain high polarization and the NMR signal is acquired at a higher field either by shuttling [44] or flowing [45] the hyperpolarized sample to the higher field. ^{13}C enhancements for halogenated compounds were demonstrated in the late 1990's [45, 46]. Han and co-workers demonstrated a continuous flow approach to polarize water in the fringe field of an MRI magnet for imaging [47]. In the sample shuttling approach, the sample is shuttled to higher magnetic field with pneumatic equipment [44].

The lower Boltzmann polarization at lower magnetic field and the relaxation losses during the sample transfer are the main drawbacks of this approach. The

Griesinger group in Göttingen, optimizes Overhauser DNP in a two-center magnet [48] to reduce losses during shuttling by both maximizing the minimum field between the two centers and minimizing the shuttling time.

Static sample Overhauser DNP

In static sample Overhauser DNP setups DNP and NMR are performed at the same magnetic field in the liquid state. The main advantage of Overhauser DNP is that the sample always remains in the same phase. Also as both DNP and NMR are performed at the same field, problems of sample transfer are avoided. Double resonance structures are required to carry out DNP and NMR at the same position. At higher frequencies the dimensions of resonance cavities are very small which limits the sample volume in the cavity. The Prisner group has reported proton signal enhancement of water using Fermy's salt radicals at 9.2 T [49]. Enhancement of water and ethanol has been previously demonstrated in our group at 3.4 T [50, 51]. The Dupree group in Warwik polarized protons of toluene using TEMPOL as the polarizing agent at 3.4 T [52].

As already described in section 1.5.1 the condition $\omega_e\tau < 1$ becomes difficult to satisfy at higher magnetic fields. Supercritical solvents have both gas and liquid like properties. Fast mobilities can be obtained for molecules dissolved in supercritical solvents. Since fast mobilities result in decreased τ, the condition for Overhauser DNP could be satisfied. The use of supercritical CO_2 has been suggested as a solvent to attain fast dynamics of molecules to improve the Overhauser effect at higher magnetic fields [53].

1.6.3 Dissolution DNP

Dissolution DNP was developed by Jan H. Ardenkjær-Larsen *et al.* and demonstrated in 2003 [54]. Dissolution DNP is generally performed at a lower magnetic field (usually 3.4-6.9 T) and at very low temperatures (below 4.2 K). After DNP, the sample is rapidly dissolved with a superheated solvent and transferred to a higher field or MRI magnet in the liquid state for signal acquisition. The reported enhancements from this method are ∼10,000 fold higher compared to room temperature Boltzmann polarization. The high enhancement is obtained due to a combination of DNP with Boltzmann enhancement at lower temperature, the latter can be ∼200-300 because of the change of temperature from ∼1.2 K to 300 K [26]. The DNP enhancement at lower temperature is high due to high starting electron polarization at sub-kelvin temperatures. The sample (10-500 μl) usually consists of the target

molecules, glassing agents and stable free radicals (free electron spins).

Although, dissolution DNP produces highly polarized samples, there are some drawbacks in its mode of operation. During the transfer of the sample from the polarizer to the NMR or MRI magnet, the liquid sample must pass through a region of low magnetic field in the presence of paramagnetic radicals; at these fields short T_1 times are encountered for the nuclear spins. For proton NMR, such fast relaxation results in a substantial polarization decay by the time of the NMR experiment. These losses are typically less severe in ^{13}C spectroscopy because of their longer T_1 times compared to protons. Various groups have tried to reduce this relaxation, for example: the Bodenhausen group in Lausanne uses a magnetic tube [55] in order to maintain a higher magnetic field strength during a sample's "voyage" from the polarizer to the NMR magnet; the Köckenberger group in Nottingham makes use of a rapid-shuttle, 2-center magnet for dissolution DNP. Additionally the sample is shuttled in the solid state until just above the NMR assembly [56] in order to take advantage of the longer T_1 times in the solid-state. The total experiment time of dissolution DNP is usually several hours because of the slow build-up of the polarization for carbon, which has a very long T_1 at lower temperatures. Cross polarization methods have been employed to shorten the DNP build-up time by first polarizing protons [57]. In dissolution DNP, the sample gets diluted because of the dissolution, amounting to overall decrease in the NMR detection sensitivity. Furthermore, the dissolution step changes the composition of the sample irreversibly, and therefore 2D experiments are difficult to implement in this setup. Various groups have employed different approaches to acquire 2D spectra in dissolution DNP. Frydman used pulse field gradients to encode different parts of a sample with coherences needed for the 2D spectrum [58]. Hilty and co-workers obtained two-dimensional chemical shift correlations from hyperpolarized samples by differential scaling of the scalar coupling to encode a second chemical shift dimension [59]. The same group later demonstrated sequential 2D experiments using variable flip angles on single hyperpolarized samples [60].

Dissolution DNP is commercially available and is mainly used for metabolic imaging [61, 62]. Other applications include biomolecular NMR [63, 64], biological assays [65, 66], detection of reaction intermediates having low concentrations [67], protein folding [68], and drug screening [69]. The use of dissolution DNP in a clinical environment is under development [70]. GE Healthcare built the SPINlab polarizer which is compatible with clinical use [71].

1.6.4 Temperature Jump DNP

The Griffin group at MIT acquired NMR spectra of low γ nuclei in the liquid state [72]. In this approach protons are first polarized in the solid state for 60-90 s using a MAS-DNP setup at 90 K. The low-γ nuclei are then polarized by cross polarization (CP) from protons. For NMR signal acquisition in the liquid state (∼300 K), the sample is melted using a CO_2 laser. In this way, the sample remains intact during freeze-thaw cycles and one can do signal averaging or even 2D NMR spectroscopy [73].

Recently, Yoon and co-workers used the high power microwaves of a gyrotron for DNP and also for melting of a static sample [74]. Enhancements of ∼550 and 40 are reported for ^{13}C and protons respectively. DNP was performed at a temperature of 20 K and NMR at 300 K. Due to the long T_1 of ^{13}C at 20 K, 3 hours of microwave irradiation was required for ∼550 fold enhancement.

1.6.5 Rapid-melt DNP

Rapid-melt DNP is our implementation of the temperature jump DNP method to allow liquid-state NMR detection in a microfluidic context combined with generic solid-state DNP which has a few distinct advantages over earlier mentioned temperature jump and dissolution DNP implementations as described below. All the experimental stages namely DNP, sample melting and NMR are completed in the same magnet. This eliminates the requirement of different magnets for DNP and NMR. All the different experimental blocks of the probe (DNP, melting and NMR) are situated within a distance of 5 cm. The sample is contained in a microfluidic glass capillary. The sample capillary can be quickly shuttled (within typically 20 ms) to different parts of the probe for DNP, sample melting and/or NMR. The shuttling mechanism is a linear actuator which is easy to operate and program. The sample is typically polarized at liquid nitrogen temperature (77 K). A high power density of microwaves can be attained due to small sample size. Klystrons can be used as microwave power source instead of high power gyrotron microwave sources. Therefore no additional magnet is required. A microwave resonator can be implemented for small microwave excitation volume, then low cost solid-state sources can be used as microwave power sources. The cryogenics is simple and less demanding. Due to the small size the sample can be melted in tens to hundreds of milliseconds by passing the capillary through a region of hot gas flow. Melting the sample through hot gas is inexpensive and very simple. In this manner, NMR of fast relaxing nuclei (e.g. protons) becomes possible, as shuttling and melting times are shorter than typical relaxation times of nuclei. The relaxation losses are limited

as the sample always remains at high magnetic field. The sample remains intact during the whole experiment. This is particularly beneficial for expensive and rare samples. The same sample can be used for further experimental cycles for signal averaging, multi dimensional NMR or for reproducing the results.

Like in other DNP methods, in principle all types of molecules can be polarized through rapid-melt DNP. Protons have a shorter DNP build-up time and a higher polarization than for instance ^{13}C [75]. This fast buildup of high polarization of the protons can be used to polarize ^{13}C at a faster rate by the implementation of cross polarization after the DNP step, when the sample is still in the solid state (this approach is similar to the study of hetero-nuclei using MAS-DNP [76]). The NMR acquisition in rapid-melt DNP is performed with a NMR stripline detector at room temperature in the liquid state in order to benefit from the higher resolution attainable with liquid-state NMR spectroscopy without recourse to sample spinning. For mass-limited samples, scaling the assembly down from a typical 5 mm NMR tube, containing around 500 μl of sample, to volumes on the order of 10 nl to 1 μl, brings a significant improvement in mass/volume sensitivity. In general, for a given sample amount the SNR of an NMR coil scales inversely with detector radius [77] if the sample can be concentrated accordingly. The stripline NMR detector is a lithographically defined structure that provides high sensitivity with low static field distortion and is cheap to produce. It is also very convenient for the present purpose, as it provides an open axial access along the static field axis [78].

In summary rapid-melt DNP can be a simple and inexpensive approach to combine effective solid state DNP with high resolution liquid state NMR in a generic way.

Chapter 2

Rapid-melt DNP

Abstract

In recent years, Dynamic Nuclear Polarization (DNP) has re-emerged as a means to ameliorate the inherent problem of low sensitivity in nuclear magnetic resonance (NMR). Here, we present a novel approach to DNP enhanced liquid-state NMR based on rapid melting of a solid hyperpolarized sample followed by 'in situ' NMR detection. This method is applicable to small (10 nl to 1 μl) sized samples in a microfluidic setup. The method combines generic DNP enhancement in the solid state with the high sensitivity of stripline ^{1}H NMR detection in the liquid state. Fast cycling facilitates options for signal averaging or 2D-NMR for structural analysis. Preliminary tests show solid-state ^{1}H enhancement factors of up to 500 for H_2O/D_2O/d8-glycerol samples doped with TEMPOL radicals. Fast paramagnetic relaxation induced by TEMPOL radicals completely annihilates the enhancement during melting. In non-polar solvents such as toluene, we find proton enhancement factors up to 400 in the liquid state with negligible relaxation losses during the melting and shuttling step, using commercially available BDPA radicals. A total recycle delay (including sample freezing, DNP polarization and melting) of about 5 s can be used. The present setup allows for a fast determination of the hyper-polarization as function of the microwave frequency and power.

Even at the relatively low field of 3.4 T, the method of rapid-melt DNP can facilitate the detection of small quantities of molecules in the pico mole regime.

2.1 Introduction

In the previous Chapter we proposed a novel method called rapid-melt DNP to acquire hyperpolarized NMR signals in the liquid state. Rapid-melt DNP combines generic solid state DNP mechanisms with high resolution liquid state NMR. In this Chapter we describe the experimental details and proof of principle of the rapid-melt DNP method.

The general experimental scheme for rapid-melt DNP approach is shown in Figure 2.1. The sequence of the experiment is first to polarize the sample (in the frozen state) using DNP, then rapid melting of the sample and finally NMR detection. The sample is contained in a micro sized capillary. DNP is usually performed in the solid state by microwave irradiation on the sample cooled at cryogenic temperatures. If required, DNP can also be performed in the solution state by turning off the cooling. The DNP build-up time for protons is usually a few seconds. After DNP the sample is shuttled to the melt block by shuttling the capillary containing the sample. The sample melting takes place within 100 ms due to small size, but strongly depends on the solvent properties like specific heat, latent heat of melting and the boiling point. The melting is performed by flowing warm nitrogen gas over the sample capillary. Once melting is completed the sample is moved to the NMR stripline detector for any general NMR experiment. After the NMR acquisition the sequence of the experiment can be repeated again for a number of times required for averaging or multidimensional NMR. The fast melting transition and shuttling limits the relaxation losses. As all the three sections for DNP, melting and NMR are within a distance of 5 cm in the same magnet the sample remains at high field during the complete experimental sequence, hence relaxation losses are minimized. Due to minimum relaxation losses hyperpolarized signals from fast relaxing nuclei like protons can be observed directly. The NMR in the liquid state has the obvious benefit of higher spectral resolution.

In the following experimental section we will first describe the general set-up of the rapid-melting DNP probe. The results obtained with aqueous and nonpolar solutions are described in Section 2.3. A more detailed analysis of the obtained DNP enhancements will follow in Chapter 3. Preliminary applications are presented in Section 2.4. In Section 2.5 we will discuss the potential of the method for future applications.

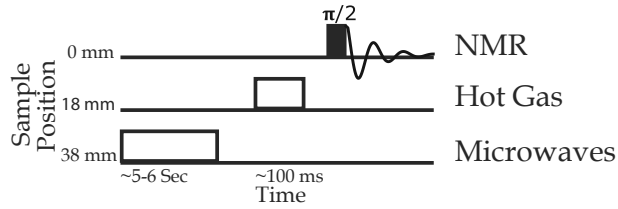

Figure 2.1: General scheme of a Rapid-melt DNP experiment. Microwave irradiation is generally irradiated for ∼5-6 seconds, depending on the temperature of the sample, and the concentration of protons and free radicals in the sample. The sample is shuttled to different parts of the probe by moving the capillary containing the sample. The shuttling of the capillary takes 20 ms to move from one functional block to another. The melting of the sample is completed in ∼100 ms depending on the heat capacity of the sample. The melted sample is transported to the NMR stripline detector for signal acquisition. After the completion of the NMR acquisition the sample can again be transferred to the cooling block for repetition of DNP and melting cycle for the same or other NMR experiment.

2.2 Instrumentation

A schematic representation of the system is provided in Figure 2.2. The core elements of the system are a sample contained within a capillary, of typically 360 μm outer diameter and 150 μm inner diameter, which is moved by an electronic actuator between three main system-regions: (1) a low temperature region at the bottom, where the sample is frozen with liquid nitrogen and irradiated with microwaves; (2) an intermediate region in which the frozen sample is subjected to a flow of heated nitrogen gas in order to melt the sample; (3) a room temperature NMR detector at the top. This is all contained within a home built probe body which is inserted into a single-center, 3.38 T, ultra-wide bore, superconducting magnet (Oxford Instruments Ltd., UK). As the microfluidic system components are miniaturized, all elements can be situated within the homogeneous part of the magnetic field. The field strength of 3.4 T corresponds to a proton Larmor frequency of around 144 MHz, and an electron Larmor frequency of around 95 GHz, which lies in the microwave W-band.

Sample shuttling

The DNP and NMR centers are brought close together to enable rapid sample shuttling, and also to allow both centers to fit within the sweet-spot of a single-center magnet. The NMR detector can be located at the center of the magnet, while the DNP resonator can be situated slightly off-center in a region that is less homogeneous but still more than adequate for DNP. The magnetic field in the magnet was mapped using a low-Q NMR probe. The resolution of magnetic resonance is

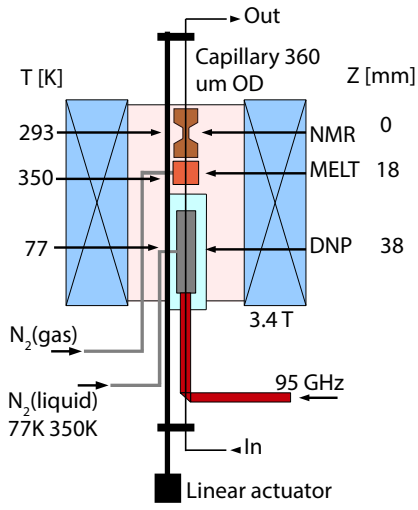

Figure 2.2: Schematic diagram of the used rapid-melt DNP. The microwave cavity, melting block and NMR stripline detector all are contained within 4 cm distance. The sample is contained in glass capillary, which can be moved by a linear actuator from below the probe. All the parts remain at different constant temperatures for optimal performance. The microwave cavity is kept at liquid nitrogen temperature for DNP. The melting block has a stream of warm nitrogen gas flowing on the capillary to melt the sample inside the capillary. The NMR stripline is kept at room temperature to acquire the NMR spectrum at room temperature. An external purge of tepid nitrogen gas keeps the probe environment at ambient temperature. The microwaves are fed by an oversized wave guide from the bottom of the probe. The cryogen is transported through a two part helium transfer siphon. The pressure of the melt gas and other gas flows are controlled from outside the probe.

determined by the magnetic field homogeneity [79]. EPR lines (100's MHz) are intrinsically much broader w.r.t. NMR lines (Hz). As DNP depends on irradiation of electron resonances, a less homogeneous field can still provide desirable results.

In the present magnet we have a space available of ±5 cm near the field center, where the homogeneity is better than ±50 ppm/cm to allow EPR/DNP. This is more than sufficient to fit both the DNP and the melting components of the system. Note that with minor effort it is possible to introduce an electrical or ferro-shim assembly that can create a second sweet spot near the DNP center with a typical homogeneity of 1 ppm/cm or better.

Positioning of the capillary with the (frozen) sample is done with a linear motor (PS01-23x80, LinMot Europe, Switzerland), which has a spatial resolution of about 20 μm. Generic motion profiles with arbitrary timing of the various freezing, polarizing, melting and detection stages can be easily programmed with appropriate synchronization to the microwave power/frequency settings and NMR spectrometer.

In the present setup, the DNP, the melting and the NMR zones are at a distance of 17.50±0.05 mm and each shuttling step is completed in approximately 20 ms.

NMR experiments were done using a Varian Infinity Plus Spectrometer (Varian, Inc., USA) modified to operate at 144 MHz running SpinSight software (Varian Inc., USA). Post-processing was carried out in MATLAB (R2014a, The MathWorks, Inc., USA) using MatNMR [80] and other home-built programs.

Cryogenics

The DNP probe has been designed [81] such that the microwave irradiation is carried out at liquid nitrogen temperatures (77 K). This system can also be used with liquid helium coolant in order to take advantage of the increased enhancement obtained via the thermal Boltzmann factor at lower temperatures. Preliminary results of DNP using liquid helium are given in Chapter 6. However, the use of liquid nitrogen results in significantly lower operational costs. In the present setup, the use of the cryogenic liquids amounts to less than 10 l per day. A dewar (L2025, Cryo Diffusion, France) of liquid nitrogen, pressurized with nitrogen gas, is used to supply cryogen to the probe via a modified, two-part helium transfer siphon (Cryogenic Ltd., UK). The demountable leg of the siphon is built into the probe and fits into the sample-cooling block. The dewar-side leg with the transfer line can be coupled to the probe once the probe has been inserted into the magnet.

The cooling block has been constructed out of PMMA using a 3D printer or machined from PTFE. Evaporation of the liquid nitrogen as it flows through the resonator, at the heart of the cooling block, is used to cool the sample. A schematic diagram of the cooling block is shown in Figure 2.3. Cold exhaust nitrogen gas from the cooling block is mixed with warm nitrogen gas and is removed through a heated outlet pipe. Temperature stabilized, nitrogen, purge gas is used to maintain a stable temperature for the rest of the probe.

Microwaves

While the sample is kept frozen, it is simultaneously irradiated with microwaves at a frequency of around 94 GHz. A low power synthesized microwave source (Wenzel Associates, Texas, USA) generates microwaves at around 12 GHz. This frequency is then up-converted to 94 GHz using an 8 times frequency multiplier (Virginia Diodes Inc., Virginia, USA). Finally the low power 94 GHz signal is fed into a 100 W extended interaction klystron amplifier (EIK) (VKB2463, CPI Canada Inc.) which feeds the

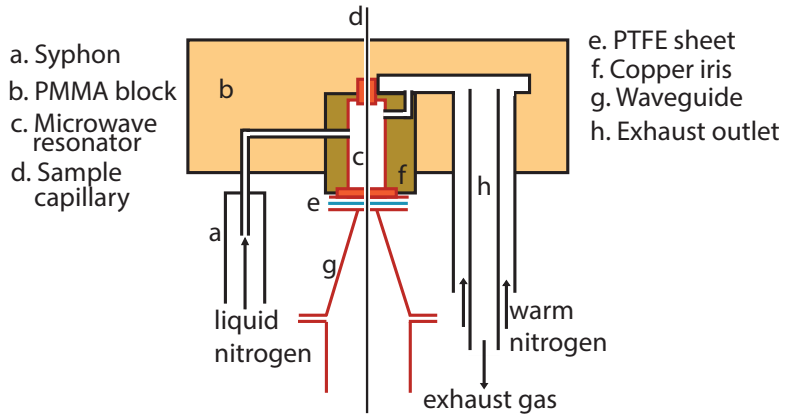

Figure 2.3: Schematic representation of the sample cooling block. Liquid nitrogen is introduced through a syphon (a), flowing through channels in a PMMA block (b) to pass through the microwave resonator (c) at the heart of the block. The sample capillary (d) passes through the resonator, below which a PTFE sheet (e) forms a seal to prevent the cryogen running down into the over-molded waveguide (g). A copper iris (f) at the lower end of the cavity is used to couple in microwaves when it is used in resonator mode. Exhaust nitrogen gas is removed via an outlet (h) that is jacketed with heated counterflow gas which mixes with the exhaust gas to stabilize the outlet temperature.

microwaves to the probe via oversized, cylindrical wave-guides. Typical insertion losses are between 3 and 5 dB. The microwave frequency and power output are both controlled by a PC running a compiled LabWindows/CVI (National Instruments) program.

A schematic of the DNP resonator/concentrator is provided in Figure 2.3. Inside the probe there is a taper (labeled as feature "g" in Figure 2.3) attached to the cylindrical waveguide, which reduces the diameter in order to couple to a non-resonant or resonant cavity ("c"). The cavity is made from copper, and the 360 μm OD capillary ("d") passes through top and bottom of the circular or rectangular cavity. Additional ports allow ingress of liquid nitrogen and allow the gaseous nitrogen to exhaust.

In the remaining part of this thesis we will restrict ourselves to non-resonant operation of the microwave cavity. Non-resonant operation of the cavity allows microwaves to be tuned to any desired frequency over the entire EPR band width. Also the absence of a tunable resonator allows a simpler probe optimization and facilitates quantitative comparison between different experiments. In principle this enables the use at higher magnetic fields without modification of the microwave assembly. The non-resonant mode of operation obviously reduces the microwave B_1 field strength. However, as the diameter is close to single mode cut-off at 95 GHz,

the irradiation volume is about one to two orders of magnitude smaller than typically used in either Dissolution DNP or MAS-DNP, and much higher power densities can be reached even in non-resonant mode of operation.

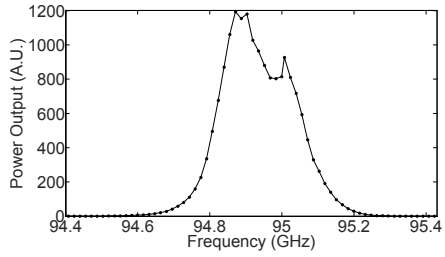

Figure 2.4: The output power profile of the used microwave source (klystron) for different frequencies. The power output is sufficient for 300 MHz window. The output power and frequency of the klystron can be changed during the experiment. The Larmor frequencies of BDPA and TEMPOL free radicals are 94.703 GHz and 94.98 GHz respectively for the current field (3.4T).

Sample melting

Sample melting is achieved by means of a stream of heated nitrogen gas, directed onto a localized section of the capillary, midway between the DNP and NMR centers. The gas is heated to a temperature of 50-70 °C using a tube with an internal electrical heating element.

This warm gas is then piped into a PTFE block through which the capillary passes, and melts the sample. The heated nitrogen gas stabilizes the temperature of the PTFE block which also acts as a thermal buffer between the cryogenic DNP section and the room temperature NMR region. The main objective of the heating stage is to allow a fast, reproducible, transition of the sample to the liquid state. Depending on the radical type, concentration, and solvent used for the DNP, proton relaxation can be quite fast. The continuous hot gas flow facilitates stable temperature settings for the NMR part, and the melting time is optimized by monitoring the NMR signal of the sample for increasing residence times in the hot zone. Alternatively, the sample can shuttle directly into the NMR detector, while still in the solid phase, for monitoring the polarization in the solid or possible NMR encoding or CP polarization transfer. The NMR signal is then recorded in either the solid phase or, after a subsequent melting step, in the liquid state.

Typical melting times (from 77 K to room temperature) can be achieved in about 500 ms for aqueous samples, which have a large latent heat at the melting transition and a large specific heat. Other solvents such as methanol, DMSO or toluene

allow melting times down to less than 50 ms. At a typical radical concentration of 20-50 mM, the effective proton T_1 relaxation time in the liquid state is about 0.1-5 s, depending on radical type and concentration. Except for the worst case of aqueous samples with high concentration TEMPOL radicals, the relaxation loss is acceptable. As indicated before, it is feasible to achieve faster melting by going to smaller inner diameter capillaries, higher heating gas temperatures or by the inclusion of additional IR laser or dielectric RF heating. For the present range of experiments we found that this is not necessary and a simple warm gas flow melting is sufficient.

Figure 2.5(a) represents a series of spectra taken after variable heating times for a frozen toluene sample with 50 mM BDPA radical. The corresponding integrated liquid-state signal is plotted in panel (b) as function of the melting time. Panels (c) and (d) show the corresponding series of spectra for a water-based sample containing H_2O, D_2O and fully deuterated glycerol in the ratio 25:70:5 (vol. %) with 5 mM TEMPOL. The first spectrum represents a direct transfer from the DNP center to the NMR center. Subsequent spectra are sequentially acquired with a 0.1 s increment of the residence time in the melting region, up to 0.8 s. The solid lines in panels (b) and (d) represent linear fits for the melting stage and exponential relaxation in the liquid phase. From Figure 2.5, the melting can be observed by the growth of the liquid-state proton resonance peak in the sample, as well as a slight narrowing of the signal, probably in part as a result of susceptibility broadening being reduced as the ice in the partially melted sample disappears. Thermal equilibration of the water sample is evidenced for example by the temperature dependent shift of the water peak. Panel (d) shows the integrated intensity of the water peak as function of the time spent in the melting zone. If we assume a specific heat of 4.2 kJ/kg for aqueous samples and a latent heat at the melting transition of 334 kJ/kg, then the total energy required to heat and melt a 50 nl frozen sample equals about 60 mJ. Using a heat conductivity of quartz of 1.4 W/K m we can estimate the average heating and melting time at 0.2 resp. 0.1 s, in reasonable agreement with the experimental observations. For toluene, which melts at -93 °C, the latent and specific heat is nearly a factor 5 resp. 2.5 lower, yielding typical estimated time constants of approximately 30 ms for melting and 70 ms for heating to room temperature, allowing a full melting transition within 0.1 s. In the experiments that will be described later we allow for temperature stabilization for another 0.1-0.4 s in the NMR chip before acquisition. A comparison of the relaxation rate in the liquid state is also favorable for the case of toluene-BDPA as the paramagnetic (Overhauser) relaxation rate is much lower compared to that of water-TEMPOL at comparable radical concentrations. Note that during the melting transition of water-glycerol, the viscosity of the liquid fraction is quite high, leading to fast relaxation. As a

result, the polarization will decrease rapidly during the melting transition. This is even more prominent if one increases the glycerol content to promote glass formation. At higher radical concentrations, the relaxation rate becomes prohibitive for DNP enhanced liquid-state proton NMR. For Toluene-BDPA this polarization loss is minimal and much higher radical concentrations can be used without seriously affecting the polarization and/or NMR resolution in the liquid state.

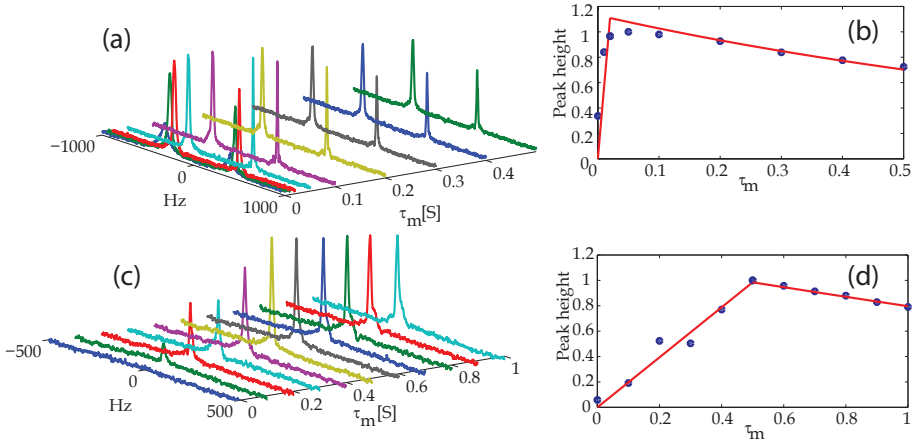

Figure 2.5: Sequence of spectra showing sample melting with increasing residence time in the warm nitrogen gas-stream. The first spectrum at time $\tau_m = 0$ is for the sample passing straight through the heating region; subsequent spectra are taken with an increasing residence time in the warm gas flow. (a) Melting of a frozen toluene sample containing 50 mM of BDPA radicals. (b) Corresponding integrated intensity of the liquid-state signal, indicating full melting within approximately 30 ms. The solid lines in panels (b) and (d) represent linear fits for the melting stage and exponential relaxation in the liquid phase. (c) Melting of a frozen water-glycerol sample, which comprises 25 % H_2O, 70 % D_2O, 5 % deuterated glycerol (by volume), with 5 mM TEMPOL. (d) The integrated liquid-state signal intensity as function of the heating time, indicating a complete melting in about 500 ms.

NMR detector

The NMR detection was done using a stripline probe [78, 82]. A chip was used with a stripline length of 3 mm, and a width of 0.5 mm as shown in Figure 2.6. The design concept of the stripline chip is described elsewhere [78]. For the present application, the main attractive point is its high sensitivity for mass limited samples. At 600 MHz a sensitivity Limit of Detection (LOD) equal to $3 \cdot 10^{13}$ proton spins in a bandwidth of 1 Hz was demonstrated. This specification for probe sensitivity implies that for a solution containing this amount of protons, a signal to noise ratio of one is obtained in a single scan for a single resonance with a spectral line-width of 1 Hz. If a 5 mm probe (sample volume 200 μl) would have a similar sensitivity, a

single CH proton resonance with a line-width of 1 Hz could be detected at unity SNR for a molecular concentration of 300 nM. At the lower fields used in this paper we expect a LOD of about $7 \cdot 10^{14}$ spins in a bandwidth of 1 Hz. In practice, our present setup performs below this predicted sensitivity with a LOD of $2 \cdot 10^{15}$ spins, probably because of additional losses in the non-ideal RF circuit. The low susceptibility distortion of the stripline design was proven to provide sub-hertz resolution at 600 MHz. In the present probe we experience field gradients due to stainless steel welds of the cryogenic transfer line. For future practical applications these gradients need to be reduced and additional shimming options need to be included. However, for the present proof of principle it is sufficient if all the individual resonances of small probe molecules can be resolved. A final attractive point of the stripline geometry is that it allows axial sample access. Helical microcoils can provide a similar sensitivity, but the orientation perpendicular on the field axis prevents on-axis sample shuttling.

The most straightforward experiments involve a long sample, i.e. long relative to the length of the sensitive region of the stripline. For such experiments it is possible to fill the capillary with sample and use the section of the sample that coincides with the DNP center for the experiment. It is then only required to know the precise distances between the different experimental regions (DNP, heating and NMR) in order to ensure that the enhanced section of sample is subsequently melted and transferred to the NMR detector. For future applications, it is desirable to study small, well-defined sample plugs. These could be contained between buffers of a susceptibility-matched, NMR-inactive liquid that is not miscible with the sample plug, such as fluorinert FC40 (3M corp.) in the case of water-based samples. For the exploratory experiments presented here, only long samples have been studied.

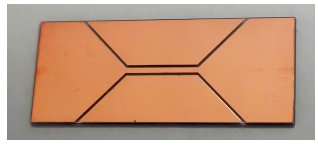

Figure 2.6: A typical stripline NMR detector used to acquire NMR signal. The stripline provides high resolution and sensitivity. The detection length for the current detector is 3 mm corresponding to 50 nl of effective sample volume. The sample capillary is placed directly on the detector, and can be moved axially.

2.2.1 Glassing Agent and Radicals

When polarizing in the solid state it is common to add a glass-forming agent to the solvent, in addition to the radical. Typical glass-forming mixtures are water-glycerol or water-DMSO for water-soluble radicals. Nonpolar solvents such as toluene naturally form a glassy state and no additives are required. The purpose of this glass formation is to ensure homogeneous distribution of the radicals in the solid phase. The glass formation was verified optically by checking the transparency of sample beads formed in liquid nitrogen. Aqueous samples were degassed by freezing at liquid nitrogen temperature with subsequent melting under vacuum.

In the present series of experiments we restricted ourselves to readily available radicals such as TEMPOL for polar solvents and BDPA for non-polar solvents Figure 2.7. A typical TEMPOL concentration of 5-20 mM was used to achieve an acceptable compromise between enhancement factors and (paramagnetic) relaxation time. BDPA was used at a higher concentration of 50 mM concentration in toluene, since this radical induces a lower paramagnetic relaxation in the liquid compared to TEMPOL.

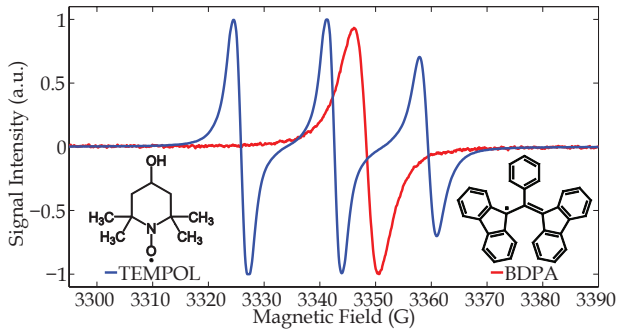

Figure 2.7: EPR spectra of BDPA and TEMPOL at room temperature. 15 mM BDPA was dissolved in toluene while 30 mM TEMPOL was dissolved in water. Both the samples were measured in capillaries.

2.3 DNP results

2.3.1 Aqueous samples: TEMPOL

In a first experiment, the polarization buildup was recorded in the solid state for a water based sample with TEMPOL radicals. To monitor the polarization, the sample was shuttled directly into the NMR chip, and the corresponding wide line spectrum

was measured with minimal delay after the shuttle step. The probe background signal was subtracted from the time domain signal. The enhancement was determined by normalization to the integrated intensity in the liquid state at room temperature. The test sample was obtained by doping a H_2O/D_2O, d_8-glycerol mixture (1:1 vol. %) with 30 mM TEMPOL. First, the Boltzmann buildup was recorded for the sample by varying the time spent in the cold DNP resonator, but with the microwaves switched off. The resulting thermal buildup curve indeed confirms a base temperature close to that of liquid nitrogen (77 K), with a typical cooling time constant of about 3 s. However, the wide line solid spectrum has a width close to that of the background and normalization accuracy prevents a more detailed analysis.

As a second step, DNP was performed by introducing microwaves at 94.99 GHz at increasing powers. For each power we determined the full solid-state polarization buildup as a function of the time spent in the cold DNP resonator for a sample that consisted of a mixture of 25 vol. % D_2O, 25 vol. % H_2O and 50 vol. % d_8-glycerol with 30 mM TEMPOL. A three-dimensional representation of the results is given in Figure 2.8(a). The microwaves were switched on immediately as the sample arrives in the cold DNP resonator and the DNP buildup was monitored as function of the irradiation time. The effective build-up time is a convolution of the actual cooling time with the (temperature-dependent) DNP rate constant. This effective time constant is about 3 s at low powers and decreases to about 2.2 s at high powers.

The DNP enhancement increases with microwave power to a maximum of -500, including the contribution from the thermal temperature jump.

Although the high glycerol concentration is essential for the glass formation, it prevents us to record liquid-state NMR spectra due to fast relaxation during and after the melting process.

TEMPOL has an exposed electron spin which effectively induces zero-single and double quantum relaxation transfers of the coupled electron-nuclear spin system in the liquid state. This is in fact the origin of the substantial Overhauser DNP that can be realized with nitroxide radicals in solution. In high viscosity solvents, such as in the present water-glycerol mixture at temperatures close to the freezing point, single quantum relaxation dominates and a substantial polarization loss is observed before one can obtain liquid-state NMR spectra. Only for samples with low glycerol content (5 vol. %) a DNP enhanced liquid-state NMR spectrum could be measured. Although reasonable enhancements (~50) were achieved, the reproducibility was poor. The build-up time for DNP in this case increased to >100 s, indicating a

slow spin diffusion in semi-crystalline ice where the radicals are presumably phase separated near the grain boundaries.

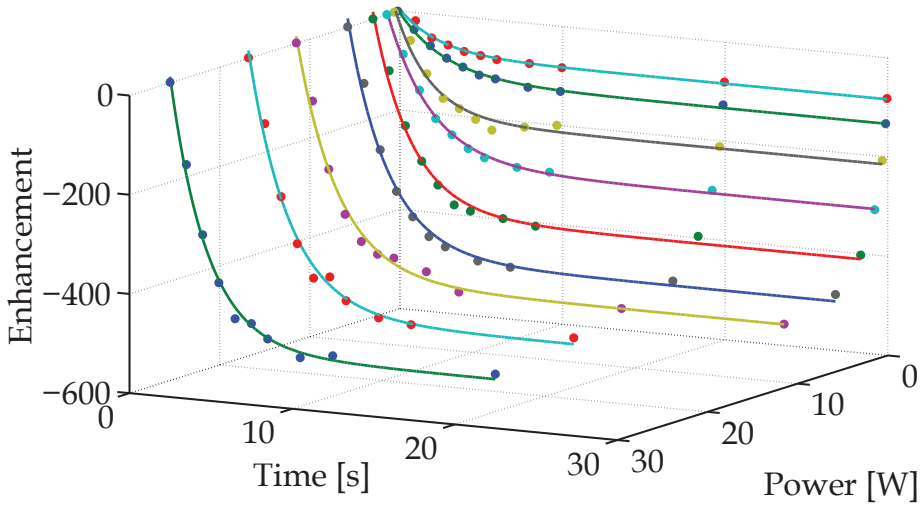

Figure 2.8: (a) Solid phase DNP buildup curves of a mixture of 25 vol. % D_2O, 25 vol. % H_2O and 50 vol. % d_8-glycerol, as function of irradiation time τ_{DNP} and microwave power. The DNP irradiation was started immediately during the cooling process.

2.3.2 Non-polar solvents: BDPA

A typical radical with a narrow, nearly homogeneously broadened EPR line is BDPA Figure 2.7. This molecule has a partly shielded electron spin on the internal carbon bonds. The long interaction distances with mobile molecules in solution lead to a low paramagnetic relaxation of the nuclear spin. Thus, the liquid-state proton T_1 of both solvent and solute is less reduced, when compared to a similar situation with for example nitroxide radicals. Experiments were performed with BDPA dissolved in toluene. At a concentration of 50 mM BDPA, the proton T_1 for both methyl and ring protons in toluene were found to be 500 ms. The melting sequence for a toluene sample was already shown in Figure 2.5. For this situation it is clear that the melting transition can be achieved well within the nuclear relaxation time, even in the presence of fairly high radical concentrations. As frozen toluene forms a natural glassy state, no glassing agents are needed. The low latent heat at the melting transition, combined with a low viscosity in the liquid state, facilitates rapid melting with negligible relaxation loss.

It is clear that even at the fastest shuttling time of 20 ms, with 0 ms spent in the melting zone, part of the sample is already in the liquid state and in less than

40 ms melting, the total sample becomes liquid. For longer melting times the NMR signal starts to relax slowly, as expected. In this case the melting transition occurs much faster than the effective relaxation time and we are able to study the DNP enhancement in more detail.

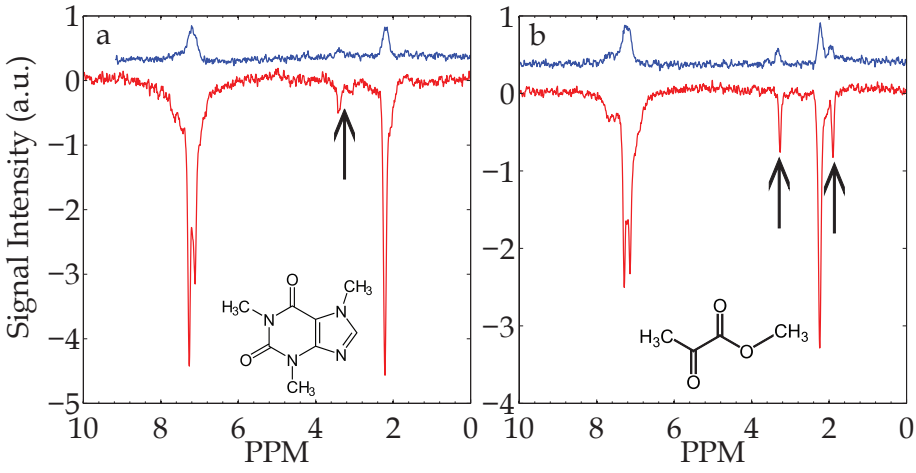

Figure 2.9: (a) Signal from a sample of deuterated toluene doped with 20 mM caffeine and 50 mM BDPA free radical. The signal in blue is a room temperature reference with 1024 scans, while the single scan signal in red is acquired after microwave irradiation of 10 seconds at 25.5 W of power. The small peaks near 3.4 ppm are due to 20 mM caffeine that was added to the toluene solvent. (b) Signal from a sample of deuterated toluene doped with 30 mM methyl pyruvate and 50 mM BDPA free radical. The signal in blue is a room temperature reference with 1024 scans, while the single scan signal in red is acquired after microwave irradiation of 10 seconds at 25.5 W of power. The peaks at 2 and 7 ppm are from the methyl and aromatic protons respectively of the residual protons of toluene. The small peaks at 3 and 1.8 are from the methyl pyruvate. The resolution for the DNP enhanced spectrum is similar to the reference spectrum.

In Figure 2.9(a) we show the DNP enhanced spectrum of a d8-toluene (99 % deuterated) sample with 50 mM BDPA. The total enhancement (Boltzmann + DNP) for toluene was approximately 300. Because of the low proton density in the sample, the room temperature reference spectrum was recorded with 1024 averages. In Figure 2.9(a) the averaged room temperature signal has been scaled by $\sqrt{1024}$ to compare it with the single scan DNP spectra at same noise level. As an illustration of the rapid-melt DNP performance, the spectrum in Figure 2.9(a) shows that sub-nanomole samples can be readily detected in a single DNP-enhanced scan, even at the present low magnetic field and with the very limited resolution that we obtain with the present prototype probe. Thermal averaging for many hours would be required to reach the same signal to noise level.

The present probe allows both solid and liquid-state DNP, in Figure 2.10 we show

a liquid-state spectrum of neat toluene doped with 100 mM BDPA radicals, compared with a liquid-state Overhauser DNP enhanced spectrum obtained with the microwaves tuned to the BDPA resonance. For this experiment, the cold nitrogen flow was switched off and both DNP microwave irradiation and NMR detection were performed near room temperature. As the present probe allows also for the option to work at high pressures, we have included in panel (b) a preliminary DNP enhanced spectrum for 20 % toluene in supercritical CO_2, doped with 20 mM TEMPO radicals and at a pressure of 100 Bar. All spectra in Figure 2.10 are obtained in a single scan. In comparison to the rapid-melt DNP shown in Figure 2.9 the Overhauser enhancements in Figure 2.10(a) and (b) are quite modest. Note however, that the BDPA radical used in (a) is definitively not the most efficient for Overhauser DNP. Also none of the parameters were fully optimized. In particular, we did not implement a microwave resonator and the radical spins are not fully saturated at the present power levels. As the microwave irradiation is nonresonant, this example does illustrate the relative absence of heating in nonpolar solvents and with suitable high-Q resonator structures, the present fast shuttling probe can be an effective way to implement high frequency Overhauser DNP with separately optimized DNP and NMR stages. The main advantage would then be that the electron spin can be irradiated at an allowed transition and full saturation can be achieved even at moderately low powers, opening the opportunity to use low-cost solid-state microwave sources.

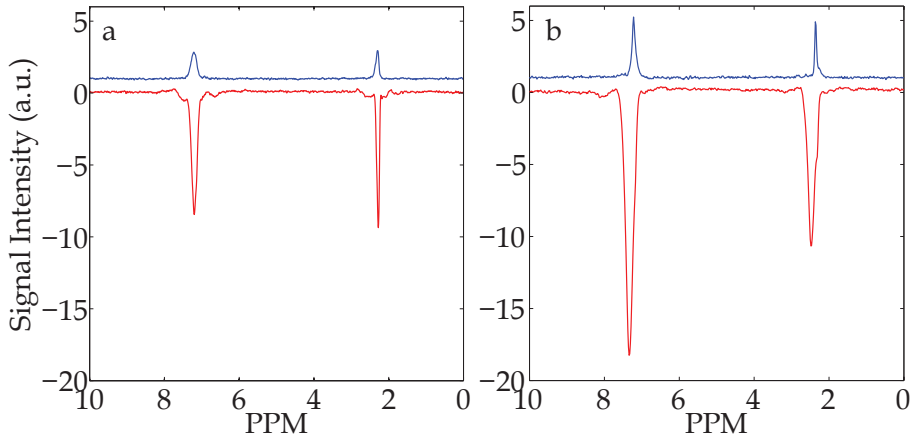

Figure 2.10: (a) Liquid State Overhauser DNP enhancement for neat toluene, doped with 100 mM BDPA. The thermal reference spectrum (blue) is displaced vertically for clarity. The sample volume is 50 nl and contains approximately 0.5 μmole toluene. (b) Liquid overhauser enhanced spectrum for 20 % toluene in supercritical CO_2, doped with 20 mM TEMPO radicals at a pressure of 100 Bar. The sample contains 100 nmol toluene. All the above spectra are single scan.

2.4 Preliminary applications

In this section, we will evaluate the potential for NMR detection of low amounts of molecules with increased sensitivity.

A small metabolite molecule that is often studied in the context of DNP for medical imaging purposes, is pyruvate. In typical dissolution DNP for in vivo or in vitro metabolic studies, a pyruvate solution of a concentration of 1 M or more is polarized for several hours and after dissolution its metabolic fate is studied at initial concentrations of 5-20 mM by ^{13}C NMR. In vitro studies are typically done in 200 μl or 1 ml volumes. In vivo voxel volumes are of comparable size and high resolution imaging is hampered by the intrinsic T_1 relaxation time in such a single shot hyperpolarization experiment. In the present setup we study nearly thousand times smaller volumes, typically 50 nl, and at 30 mM concentration, the total amount of molecules that is interrogated is of the order of 1 nano mole. A typical result is shown in Figure 2.9(b). The NMR is based on a simple one-pulse acquisition with no solvent suppression. The main peaks are due to the solvent signal of the 1 % protonated toluene in the solvent. The pyruvate signals are indicated by the black arrows. The DNP enhancement of the pyruvate signal at this microwave power is about 100, including the contribution from the temperature jump.

Although Figure 2.9 shows a typical spectrum, this method can be used with even lower concentration of target molecules. In Figure 2.11, the top spectrum is a single scan and the bottom spectrum is acquired with 100 averages after DNP for a sample of 3 mM (150 pico-mole) methyl pyruvate dissolved in d8-toluene with 50 mM BDPA. The total measurement time for this spectrum was about 10 min, with 100 averages and a total cycle delay of 6 s (5 s DNP, 30 ms melting and 200 ms stabilization time). In the thermal signal it was not possible to discern the pyruvate signals except after excessive signal averaging. With DNP the signals are visible in a single scan and with modest averaging, a good sensitivity is achieved. Actually, despite the higher DNP temperature (77 K versus 1.2 K) and the lower field at which NMR signals are detected (3.4 T versus 14.1 T), the signal SNR can surpass that of dissolution DNP. As indicated in the introduction, this is mainly due to the following aspects: (a) Proton detection is more sensitive than ^{13}C detection. (b) Microcoil detection can be a factor 10 more sensitive than more common large volume saddle coil detection. (c) Proton DNP buildup is much faster than for ^{13}C, in particular at the higher temperature of 77 K. At the much larger microwave B_1 field strength that can be applied, the build-up time for the polarization is a few seconds, instead of a few hours for the ^{13}C dissolution counterpart. (d) Rather than a single

shot experiment, the present implementation allows multiple scans averaging with relative short cycle delay times. A final remark concerning the comparison of concentration in microfluidic volumes versus dilution in a larger volume concerns the need for solvent suppression. Assuming that a similar deuterated solvent is used (99 % deuteration), a similar amount of pyruvate measured in diluted form with a 5 mm probe would show relative intensities of the solvent peaks that are about 4000 times larger and the small pyruvate signals could be masked in this strong background. With microfluidic detection and with modern high dynamic range data acquisition, solvent suppression is often not required. The main applications of dissolution DNP lie in metabolic imaging and study of metabolic pathways where the above mentioned drawbacks may not limit its application. However, this may not be the case for analytical applications where high resolution proton NMR and multidimensional NMR are indispensable. The main aspect that presently prevents a direct application of the prototype probe is the unsatisfactory resolution. This is partly due to problems related with welding joints of the cryogenic transfer line that become magnetic at low temperatures. In the future we intend to avoid these problem and with the implementation of additional dedicated shimming at the NMR part we hope to improve this aspect.

A second example was already given in Figure 2.9(a). Caffeine was dissolved in d8-toluene at a concentration of 20 mM. This corresponds to a total amount of 1 nanomole caffeine in the detection volume of 50 nl. DNP enhancement for the caffeine was in this case about 100, compared to an enhancement of 300 for the toluene signals. Although the sensitivity is quite sufficient, it is clear that the NMR resolution needs to be improved to resolve the different resonances. If the required resolution can be obtained, this will also help to further improve the sensitivity in the frequency domain, and avoid overlap with solvent resonances. However, the main conclusion is that DNP polarization in the solid state, followed by rapid melting and NMR detection in the liquid state can indeed be a successful and generic method for a wide range of both smaller and larger molecules.

2.5 Conclusions and future prospects

Rapid-melt DNP is a new method to achieve high nuclear proton polarization in liquid-state samples by rapidly melting a frozen hyperpolarized sample. The new configuration is situated within the homogeneous region of a superconducting magnet and comprises a cold DNP resonator, a heated gas melting stage and NMR detection in a stripline chip. Sample shuttling is done by translation of the sample

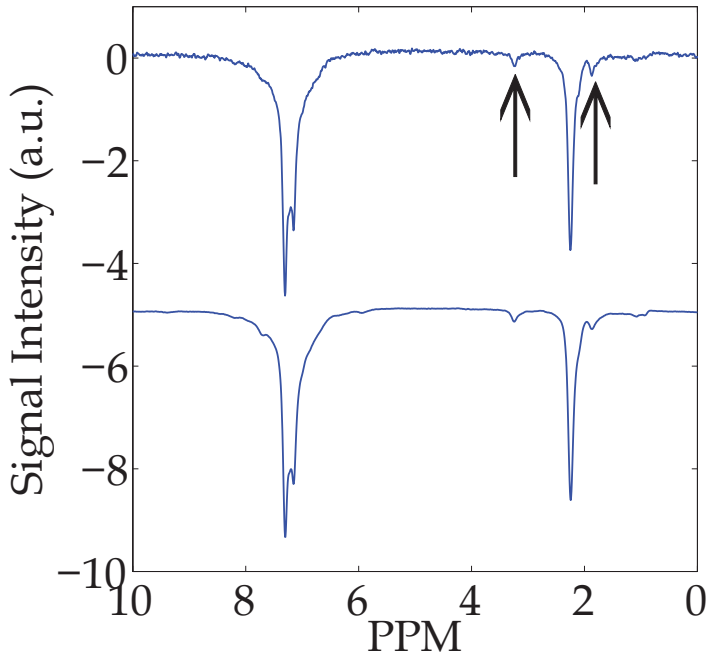

Figure 2.11: The DNP enhanced spectrum of 150 pico moles of methyl pyruvate (3 mM) dissolved in d8-toluene with 50 mM BDPA. The top spectrum is a single scan for 25.5 watts of microwave power for 5 seconds. The bottom spectrum is averaged for 100 scans at the same settings as the top spectrum. A single scan including DNP, melting, NMR and shuttling can be completed in ∼6 seconds. The two big peaks at 7.2 and 2.1 ppm are from the residual protons of toluene for aromatic and methyl groups. The two small peaks around 2 ppm are from the two methyl groups of methyl pyruvate.

capillary using a linear actuator. This approach allows repetitive signal averaging or multidimensional NMR experiments, for example aimed at structure elucidation. For aqueous samples we obtain a typical melting time of 500 ms, which is rather long compared to proton relaxation times in the presence of high concentration radicals such as TEMPOL. The main point we would like to emphasize here is that the capability to invoke solid-liquid phase changes within the nuclear coherence times of protons and low gamma nuclei may allow a novel optimization of general NMR experiments, combining the potential of solid and liquid NMR in a single experiment.

Melting of non-polar solvents such as toluene, with a low specific heat and low latent heat for melting, can be achieved in less than 30 ms for a typical sample volume of 50 nl. As the paramagnetic relaxation of BDPA in this low viscosity solvent

is small, we observe acceptable relaxation losses during the melting transition. A viable road for high sensitivity detection was demonstrated by the measurement of low amounts of molecules (typically 1 nano mole), with a typical DNP enhancement in the final state of more than a factor 100 in a single scan. In principle this could reduce measurement times by a factor 10,000, reducing demanding experiments to single or few scan experiments. From a practical point of view we should note that the operational costs in terms of chemicals (including radicals) and cryogenic liquids are negligible, compared to the present commercial options. In the present study we used only the widely available and cheap TEMPO(L) and BDPA radicals. Also the investment costs are quite modest, as the use of a second superconducting magnet for either polarizer (Dissolution) or gyrotron oscillator is avoided. In the present test measurement we opted for the relatively low sample volume of 50 nl. The fast shuttling technique within the homogeneous bore avoids relaxation losses and as the microwave DNP resonator is physically separated from the NMR detection both can be optimized separately.

Chapter 3

Mechanistic studies in rapid-melt DNP

Abstract

Dynamic Nuclear Polarization (DNP) has become a key element in nuclear magnetic resonance (NMR). Rapid-melt DNP is a novel approach to DNP enhanced liquid-state NMR based on rapid melting of a solid hyperpolarized sample followed by 'in situ' liquid-state NMR detection. This method allows ^{1}H detection with fast cycling options for signal averaging. In non-polar solvents, doped with BDPA radicals, proton enhancement factors were achieved of up to 400. A short recycling delay of about 5 s allows for a fast determination of the hyperpolarization dynamics as function of the microwave frequency and power. Here, we use the rapid-melt DNP method to study the mechanisms of DNP in the solid phase in more detail. Solid Effect, Cross Effect, Solid Overhauser and Liquid-state Overhauser DNP enhancement can be observed in the same setup. Here, we concentrate on Solid Effect DNP observed with both homogeneous narrow line radicals such as BDPA and with wide line anisotropic nitroxide radicals such as TEMPOL. We find indications that BDPA protons play an important role in Solid Effect DNP with this radical. A simplified spin diffusion model for BDPA can give a semiquantitative description of the enhancements as function of the microwave power and as function of the proton concentration in the solid solution. For aqueous frozen samples we observe a similar Solid Effect DNP enhancement, which is analyzed within the simplified spin diffusion model.

3.1 Introduction

In the previous Chapter, we introduced the rapid-melt DNP method to allow liquid state NMR detection combined with generic solid-state DNP [83]. In this Chapter we focus on the mechanistic studies performed in the rapid-melt DNP setup.

Three mechanisms for solid-state DNP have been identified: a two-spin (electron-nuclear) interaction (Solid Effect DNP [16, 84, 85]), a three spin interaction (Cross Effect DNP [18]) and a generalized multiple spin interaction (Thermal Mixing DNP [86]). The DNP mechanism can usually be identified by the frequency dependence of the enhancement. The in situ melting approach of rapid-melt DNP allows detailed studies of power and time dependent polarization buildup. Also, it is feasible to use high-power/high-B_{1e} microwave fields to explore different DNP mechanisms, as microwave heating effects can be minimized by efficient cryogenic cooling of small capillary samples. In the present set-up we can use up to 100 W of microwave power, and with proper high Q resonator structures it is conceivable to excite with a very high B_{1e} field strength. In this Chapter we will use non-resonant excitation only, to allow for flexible frequency dependent studies. In contrast to most CW gyrotron sources, the extended interaction klystron is an amplifier which allows frequency stepped pulsed mode operation synchronized with the NMR spectrometer. The NMR is performed in the liquid state at room temperature in order to benefit from the higher resolution attainable with liquid-state NMR spectroscopy.

In the experimental results we will describe detailed mechanistic studies of the DNP process in apolar frozen toluene with BDPA radicals and in polar $H_2O/D_2O/d8$-glycerol mixtures with TEMPOL radicals. As the analysis will be mainly focused on the Solid Effect, we will summarize and extend the basic theory for this mechanism using simplified rate equations.

3.2 Theory of Solid Effect DNP

The classical description of Solid Effect DNP for excitation of a single unpaired electron spin coupled with N_n proton spins for $W^{\pm}$ excitation rates at frequency $\omega^{\pm} = \omega_e \pm \omega_n$ can be summarized by the rate equations:

$$\frac{dp_e}{dt} = -\frac{p_e - p_e^0}{T_{1e}} - W^{\pm}(p_e \mp p_n) \tag{3.1}$$

$$\frac{dp_n}{dt} = -\frac{p_n - p_n^0}{T_{1n}} - \frac{W^{\pm}}{N_n}(p_n \mp p_e) \tag{3.2}$$

where p_e and p_n are the electron and proton spin polarization levels. The frequencies ω_e and ω_n are the electronic, resp. nuclear Larmor frequencies and p_e^0 and p_n^0 are the corresponding Boltzmann polarization levels at the temperature of interest. We have assumed that the EPR linewidth is narrow compared to the nuclear Larmor frequency (well resolved Solid Effect), where the W^+ and W^- transition do not overlap and single quantum transitions W^0 can be neglected. The transition rate $W^\pm$ will be proportional to the applied microwave power $W^\pm = \alpha P_{mw}$, where the constant α depends on the electron-nuclear hyperfine coupling and will scale with experimental parameters such as cavity conversion factors that relate microwave power to local B_{1e} field strength. T_{1n} is the longitudinal nuclear relaxation time, including the paramagnetic relaxation induced by the unpaired electrons spin. It is common to assume Boltzmann equilibrium for the electron polarization ($p_e = p_e^0$), however this approximation is not needed and if $T_{1e} \ll T_{1n}$ the coupled differential equations for Solid Effect DNP can be solved as (see also Ref. [87], with a slightly different notation)

$$\epsilon_s = \frac{(1 + f_e S^\pm) \mp \epsilon_i S^\pm}{1 + S^\pm(1 + f_e)} \tag{3.3}$$

for the saturation (steady-state) proton enhancement and a DNP build-up time constant given by

$$\tau_{dnp} = T_{1n} \frac{1 + f_e S^\pm}{1 + S^\pm(1 + f_e)} \tag{3.4}$$

where we have introduced a proton saturation level $S^\pm = W^\pm T_{1n}/N_n$, $\epsilon_i = \gamma_e/\gamma_n$ is the maximum enhancement and the electronic 'leakage' factor f_e is defined as $f_e = N_n T_{1e}/T_{1n}$. The main underlying assumption is that the nuclear polarization is instantly shared among all protons, in other words that the proton spin diffusion is fast on the scale of the excitation rate $W^\pm$. The maximum enhancement at full saturation $S^\pm \gg 1$, reduces to

$$\epsilon_s = \frac{f_e \mp \epsilon_i}{f_e + 1} \tag{3.5}$$

The main result within this model is thus that for the usual case where $f_e \ll 1$ a maximum DNP enhancement approaching 660 can be reached if the 'forbidden' cross transition can be pumped efficiently ($S^\pm \gg 1$). At the same time the DNP build-up time τ_{dnp} becomes much smaller than the nuclear relaxation time $\tau_{dnp} \approx T_{1n}/S^\pm \propto P_{mw}^{-1}$. So far, for practical situations described in literature, a full saturation is generally not achieved and detailed measurements of the build-up time is difficult with for example CW gyrotron sources. In a few cases a reduction of τ_{dnp} below T_{1n} is reported [88], but a tendency towards zero, as predicted by the Solid Effect theory has not been reported. Only in the case for very low concentration radicals with an exceptionally long T_{1e} it becomes relevant to correct for the factor f_e, but in practical situations the approximation $f_e = 0$ is justified.

In the following, we will extend the basic Solid Effect model to a more realistic situation where spin diffusion is not infinitely fast. We will assume that the unpaired electron spin is coupled to a local bath of N_c core nuclei as described by Equations 3.1 and 3.2. We will further assume that the diffusion of polarization from core to the bulk protons can be described by a rate constant W_d:

$$\frac{dp_e}{dt} = -\frac{p_e - p_e^0}{T_{1e}} - W^{\pm}(p_e \mp p_c) \tag{3.6}$$

$$\frac{dp_c}{dt} = -\frac{p_c - p_n^0}{T_{1c}} - \frac{W^{\pm}}{N_c}(p_c \mp p_e) - \frac{W_d}{N_c}(p_c - p_b) \tag{3.7}$$

$$\frac{dp_b}{dt} = -\frac{p_b - p_n^0}{T_{1b}} - \frac{W_d}{N_b}(p_b - p_c) \tag{3.8}$$

where p_c is the proton polarization in the core region with a longitudinal relaxation time T_{1c} and p_b the proton polarization in the bulk with a relaxation time T_{1b}. W_d is the effective rate constant for diffusion between the two regions. The normalization with respect to the respective pool sizes (N_c and N_b) takes care of the conservation of nuclear magnetization in the diffusion process. Direct Solid Effect transitions from electron to bulk protons are neglected. The core protons may have a shorter longitudinal relaxation time ($T_{1c} < T_{1b}$) due to the close vicinity of the fluctuating electron spin.

In general, these coupled rate equations need to be solved numerically. However, it is instructive to evaluate the simplified situation where we assume that the electronic polarization is constant during the DNP buildup of the core polarization ($T_{1e} \ll T_{1c}$). Also, we will assume that diffusion is the rate limiting step in the buildup of the bulk polarization. For high microwave pumping rates, the core polarization reaches an equilibrium in a time much shorter than the bulk proton relaxation time T_{1b}. For full saturation of the coupled electron-nuclear satellite transitions in the direct vicinity of the unpaired electron spin, the core polarization will then approach the theoretical maximum given by the basic Solid Effect theory $p_c = \epsilon_c \cdot p_n^0 \approx \gamma_e/\gamma_n \cdot p_n^0$. Equation 3.7 can be solved as in the basic Solid Effect model if we can neglect the diffusion term, with the result shown in Equation 3.3, and assuming $f_e = 0$.

$$\epsilon_c = \frac{1 \mp \epsilon_i S^{\pm}}{1 + S^{\pm}} \tag{3.9}$$

Under these assumptions, the rate equation for the bulk polarization can be rewritten as

$$\frac{dp_b}{dt} = -\frac{p_b - p_n^0}{T_{1b}} - \frac{W_d}{N_b}(p_b - \epsilon_c p_n^0) \tag{3.10}$$

which can easily be solved and the saturation (steady-state) enhancement in the bulk is given by

$$\epsilon_b = \frac{f_d + \epsilon_c}{f_d + 1} = \frac{1 \mp S^{\pm}\epsilon_i^{'}}{1 + S^{\pm}} \tag{3.11}$$

where

$$\epsilon_i^{'} = \frac{\epsilon_i \mp f_d}{f_d + 1} \approx \frac{\epsilon_i}{1 + f_d} \tag{3.12}$$

and the diffusion 'leakage' factor f_d is defined as $f_d = N_b/(T_{1b}W_d)$. The bulk enhancement will not follow a simple exponential buildup. At high microwave powers, where the core polarization reaches equilibrium in a time $T_{1c}/S^{\pm}$ much shorter than the bulk T_{1b}, the approximate build-up time constant for the bulk protons becomes

$$\tau_b = \frac{f_d T_{1b}}{1 + f_d} \tag{3.13}$$

This shows that under the above assumptions with a rate limiting diffusion step, the bulk enhancement is reduced from the theoretical upper limit. For fast polarization transport from core to bulk (high W_d), low proton densities in the bulk (low N_b) and long T_{1b} relaxation times, the diffusion leakage term f_d becomes small and the bulk polarization follows the core polarization. On the other hand, for high proton densities with short relaxation times, the bulk polarization is strongly reduced from the theoretical maximum. Also, the build-up time constant for the bulk polarization becomes comparable to T_{1b} and will become independent of the microwave power if the above conditions are met. In particular, the build-up time constant will not tend to zero at high pumping rates as predicted by the basic Solid Effect theory.

In a physical sense, the electronic 'leakage' factor $f_e = N_n T_{1e}/T_{1n}$ represents the fact that the DNP pumping process cannot be repeated faster than T_{1e} and the polarization level is limited by the nuclear relaxation rate N_n/T_{1n} during this time interval. If spin diffusion becomes the rate limiting step, then the diffusion rate W_d into the bulk region is balanced by the bulk relaxation rate N_b/T_{1b}. In general, the electronic 'leakage' can be neglected ($f_e \approx 0$), but this is not the case for the diffusion 'leakage' term f_d.

In the present experiment, we have performed the DNP experiment at liquid nitrogen temperatures and the maximum nuclear polarization that can be reached is limited by the electron polarization level in the solid with $T_s \approx 77$ K. The detection will be done in the liquid state and the effective enhancement, normalized on the room temperature (T_l) Bolzmann polarization is then simply

$$\epsilon_l = \frac{T_l}{T_s}\epsilon_i^{'} e^{-t_m/\tau_r} \tag{3.14}$$

where t_m is the time taken by the melting process, and τ_r is the effective relaxation in this time interval. For rapid melting of toluene samples, where the relaxation losses are minimal, the measured enhancement in the liquid state equals the solid enhancement multiplied by the temperature jump ratio. Assuming a sample temperature during microwave irradiation in the range 77-90 K (allowing for microwave heating) and 293 K during detection, the temperature jump factor is approximately 3.5 ± 0.3 and the maximum upper limit for the enhancement is about $660 * 3.5 = 2300$. Note that for Dissolution DNP, a similar effect is seen, where a low temperature DNP enhancement factor of 100 (15 % absolute polarization) and a temperature jump from 2 K to 300 K results in a typical effective enhancement of 15,000 relative to room temperature Bolzmann polarization.

For radicals with an inhomogeneously broadened EPR spectrum only a fraction of the radicals have the proper orientation for Solid Effect DNP at a given magnetic field and microwave frequency. Also, excitation at frequencies $\omega_e \pm \omega_n$ may both be present and the net excitation is the balance between the two rates. In addition, multiple spin effects such as Cross Effect DNP may overlap with Solid Effect DNP. For a simplified treatment of this case we will assume that the fraction of 'active' electron spins with the proper orientation and resonance frequency to match the Solid Effect conditions is given by:

$$\chi = \xi[G(\omega - \omega_n) - G(\omega + \omega_n)] \tag{3.15}$$

where $G(\omega)$ represents the normalized EPR resonance at frequency ω and ξ is a dimensionless effective excitation bandwidth, determined by the homogeneous linebroadening and the microwave B_{1e} field strength. The remaining electron spins are not contributing to Solid Effect transitions, but do contribute to enhanced relaxation of the bulk protons. A crude, but not unrealistic, treatment would then be to adapt the above analysis where the effective radical concentration is reduced by the factor χ. The pumping rate of the 'active' radicals is determined by the local hyperfine couplings and depends on the molecular structure of the radical. In the case of infinitely fast diffusion, the maximum enhancement levels remain practically the same [87] as the renormalized electronic leakage factor f_e remains small. On the other hand, if the diffusion from the core protons to the bulk, is the rate limiting step, then the diffusion leakage term $f_d = N_b/(T_{1b}W_d)$ becomes larger both because the number of bulk protons per active radical increases by the factor χ and because of the reduction in T_{1b} by the 'unactive' radicals. Compared to the homogeneous case, this will in general lead to lower effective enhancement, unless this is offset by a faster diffusion rate W_d. At low microwave powers and in the usual situation where the homogeneous linebroadening is much smaller than the inhomogeneous EPR linewidth the shape of the frequency dependent Solid Effect DNP for

the inhomogeneous case resembles the discrete difference $G(\omega-\omega_n)-G(\omega+\omega_n)$ of the EPR resonance curve.

3.3 Experimental

Experimental details of rapid-melt DNP are given in Chapter 2. Aqueous samples consist of glass-forming mixtures of water-glycerol or water-DMSO doped with water-soluble nitroxide radicals. Nonpolar solvents such as toluene form a natural glassy state and no additives are required.

DNP experiments of aqueous samples were performed in the solid state by skipping the melting step. DNP of non-polar solvents was examined in the regular fashion (DNP-melt-NMR) described in Chapter 2.

3.4 DNP results

3.4.1 Non-polar solvents: BDPA

To identify the DNP mechanism for BDPA, we varied the frequency of the microwave excitation source. In Figure 3.1 we show the observed frequency dependence of the DNP enhancement for different modes of operation. The top graph indicates the solid-state DNP enhancement curve for BDPA radicals in toluene. BDPA has a homogeneous narrow line EPR spectrum leading to a well resolved Solid Effect DNP. The positive Solid Effect DNP peak at lower frequencies is outside the amplifier window of our Extended Interaction Klystron (EIK) amplifier and is not shown in this graph. At a frequency near 94.7 GHz, we observe a weak positive enhancement, tentatively attributed to Overhauser cross relaxation with a scalar interaction between electron and nuclear spin (Solid Overhauser). Panel (b) in Figure 3.1 shows the observed Overhauser enhancement in the liquid phase. The negative enhancement indicates a dipolar interaction with predominant double-quantum cross relaxation. Usually, BDPA is not the preferred radical for liquid-state Overhauser DNP, due to the relatively shielded site of the unpaired electron spin, leading to small dipolar couplings in the dynamic spin-spin interaction. Nevertheless, even in the present nonresonant microwave setup we observe a clear liquid-state enhancement. Finally, in the bottom panel of Figure 3.1 the frequency dependent rapid-melt DNP enhancement is shown for a mixture of BDPA and TEMPO radicals in toluene. In this example we observe the usual Solid Effect as well as the positive Cross Effect enhancement. In this case, we irradiate on the center of the BDPA

EPR resonance, saturating this electron spin. Cross relaxation with nearby TEMPO radicals are most effective to produce proton polarization if the anisotropic TEMPO resonance differs from the BDPA resonance by the nuclear Larmor frequency. In this case an energy conserving three spin flip process is possible that effectively transfers the BDPA electron polarization to the nuclear system. This mode of operation has in common with Overhauser DNP that one irradiates an allowed transition, which requires less microwave power. Clearly, the TEMPO radical is not the best candidate for this effect and it would be desirable to engineer a homogeneous narrow line radical with the proper offset in g-factor with respect to BDPA. Note that the present comparison of DNP mechanisms, although all taken with the same or similar samples and at comparable microwave powers (varying from 5 to 15 W), the liquid state Overhauser mode of operation is far from optimized and does not represent ultimate capabilities. Apart from the frequency dependence of the DNP enhancement, the mechanisms can also be distinguished by its power dependence. The Solid Overhauser DNP turns out to saturate at very low power, indicating a fast saturation of an electron spin at an allowed transition. Previous experiments have shown that liquid state Overhauser DNP saturates at relatively low powers. If a high Q resonator is employed, as the narrow EPR line is pumped at resonance [50]. In the present non-resonant setup, we do not reach full liquid state saturation. The Cross Effect is a solid state mechanism based on full saturation of an electron spin, coupled to a second spin with a different g-factor. Again, this process saturates at rather low powers. In contrast, the solid effect DNP requires much higher microwave power and for BDPA, a full saturation is only achieved at powers above 10-20 W. This indeed indicates a low probability, nominally forbidden, transition. As shown in the top graph of Figure 3.1, the frequency dependence of the DNP enhancement strongly points towards the Solid Effect as the dominant mechanism for BDPA in frozen toluene. The frequency dependence of the DNP enhancement for water-TEMPOL is not conclusive to identify the Solid Effect as the main mechanism, and a more detailed modeling is required. Overhauser DNP and in its simplest version also Cross Effect DNP rely on the saturation of an allowed EPR resonance, leading to nuclear polarization by cross relaxation. In this case the build-up time is basically equal to the nuclear relaxation time T_{1n} and independent of the microwave power. This is not the case for Solid Effect DNP, where at high microwave power, the build-up time becomes shorter than T_{1n}. In literature, there are very few systematic studies of the relevant time constants [88, 89]. This is partly due to the fact that the most common microwave sources, such as gyrotron oscillators, are continuous wave instruments.

In the rest of this Chapter we will focus only on the Solid Effect DNP mechanism

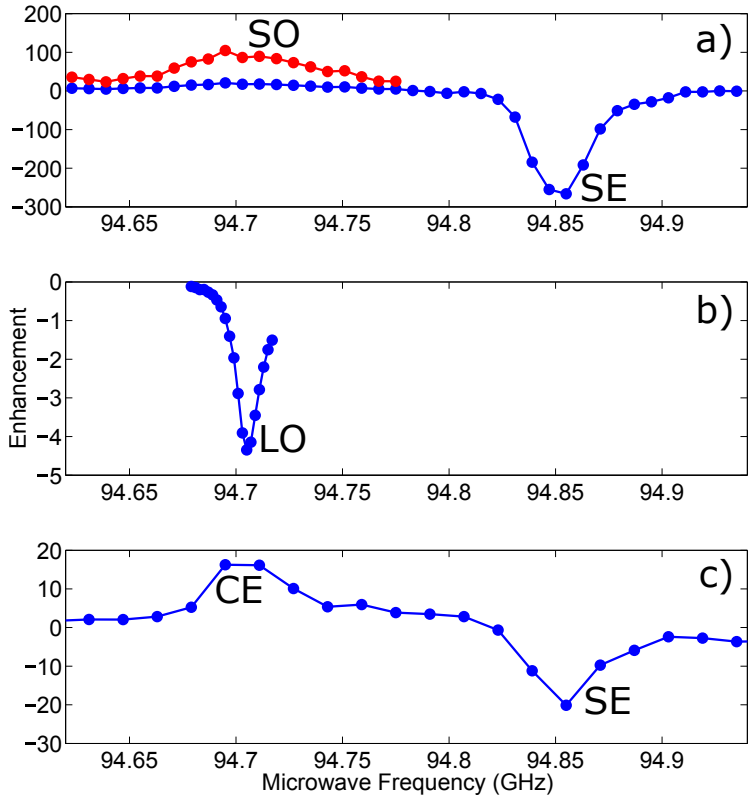

Figure 3.1: (a) Frequency dependence of rapid-melt DNP for a 99 % d8-toluene sample with 50 mM BDPA radical doping (blue). The main peak, is the solid effect DNP enhancement. In red we have multiplied the low frequency part of the enhancement curve by a factor 10. The broad positive peak is on resonance with the BDPA radical and possibly due to a Solid Overhauser cross relaxation dominated by scalar couplings. (b) Frequency dependent liquid State Overhauser (LO) DNP enhancement for neat toluene, doped with 100 mM BDPA. (c) Frequency dependent DNP enhancement for a mixture of BDPA (40 mM) and TEMPO (20 mM) radicals in toluene. In this case we observe a mixture of Solid Effect and Cross Effect DNP.

and we will attempt to analyze in detail the microwave power dependence of both enhancement and DNP build-up time for two representative cases: BDPA in toluene and TEMPOL in water/glycerol mixtures.

3.5 Rapid-melt Solid Effect DNP for BDPA-toluene

In the next experiment, we measured a series of spectra using the rapid-melt technique for increasing values of the microwave irradiation time (typically 0-30 s.). A single exponential fit to the enhancement values, normalized to the liquid state

room temperature spectral intensity, allows the determination of the saturation level and build-up time constants. The DNP enhancement limit at high microwave power for fully protonated toluene increases from -4 to -17, resp. -42 when increasing the BDPA concentration from 10 to 30 resp. 50 mM. At a very high radical concentration ($\geq$100 mM), T_1 in the liquid state becomes very short which results in loss of DNP enhanced signal during melting, and the maximum observed DNP enhancement in the liquid state drops to -12. The optimal concentration is close to 50 mM as a compromise between enhancement in the solid phase and relaxation in the liquid state. For this concentration we find a solid-state T_1 for toluene protons of a few seconds, and a liquid-state T_1 of about 1 s. A more prominent effect on the final enhancement is found for the protonation level of the solvent. For this purpose, the protonation level was modified by mixing nominally pure d8-toluene (99.6 %) with neat toluene. The enhancement increases from -40 for neat toluene to -50, -80 and -175 for d8-toluene/toluene deuteration levels of 20 %, 80 % and 90 %. For the lowest protonation levels, the enhancement saturates at about -400 for 99 % and 99.6 % d8-toluene.

In Figure 3.2 we have reproduced the typical EPR spectrum of BDPA (a), together with the predicted enhancement for the frequency dependent Solid Effect enhancement. Apart from the small additional contribution of possible solid Overhauser DNP near the BDPA resonance, the normalized experimental enhancement for a radical concentration of 50 mM BDPA in 99 % deuterated toluene (solid symbols) follows the predicted curve quite well and we may assume that at frequencies near the minimum of the negative peak in the enhancement curve, the Solid Effect is indeed the dominant process. Note that at the highest frequencies a shoulder appears that is not understood.

An additional positive DNP effect is observed for microwave frequencies near the BDPA resonance frequency. The on-resonance DNP appears to saturate at much lower microwave powers, as compared to the Solid Effect DNP. This would be consistent with an allowed microwave transition, as for example in Overhauser cross relaxation DNP with scalar coupling terms. The frequency dependence for Overhauser DNP is expected to mimic the EPR spectrum and even in the case of high B_1e off resonance excitation we would not expect the broad Gaussian distribution. The exact origin for the on resonance enhancement remains therefore uncertain. For the present discussion, we will focus on the Solid Effect as this provides the largest enhancement under the present circumstances.

In Figure 3.3 we have reproduced the experimental enhancement and build-up time as function of microwave power (black solid circles), for the sample with a low

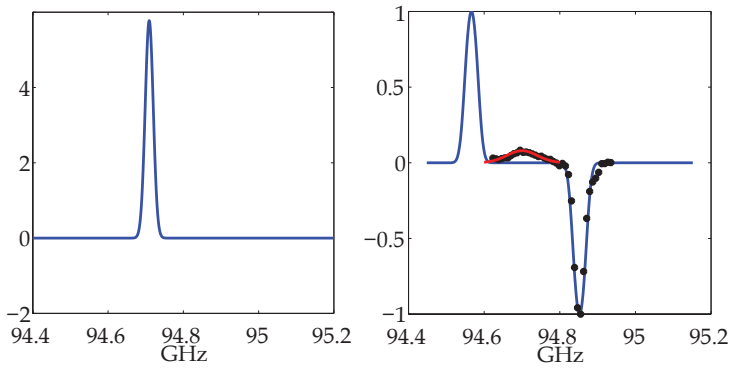

Figure 3.2: (a) Simulated EPR spectrum for BDPA, assuming a g-factor of 2.0026, A hyperfine tensor A = (1, 1.5, 5) MHz and a (homogeneous) linebroadening of 25 MHz. (b) The blue line represents the prediction for Solid Effect DNP, normalized to 1 at the maximum, for an excitation bandwith of 35 MHz, larger than the homogeneous linewidth shown in (a). The solid dots represent the experimental results for the normalized DNP enhancement as function of the microwave frequency. The red line is a superposition of the Solid Effect DNP with an on resonance DNP contribution, assuming a Gaussian contribution for the latter.

proton content (99 % d8-toluene). The blue curve represent a calculation using Equation 3.10 for the polarization of the core protons. In the basic Solid Effect theory, the bulk proton polarization would follow the same curve. The red line is a calculation using Equation 3.11 assuming a diffusion leakage factor $f_d = 3.6$ and a Solid Effect satellite saturation level for the core protons given by $S^{\pm} = 0.19/\mathrm{W}$ in the present setup. If we make the rather crude assumption that the core protons are all located on the BDPA molecule ($N_c = 21$), then for a deuteration level of 99 % the number of toluene protons per BDPA radical equals $N_b \approx 15$ and using the experimental relaxation time $T_{1b} \approx 6.5$ s we can estimate the diffusion rate per bulk proton $W_d/N_b \approx 0.05\ s^{-1}$. Under these conditions, the diffusion rate is indeed slower than the bulk nuclear relaxation rate and the maximum enhancement that can be reached is considerably lower than the prediction from simple Solid Effect theory.

In order to verify this rather crude assumption, we performed additional temperature dependent T_1 relaxation measurements for a sample containing 50 mM BDPA in 99 % deuterated toluene. The results for the saturation recovery at a temperature of 120 K is reproduced in Figure 3.4(a). The solid line is a fit for a two component relaxation with different T_1 values. The relative weight for the two components is chosen at 60 % for the short T_1 fraction and 40 % for the long T_1 fraction. The T_1 fit parameters are reproduced in Figure 3.4(b) and (c), with phenomenological T_1 fits to guide the eye. Although the accuracy in this analysis is limited, it does confirm the presence of two protonated species with substantially

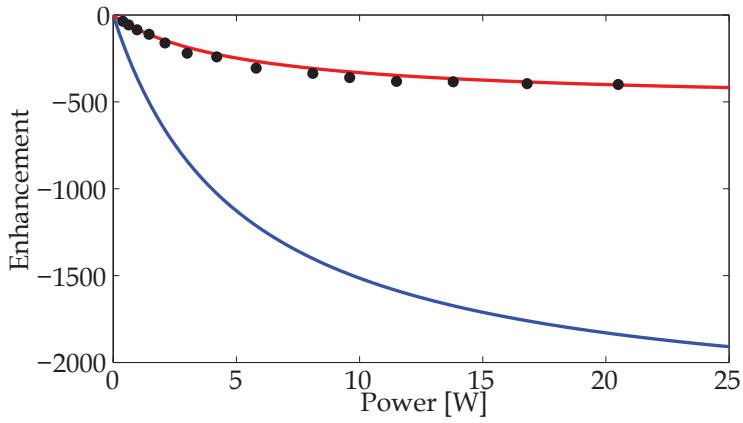

Figure 3.3: Equilibrium DNP enhancement levels (absolute values) for microwave excitation at 94.85 GHz (solid dots) as function of the microwave power for a BDPA concentration of 50 mM and 99 % deuterated toluene. The solid blue line is a prediction for the core proton polarization (including temperature jump factor), which follows the basic Solid Effect theory (Equation 3.9). The red line is the predicted polarization for bulk protons (Equation 3.11) under the assumption that the spin diffusion is the rate limiting process (diffusion leakage factor f_d=3.6).

different T_1 parameters. For the ratio of radical protons versus toluene protons we indeed expect a ratio 0.6 versus 0.4. Thus we identify the fast relaxing protons with the (core) BDPA protons and the slow relaxing fraction is attributed to the (bulk) toluene protons.

In Figure 3.5 we have reproduced the experimental results for the equilibrium DNP enhancement and corresponding build-up time as a function of the microwave pumping rate (solid symbols), for four different levels of protonation in the toluene solvent. From this series it is clear that for an increasing amount of protons in the sample, at constant radical concentration, the build-up time is reduced and becomes less dependent on the microwave power. At the same time, the maximum achievable enhancement is strongly reduced.

The blue solid lines in Figure 3.5 are solutions to the full set of coupled differential equations. These solutions are not free fits, as the number of parameters does not allow for a single solution. All parameters used to generate the solid curves are summarized in Table 3.1. The deuteration level is defined by mixing the appropriate volumes of fully deuterated d8-toluene (99.6 %) with normal fully protonated toluene. The number of core protons is assumed to equal the number of protons in the BDPA molecule. The number of solvent protons (N_b) per unpaired electron spin follows from the molar density of toluene and using the fixed radical concentration of 50 mM for all samples. The relaxation time of the BDPA protons is derived

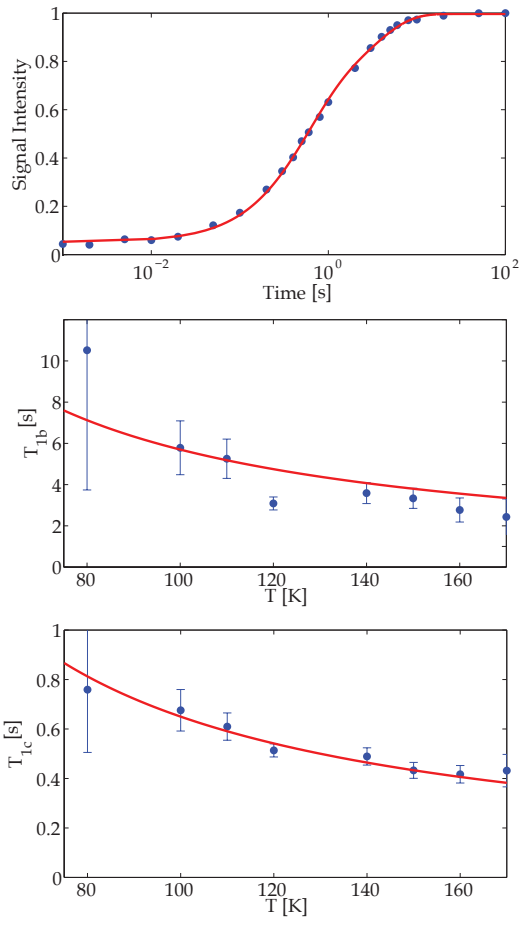

Figure 3.4: (a) Saturation recovery signal for a sample with 50 mM BDPA in 99 % deuterated toluene at a temperature of 120 K (symbols). The solid line is a two component exponential fit with relative weight 0.6 and 0.4 for the short, resp. long T_1 fraction. In panels (b) and (c) the T_1 fit parameters for different sample temperatures are plotted. The solid curves are fits to a T^{-1} power law to guide the eye.

from the T_1 relaxation experiment in Figure 3.4, assuming a sample temperature of approximately 90 K in the presence of high power microwave radiation. The BDPA proton relaxation time T_{1c} is assumed to be independent of the protonation level of the solvent. The value for T_{1b} is adjusted to match the observed DNP build-up times. For the case of 99 % deuteration, this corresponds well with the T_1 measurements assuming an elevated temperature of about 90 K. The diffusion rate from core to bulk protons (W_d), divided by the number of bulk protons (N_b) in the solvent, is assumed to be independent of the protonation level, except for the highest protonation level of 50 %. Finally, the excitation rate per unit of applied microwave power is

adjusted as losses and microwave mode structure may vary from experiment to experiment. The important parameter that determines the saturation (steady-state) enhancement levels is the diffusion rate. We find very good agreement for the full set of data with a diffusion rate per bulk proton that equals approximately 0.05 s^{-1}, except for the highest proton concentration. Most important is the observation that higher proton concentrations, with a simultaneous reduction in T_{1b}, leads to strong reduction in saturation (steady-state) enhancement combined with a simultaneous reduction of the power-dependent decrease in the DNP build-up time. Note that the bulk polarization does not follow a strict mono-exponential behavior, in particular at low microwave power, where the different time constants are comparable in size. Also, the variation in sample temperature for the different microwave powers may affect the details in the build-up rate constants. For both experiment and in the analysis of the numerical results of the coupled differential equations we have used a mono exponential fit which may lead to errors in the low power region of the τ_{dnp} curves.

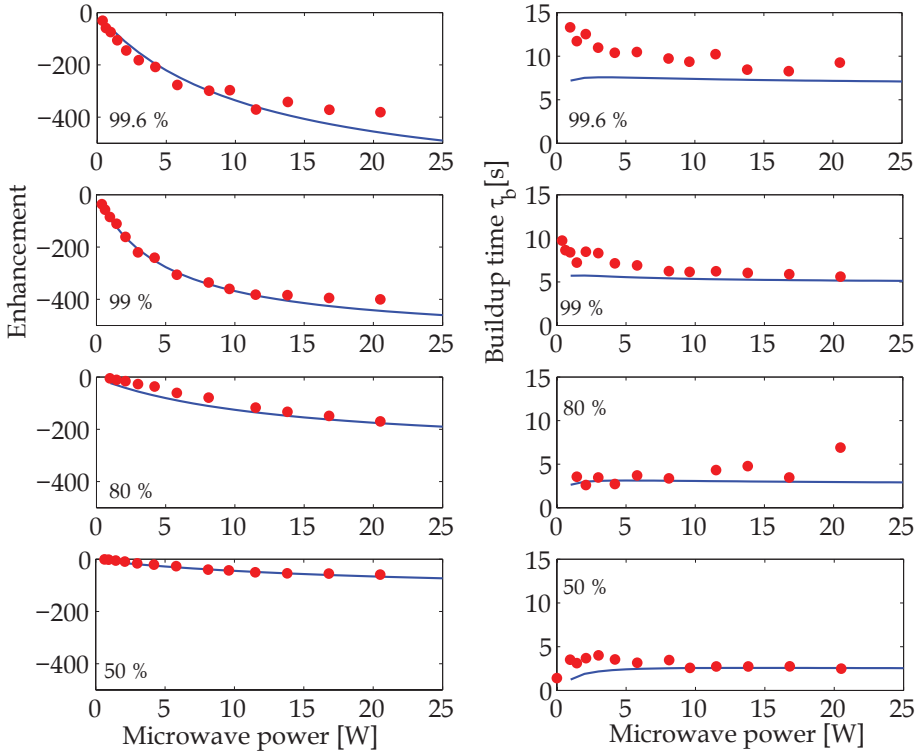

Figure 3.5: Experimental saturation DNP enhancement and build-up time constants (solid dots) as function of the applied microwave power for different deuteration levels of a toluene/d8-toluene mixture. The lines are theoretical predictions from the model as described in the text.

Table 3.1: Parameters used in the calculations shown in Figure 3.5. D represents the deuteration level of the toluene solvent, α is the core proton saturation per Watt microwave power as defined in the text. N_c and N_b are respectively the number of core and bulk protons for each radical molecule. The last column represents the diffusion rate W_d from core to bulk, divided by the number of bulk protons per radical in each sample.

D [%]	$1/\alpha$ [W s]	N_c	N_b	T_{1c} [s]	T_{1b} [s]	W_d/N_b [s^{-1}]
99.6	0.38	21	6	0.7	10	0.05
99	0.17	21	15	0.7	6.5	0.05
80	0.33	21	303	0.7	3.0	0.05
50	0.47	21	756	0.7	2.5	0.025

In summary, we observe good quantitative agreement of the measured DNP enhancement and the associated build-up time constant with the simplified model presented in the theory section. In this analysis the only free parameter is the spin diffusion rate. The main implication then is that the Solid Effect DNP for BDPA in a toluene matrix is in essence a two step process, where the initial 'forbidden' transition occurs for local proton spin states at the BDPA molecule. These protons are strongly coupled to the electron spin by hyperfine couplings which actually makes these transitions weakly allowed. This situation is in agreement with the results obtained by the Griffin group [21], where they studied the effect of BDPA deuteration on the efficiency for MAS-DNP both in the case of Solid Effect and 'Solid Overhauser Effect' mechanisms. For both mechanisms, they found a crucial role played by the BDPA protons. The practical level of hyperpolarization that can be obtained for the BDPA-toluene system is limited by the spin diffusion from BDPA protons to the frozen solvent. In the regime of low protonation, the normalized diffusion W_d/N_b is found to be constant. As the present setup with high power microwaves allows for a nearly complete Solid Effect saturation of the BDPA nuclear polarization, this insight may provide a useful road towards further optimization. For example it would be tempting to increase the number of protons in the BDPA structure by adding various protonated molecular side chains to the radical.

3.6 Rapid-melt Solid Effect DNP for H_2O/D_2O-TEMPOL

As a second class of experiments, we recorded the polarization buildup in an aqueous solvent with TEMPOL radicals in the solid state. Because of the anistropic g-factor of this radical, the Solid Effect DNP is reduced, as only a limited fraction of radicals has the proper orientation to satisfy the solid effect matching conditions. This fraction will depend on the chosen microwave frequency offset and on the effective excitation bandwidth. For water-glycerol mixtures the melting transition

is rather slow and the high viscosity of the low temperature liquid phase leads to fast relaxation. Reliable quantitative estimates of the polarization level can only be obtained in the solid phase. To monitor the polarization, the sample was shuttled directly onto the NMR chip, and the corresponding wide line spectrum was measured with minimal delay after the shuttle step. As we observe a substantial broad background signal from the probe, this background was subtracted from the time domain signal. The enhancement was determined by normalization to the integrated intensity in the liquid state at room temperature. The test sample was obtained by doping a H_2O/D_2O, d8-glycerol mixture (25 vol % D_2O, 25 vol % H_2O and 50 vol % d8-glycerol) with 30 mM TEMPOL. First, the Boltzmann buildup was recorded for the sample by varying the time spent in the cold DNP resonator but with the microwaves switched off. The resulting thermal buildup curve indeed confirms a base temperature close to that of liquid nitrogen (77 K), with a typical time constant of about 3 s. The experimental results for the (normalized) frequency dependent enhancement is reproduced by solid dots in Figure 3.6(b), compared with the predicted enhancement as shown by the solid blue line. For frequencies near the EPR central transition we observe an enhancement that is more positive than predicted by solid effect theory. An additional Cross Effect and/or Overhauser effect contribution, modeled by a Gaussian on resonance curve is represented by the green curve and the total enhancement in red. Note that at frequencies below 94.8 GHz, the EIK amplifier output diminishes rapidly and a comparison of the low frequency positive enhancement is not possible. Although the model calculation reproduce the experimental results quite well, it should be noted that the results are not very sensitive to the exact choice of the excitation bandwidth. In Figure 3.7 the experimental enhancement data for this aqueous test sample is reproduced by the solid dots for microwave irradiation near the negative peak at 94.99 GHz. The build-up times that were measured simultaneously, gradually decrease from 2.8 to 2.4 s. For the present preliminary analysis we will focus on the enhancement data. The solid line is a calculation using Equation 3.11 for a leakage factor f_d=3.1 and again using a Boltzmann temperature jump factor of 293/90. The microwave conversion factor α was adjusted to fit the experimental data. Note that in comparison to the BDPA experiments, the saturation of the core protons can be achieved at a lower microwave power, indicating a stronger hyperfine coupling for the case of TEMPOL-water system. The diffusion leakage term for this fit is similar to that of the previous BDPA example for a 99 % deuteration level of the toluene solvent. In the aqueous sample, the bulk proton density per 'active' TEMPOL radical is much higher and the relaxation time T_{1b} is lower. This indicates that the diffusion rate W_d for TEMPOL must be much higher than for BDPA. This makes sense if the core region for TEMPOL is larger and includes water protons from the solvent. As the pro-

ton relaxation during the melting phase is quite fast, it is presently not possible to analyze the DNP dynamics in more detail. It is therefore not possible to determine reliable estimates for the actual size of the core region and its related diffusion rate from core to bulk protons. Also, the glassy nature of the aqueous sample appears to add some additional slow dynamics during the cooling process that is the subject of ongoing further research.

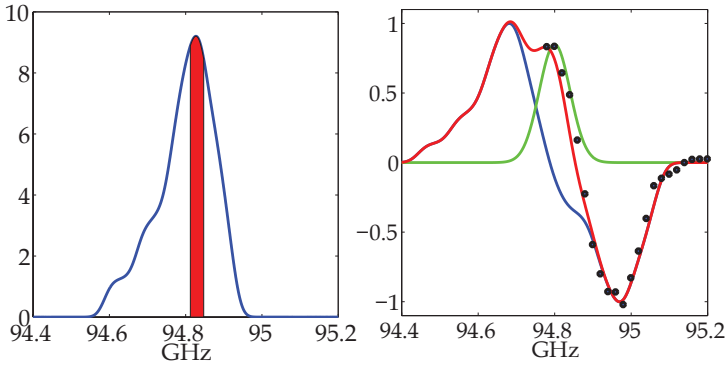

Figure 3.6: (a) Simulated EPR spectrum for TEMPOL, assuming a g-tensor of (2.008, 2.006,2.003), A hyperfine tensor A = (20,20,85) MHz and a (homogeneous) linebroadening of 40 MHz. The area, highlighted in red, corresponds with a fraction of the TEMPOL radicals that are in resonance within a bandwidth of 35 MHz near the maximum in the EPR spectrum. (b) The blue line represents the prediction for Solid Effect DNP, normalized to 1 at the maximum, for an excitation bandwith of 35 MHz as shown in (a). The solid dots represent the experimental results for the normalized DNP enhancement as function of the microwave frequency. The red line is a superposition of the Solid Effect DNP and Cross Effect DNP, assuming a gaussian contribution (green) for the latter.

3.7 Conclusions and future prospect

We have used the rapid-melt DNP method to study the dominant polarization pathways under rapid-melt DNP conditions. We have demonstrated the feasibility of using four different mechanisms as a way to achieve polarization enhancement in the present setup: solid and liquid-state Overhauser, Cross effect and Solid effect. None of these pathways were fully optimized in terms of radical design and substantial improvements could still be made. The observation of liquid-state Overhauser DNP shows that with low viscosity solvents with low dielectric loss factors, substantial enhancements are possible even with sub-optimal radicals. Although high Q resonators are still needed to obtain full saturation. Detailed measurements of the solid effect DNP enhancement using BDPA radicals and its related time constants have indicated the importance of spin diffusion in a polarization pathway via the

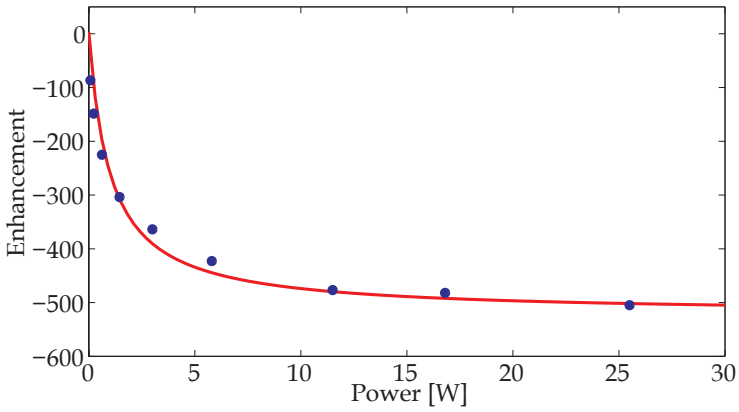

Figure 3.7: Equilibrium DNP enhancement levels of 25 vol % D_2O, 25 vol % H_2O and 50 vol % d8-glycerol for microwave excitation at 94.99 GHz, including a thermal jump Boltzmann contribution (solid dots). The solid red line is a theoretical prediction from theory for inhomogeneous Solid Effect DNP (including temperature jump), with an excitation bandwidth as in Figure 3.6 and a diffusion leakage factor $f_d = 3.1$. The horizontal scale was adjusted to match the experimental power levels.

BDPA protons. A set of rate equations is introduced to describe the DNP dynamics in both the core and bulk regions of the sample. This analysis can help in identifying the rate limiting steps and can guide the way for further optimized radical design. The solid effect DNP for TEMPOL radicals in an aqueous mixture shows that in this case, spin diffusion forms a less severe restriction. Full saturation of the core-protons becomes possible, even in the absence of high Q resonant structures. In this case, the enhancement levels are partially limited by the in-homogeneously broadened EPR spectrum where only a small fraction of radicals is in the relevant excitation bandwidth. Both BDPA and TEMPOL radicals are thus not ideal in their DNP performance and further optimizations can be made by tailoring the molecular structure or local environment. Nevertheless, the present enhancement levels of 100-500, relative to the liquid state thermal intensity at room temperature, are sufficiently high to provide a substantial reduction in measurement time. Alternatively, it may help to lower the sensitivity boundaries of NMR for mass limited samples and thus extend the field of applications in for example online hyphenated NMR analysis. Further improvements of radical design may help to increase the enhancement to approach the theoretical maximum of about 2500 for protons that are polarized by the Solid Effect at 77 K. BDPA is presently the preferred radical as it shows low relaxation rates in the liquid state and in the rapid-melt setup, the low temperature polarization is preserved for in situ liquid state NMR detection.

Chapter 4

Applications, radicals and solvents for rapid-melt DNP

Abstract

Recently we demonstrated a novel experimental technique to obtain hyperpolarized signals in the liquid state performing NMR and solid-state DNP in the same spectrometer, called rapid-melt DNP. We further investigated the DNP mechanisms involved in the rapid-melt DNP setup. Here we explore the generic nature of the setup to hyperpolarize different molecular species. The experiments were performed with various solvents and solvent mixtures containing different types of solute molecules. The T_1 in the liquid state, DNP enhancement, DNP build-up time and time required for sample melting in rapid-melt DNP were measured for various radicals, solvents and solvent mixtures. For the present setup radicals with shielded electron spin (BDPA) are found to be best suited to acquire DNP enhanced spectra in the liquid state. Solvents with lower latent heat of melting and lower specific heat are preferred to minimize the relaxation losses during the melting transition. The NMR signals of all the molecules examined in this study have been successfully hyperpolarized.

4.1 Introduction

NMR is a quantitative and non-invasive technique and it can provide information about molecular structure and dynamics that makes it an excellent analytical tool. However the sensitivity of NMR is rather low because of the low polarization of spins at room temperature. DNP was introduced in the 1950's as a solution to the low sensitivity of NMR [12, 13, 14] by transferring the high polarization of electrons to nuclei. Although DNP was introduced in the last century, technological development of DNP methods have only come to bloom in the last decade. The main DNP methods employed today are dissolution DNP [54], MAS-DNP [90] and Overhauser DNP [50]. Details of these methods can be found elsewhere [91, 92]. Dissolution DNP is used for metabolic imaging, biomolecular NMR [63, 64] and biological assays [65, 66] while MAS-DNP has found its applications in surface chemistry, protein structure determination and polymer studies [41, 40]. Dissolution DNP is limited to slow relaxing nuclei and only a few number of scans are possible within the T_1 of the nuclei of interest [70]. Usually, hyperpolarized proton signals are not measured in the liquid state through dissolution DNP because the fast relaxation of proton spins results in nearly complete loss of the hyperpolarized signal. Although MAS-DNP is not limited to the slow relaxing nuclei, the spectrum is acquired in the solid state which may lead to a low resolution due to dipolar broadening and structural/conformational disorder. Generally, Overhauser DNP provides low enhancements at higher magnetic field or for bigger molecules due to the dependence on the correlation time of the electron-nuclear spin interaction. However, it can be used to study dynamics [93].

In the previous Chapters we introduced a novel method to hyperpolarize nuclear spins in the solid state and measure the spectrum in the liquid state [83]. As a preliminary example proton spins of methyl pyruvate were hyperpolarized in a solution of d8-toluene doped with BDPA free radicals [83]. Here we explore the general applicability of the rapid-melt DNP method to hyperpolarize different types of molecular species. Different solvents were used to dissolve different type of molecules. We have examined both apolar and polar solvents for the rapid-melt DNP.

In this Chapter, we first discuss the desired properties of solvents and radicals for rapid-melt DNP. Afterwards the results of DNP of apolar molecules and solvents are given. In the next section the results of DNP of polar molecules are presented. In the conclusions section we review the results and discuss the future possibilities.

4.2 Solvents and radicals for rapid-melt DNP

4.2.1 Solvent for rapid-melt DNP

The general concept of rapid-melt DNP is to perform DNP in the solid state and signal acquisition in the liquid state. The sample is rapidly melted from solid to liquid. The melting transition is required to be completed in short time w.r.t longitudinal relaxation (T_1) to observe hyperpolarized signals in the liquid state. Usually, the T_1 is much shorter in the vicinity of the melting point for a solution due to higher viscosity at lower temperatures. Figures 3.4 and 4.1 show that the T_1 of toluene protons of a sample doped with 50 mM BDPA is indeed shortest near the melting point of toluene at 178 K. The duration of the complete melting transition from a frozen solid to an ambient temperature liquid for a sample is governed by the latent heat of melting, specific heat and the melting point. Various physical properties of common NMR solvents are given in the Table 4.1. All of these solvents have low specific heat and low latent heat of melting, so they are expected to complete melting transition in a short time. Toluene, chloroform and DMSO have been tested for the melting transition and subsequent measurement of hyperpolarized NMR signals in the liquid state. Hyperpolarized NMR signals with all the solvents have been observed in the liquid state.

The energy (Q) required to change the temperature by (ΔT) of a given mass (m) of a substance having specific heat (C) can be calculated from $Q = C \cdot m \cdot (\Delta T)$. The sample capillary has an inner and outer diameter of 150 μm and 360 μm respectively, while the length of the heating block is 5 mm. The energy required to change the temperature of a sample of the solvents with the properties given in Table 4.1 from 77 K to 350 K including melting is ∼30 mJ and ∼40 mJ for toluene and DMSO respectively. Although the NMR measurement is performed at room temperature, the heating block is kept at higher temperature to melt the sample quickly. Heating block temperature for acetone and chloroform was kept at 315 K and 325 K respectively due to their lower boiling points, the energy required to melt and heat up the sample is ∼35 mJ for both of these solvents. The time required to heat up the sample can be estimated as $t = \frac{Q \cdot d}{K \cdot A \cdot \delta T}$, where t is the time, Q is the energy required to heat/melt the sample, d is the thickness of the capillary wall, K is the thermal conductivity of the capillary material, A is the area available for heat transfer, δT is the temperature difference across the capillary wall. The thermal conductivity of fused quartz is 1.4 W/(K m) at room temperature, the time required to melt the sample will be ∼10 ms for toluene and acetone, ∼20 ms for chloroform, and ∼60 ms for DMSO in the current configuration. The time required to heat up

the sample from the melting point to the desired final temperature will be ∼30 ms for toluene, chloroform and acetone and ∼ 50 ms for DMSO. The relaxation losses during the heating of the sample till the melting point can be neglected as the time required to heat up the sample till its melting point is negligible compared to the T_1 in frozen state. The highest losses occur during the melting transition where the T_1 is shortest. The measured T_1 for d8-toluene doped with 50 mM BDPA was ∼80 ms for both the methyl and aromatic protons at 180 K (Figure 4.1), so the expected relaxation losses are ∼10 % for both the functional groups during the 10 ms of melting time. The delay before the acquisition and time to heat the sample is 60-70 ms in total. The T_1 is around 600 ms at these temperatures, this results in additional decay of about 10 % of the hyperpolarized signal.

One other requirement for efficient DNP is glass formation of the sample upon freezing for homogenous distribution of radical spins in the sample. Usually, a glass forming agent is added to the sample to facilitate glass formation. If a solution does not form a glass upon freezing the build-up time becomes longer due to inhomogeneous distribution of radicals in the sample. In this case, the build-up time is dominated by the spin diffusion of hyperpolarization from the nuclei close to the radical spin to the nuclei far from the radical spin. It is advantageous to have a solvent like toluene which forms a glass by itself upon freezing to avoid alteration of the sample properties like viscosity by addition of glass forming agent. For example glycerol is a common glassing agent for water samples. As glycerol is highly viscous the overall viscosity of the final solution is also much higher. The higher viscosity of the solution results in relatively short T_1 of water protons. In this case DNP enhanced signals of water protons decay completely during melting transition in rapid-melt DNP.

Table 4.1: Parameters for different solvents.

Solvent	Specific heat (kJ/(kg K)) at room temperature	Specific heat (kJ/(kg K)) at 100 K	Latent heat of melting (kJ/(kg K))	Melting point (K)	Forms glass
Toluene	1.72	0.68	72	178	Yes
Chloroform	1.05	-	77	210	No
Acetone	2.15	1.13	98	179	No
DMSO	1.96	0.70	172	292	Yes

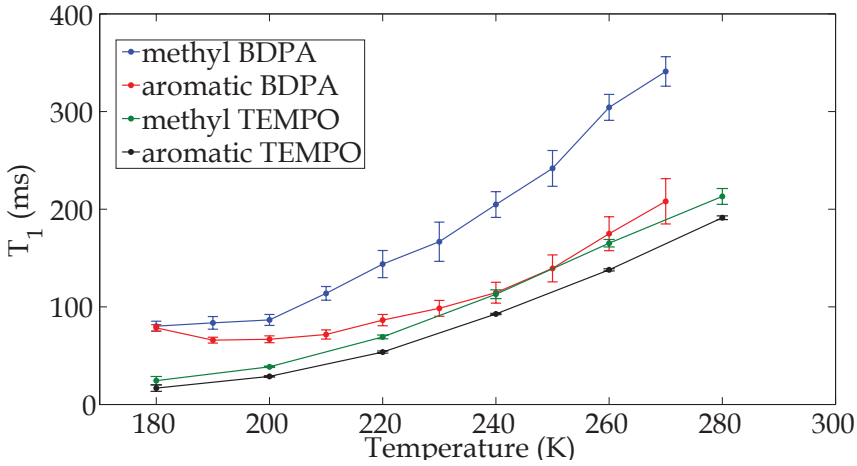

Figure 4.1: T_1 of methyl and aromatic protons of toluene vs temperature for toluene doped with BDPA and TEMPO free radicals doped at 50 mM concentration.

4.2.2 Radicals for rapid-melt DNP

The source of polarization in DNP is the free radical spin. Although, radical spins are the source of polarization in DNP, they also induce fast paramagnetic relaxation of the target molecules. This fast paramagnetic relaxation can annihilate the hyperpolarization during the melting transition. Free radicals having less exposed electron spin induce slower paramagnetic relaxation. 1,3-bisdiphenylene-2-phenyl allyl (BDPA) has a free electron spin which is delocalized on the aromatic rings. The free electron spin is less exposed due to bulky aromatic rings. As the electron spin is less exposed, the induced paramagnetic relaxation of target molecules is limited while the polarization can be transferred from the BDPA protons via spin diffusion to the solvent protons. On the other hand (2,2,6,6-Tetramethylpiperidin-1-yl)oxyl (TEMPO) has exposed electron spin which induces very fast paramagnetic relaxation in liquids. The T_1 of toluene doped with 50 mM TEMPO at the melting point was measured to be ∼20 ms for both the methyl and aromatic protons of toluene, which is indeed much shorter than the T_1 in the presence of BDPA. For the melting duration of 10 ms the relaxation loss will be 40 %, which is 4 times higher than losses for BDPA doped samples at the same concentration of the radical spins. The room temperature T_1 for TEMPO based samples was 200 ms, so the relaxation losses during heating the sample and stabilization delay before starting the acquisition are additionally 25 %, compared to only 10 % for BDPA based samples. Figure 4.2 shows reference and DNP enhanced spectra of toluene doped with 50 mM BDPA (in red) and 50 mM TEMPO (in blue). The spectra were measured for similar experimental conditions and at optimal frequency for respective radi-

cals. (94.850 GHz for BDPA and 95 GHz for TEMPO). In Figure 4.2, the enhancement factor for TEMPO based spectrum is much lower than BDPA. Enhancement factors are found to be up to 3 times smaller for TEMPO based samples w.r.t. BDPA based samples for similar experimental conditions. Enhancement in the solid state could not be measured for toluene based samples as toluene starts to melt even without stopping the frozen sample in the warm gas flow region. Different enhancement factors have been observed for aromatic and methyl protons of toluene doped with 50 mM TEMPO. The reason for different enhancement of different groups of toluene is not clear.

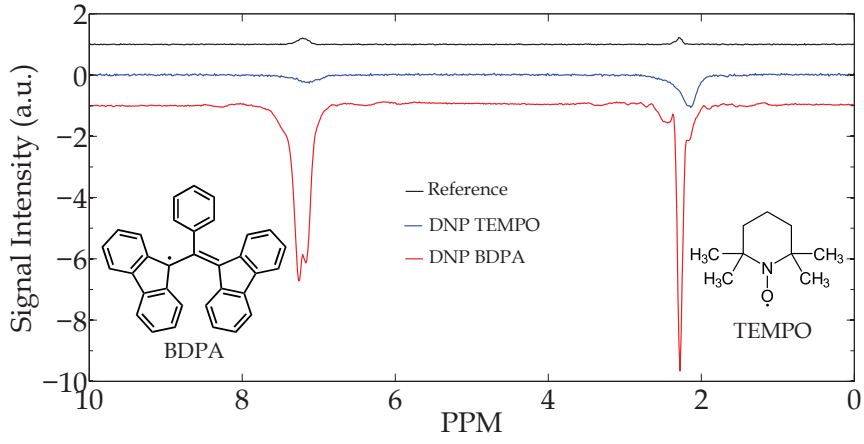

Figure 4.2: The comparison of reference and DNP enhanced spectrum of toluene for BDPA and TEMPO radicals. The DNP enhanced spectra were acquired for the same duration and power level for microwaves. The microwave frequency was 94.850 GHz and 95 GHz for BDPA and TEMPO respectively. The spectra are displaced vertically for clarity.

The DNP mechanisms can be fully exploited with the use of radicals with specific properties, e.g. special bi-radicals are synthesized for optimal Cross Effect in MAS-DNP [94, 95]. The Solid Effect is most efficient in case the line width of the radical spin is smaller than the Larmor frequency of the nucleus. We have used commercially available BDPA and TEMPOL radicals for the current setup. Although BDPA has a narrow homogenous EPR line width resulting in efficient solid effect, it is highly non-polar hence a limited solubility in polar solvents. TEMPOL (water soluble derivative of TEMPO) on the other hand has a broad inhomogeneous EPR line width. Despite this broad line width enhancements of up to 500 are observed in the solid state [83]. A frequency modulated microwave irradiation (integrated solid effect) for TEMPOL can further improve the enhancement [96, 97]. An ideal radical for rapid-melt DNP should have a narrow EPR line width compared to the nuclear Larmor frequency and high solubility in polar solvents. Section 4.4.2 summarizes the details of water soluble BDPA derivatives synthesized for rapid-melt DNP.

4.3 Apolar solvents

Toluene is a widely used solvent in various fields including NMR [98] and has already been used to demonstrate the proof of principle and to probe the solid effect in the rapid-melt DNP setup [99]. To test the potential of rapid-melt DNP to hyperpolarize different types of molecules, apolar molecules were dissolved in toluene doped with BDPA. We have examined different types of molecular species like flavor molecules (hexanal), lipids (stearic acid), and steroid hormone (testosterone) in toluene. All the molecules were successfully hyperpolarized. The enhanced spectra of hexanal, stearic acid and testosterone are shown in Figure 4.3. The peaks can be assigned to the corresponding nuclei even with the limited resolution of the current setup. Testosterone has many resonances between 0 to 2 PPM and they can't be resolved. The spectra in Figure 4.3 are not to scale and just represent the enhanced signals of solvent and solute molecules. The enhancements and the build-up times for solvents and solutes are summarized in Table 4.2. The build-up times for both the solvent and solute molecules are found to be comparable and are usually less than 5 seconds, within the confidence level of the fit. The enhancement given in Table 4.2 includes the DNP enhancement as well as the enhancement due to the temperature jump. Usually the melting transition is completed in less than 50 ms for toluene. An additional 50-100 ms delay is employed after the sample has been shuttled to the NMR detector for stabilization. The stearic acid sample is found to be peculiar. Stearic acid signals are only observed after 350 ms of melting delay and an additional 50 ms delay before NMR acquisition. However the signals from toluene protons were observed with the usual 50 ms delay for melting. This peculiar behavior of stearic acid may arise due to its well known surfactant nature [100]. Stearic acid may form aggregates while freezing, which only dissociate later after melting.

Although the build-up times and enhancement factors for toluene based samples are apt for hyperpolarization experiments, it is not the ideal solvent for analysis. Toluene has proton resonances in both the aromatic and methyl region of NMR spectrum. The residual signals from toluene, even at 99 % deuteration crowd, the spectrum which is a disadvantage particularly in the limited resolution of the current setup.

Chloroform is also a common solvent which is used extensively in NMR [98]. Chloroform has only one proton resonance in the aromatic region of the NMR spectrum at 7.2 PPM. The latent heat of melting and the specific heat of chloroform are similar to toluene (see Table 4.1). The boiling point of chloroform is only 334 K, while

Table 4.2: Build-up times and enhancements for different solute and solvent (toluene) molecules. All samples contained 50 mM BDPA. Enhancement and build-up time of toluene could not be measured for the sample with water and Triton X-100 because the toluene signals were masked under Triton X-100 signals.
*Target concentration was 50 mM, but the actual concentration was unknown due to precipitation.
#D_2O (99 % deuterated) was added to solution of d8-toluene and Triton X-100. toluene:triton:water 9:3:1 vol.

Solute and concentration	Solvent	$\tau_{solvent}$ (Sec)	τ_{solute} (Sec)	$\epsilon_{solvent}$	ϵ_{solute}
Hexanal 20 mM	d8-toluene	5.4±1.1	6.5±1.8	-181	-110
Stearic acid 100mM	d8-toluene	9.3±1.3	17.8±6.1	-181	-77
Testosterone 50mM	d8-toluene	4.1±2.2	5.6±2.6	-237	-182
Thymol 100 mM	d-chloroform	6.2±2.6	6.4±3	-109	-32
l-Ascorbic acid*	d8-toluene d4-methanol	5±0.8	4.4±2.7	-249	-77
l-Lysine*	d8-toluene d6-DMSO (9/1 vol)	3.7±1.2	3.4±1	-165	-170
Pyruvic acid 50 mM	d8-toluene d4-methanol	6.7±1	12.8±4.7	-192	-110
Water#	d8-toluene Triton X-100(3/1 vol)	-	4.1± 1.2	-	-116

the temperature of the warm gas used for toluene based samples is 350 K. To avoid boiling of chloroform, the temperature of the gas used for melting was decreased. The lower temperature of the gas used for melting resulted in longer melting time, 100 ms of delay was employed for melting. The free radical used for chloroform was BDPA. The employed concentration of BDPA was 40 mM, as dissolving higher concentration requires extra time. Chloroform does not form a glass upon freezing. However, the build-up time for chloroform is found to be ∼12 seconds. This implies that chloroform freezes into nano sized crystals. The intensity of the residual signals of deuterated chloroform vs microwave irradiation time and the corresponding exponential fit is shown in Figure 4.4. As a test molecule 100 mM thymol was dissolved in deuterated chloroform doped with 40 mM BDPA. Thymol is used for it's strong antiseptic properties. The DNP enhanced spectrum of thymol can be seen in Figure 4.3. The small peak at 0 PPM is from TMS which was present in chloroform at 0.05 vol. %. TMS is a standard reference compound for chemical shift, which is usually present in commercial NMR solvents. The TMS signal has been observed in the DNP enhanced spectrum in single scan making it possible to reference the spectrum. The enhancement and build-up time for thymol and chloroform can be found in Table 4.2.

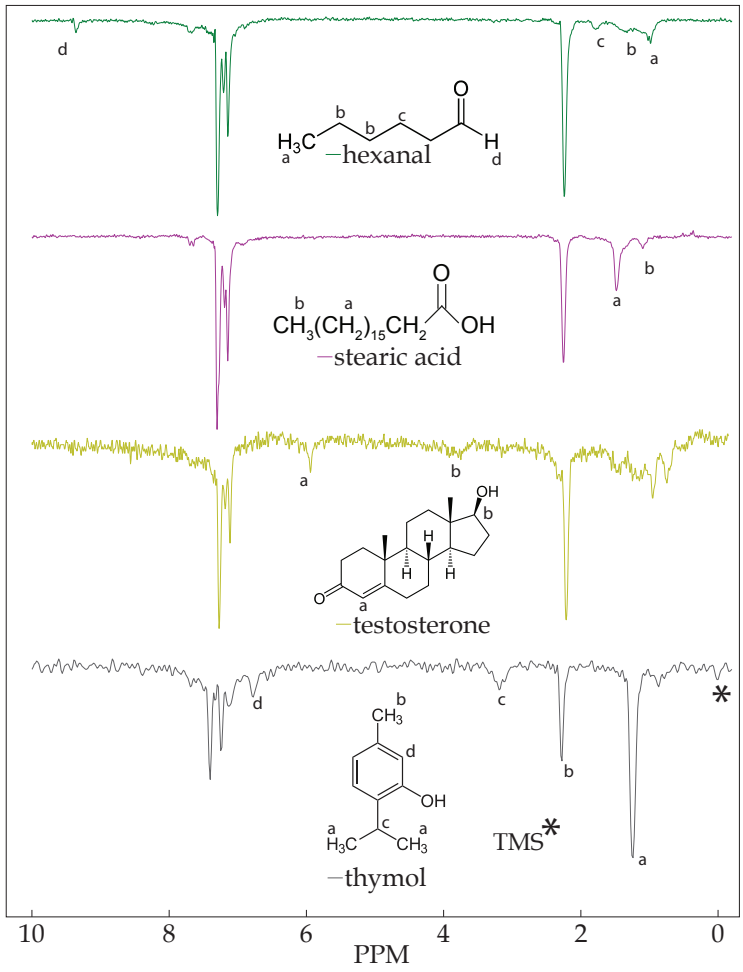

Figure 4.3: The DNP enhanced spectra of various apolar molecules dissolved in toluene (top three) or chloroform (bottom) with BDPA. The spectra are not to scale. All spectra are single scan with 10 seconds of microwave irradiation at 25.5 Watts of power. The noise level in the testosterone spectrum is higher as a small flip angle (10°) was used to acquire the spectrum. In the testosterone spectrum, the signals around 1 PPM region are from various protons of testosterone. The small signal around 0.8 PPM in the thymol spectrum is from some unknown impurity. The letters a,b,c,d are used to indicate the peak positions of the corresponding nuclei.

4.4 Polar Solvents

Water has already been examined for hyperpolarization in the rapid-melt DNP setup (Chapter 2). Enhancement factors of up to 500 relative to the room temperature reference have been observed in the solid state for water-glycerol mixtures doped with

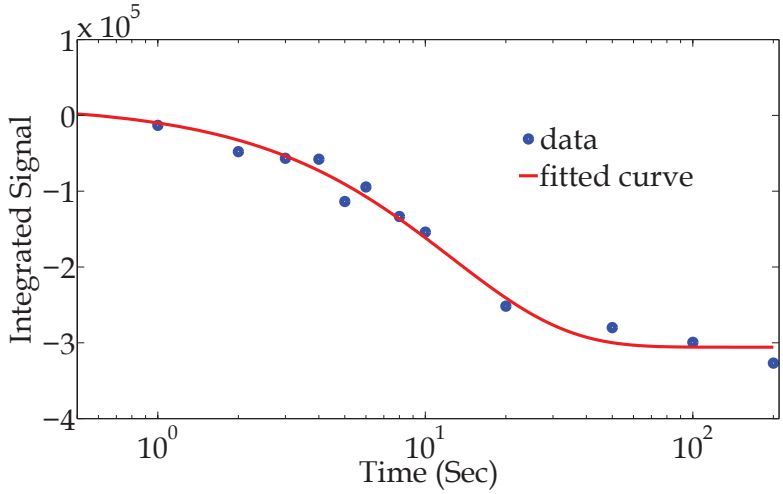

Figure 4.4: The intensity of hyperpolarized signal of d-chloroform (99.8 % D) doped with 40 mM BDPA versus microwave irradiation time. The microwaves are applied with 25.5 Watts power. The build-up time was found to be ∼12 seconds for the above fit.

4-hydroxy-TEMPO. The relaxation losses during the melting transition limit the hyperpolarized signals to be observed in the solid state only, due to the slow melting transition of water combined with fast paramagnetic relaxation induced by TEMPOL radicals. As already discussed in 4.2.2 BDPA is a favorable molecule for rapid-melt DNP, but it is not readily dissolved in polar solvents.

Polar molecules were dissolved in toluene by tuning the polarity through addition of a suitable co-solvent. DMSO and methanol were used as co-solvents. Different types of molecular species like vitamin (l-ascorbic acid), amino acid (l-lysine), small metabolite (pyruvic acid) and dicarboxylic acids (succinic acid and furamic acid) were examined for hyperpolarization after dissolving in toluene with a suitable co-solvent.

The DNP enhanced spectra for these polar molecules are shown in Figure 4.5. The peaks for various protons can be assigned in the limited resolution of the current setup with solvent, co-solvent and solute molecule peaks. Succinic acid and fumaric acid have their peaks right on top of aromatic and methyl protons of toluene respectively, so their spectra are not included here. The build-up times and enhancements for the different molecules is given in Table 4.2. The build-up times for all the molecules were found to be less than 10 seconds. The enhancement of solute molecules are moderate but peaks of different proton resonances can be clearly seen in the spectrum.

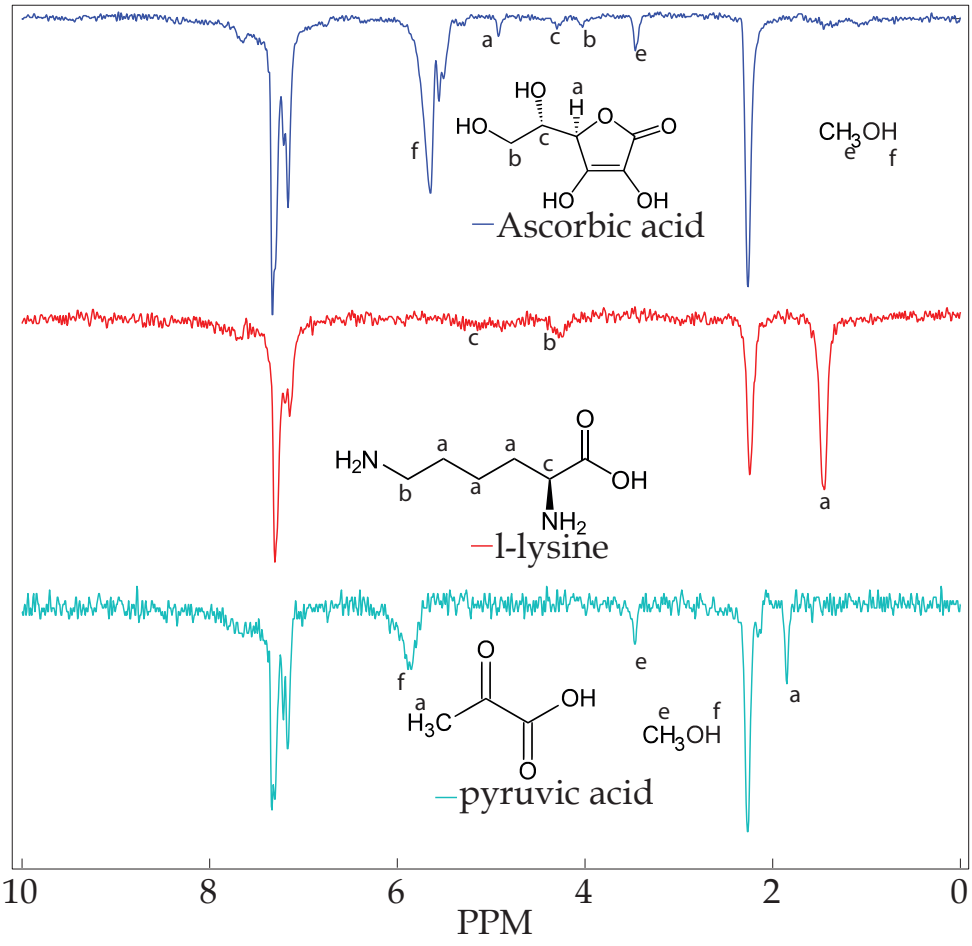

Figure 4.5: The DNP enhanced spectra of various polar molecules dissolved in d8-toluene with addition of a co-solvent. The spectra are not to scale. All the above spectra are single scan with 10 seconds of microwave irradiation at 25.5 Watts of power.

The room temperature reference spectrum for 50 mM pyruvic acid dissolved in d8-toluene and d4-methanol (11 mM) shows that pyruvic acid peaks cannot be observed even after 1024 scans Figure 4.6(1). The reference spectrum is normalized to the same noise level as the hyperpolarized spectrum. The reason for the poor signal-to-noise ratio in Figure 4.6(1) is that both the spectra were recorded with a tip angle much smaller than 90°.

DMSO is a common aprotic polar solvent. A solution of sulfolane in DMSO (1:1 volume) can be used to dissolve BDPA. The DNP enhanced spectrum of 20 mM BDPA doped in the solution is shown in Figure 4.6(2). The small peak around 3.9

PPM in the DNP spectrum is assumed to be of water present in DMSO. The DNP build-up time for the sample is 6.4±3.4 second, while the enhancement is around 11. The observed enhancement is moderate because of the lower concentration (20 mM) of BDPA and relaxation losses during melting. T_1 for the sample was ∼400 ms, while a delay of 100 ms was used for melting transition. Although a lower enhancement factor has been observed for the DMSO-sulfolane mixture, the build-up time is reasonably short. This solution can be used for hyperpolarization of molecules combined with signal averaging which has already been demonstrated for the rapid-melt DNP in Chapter 2.

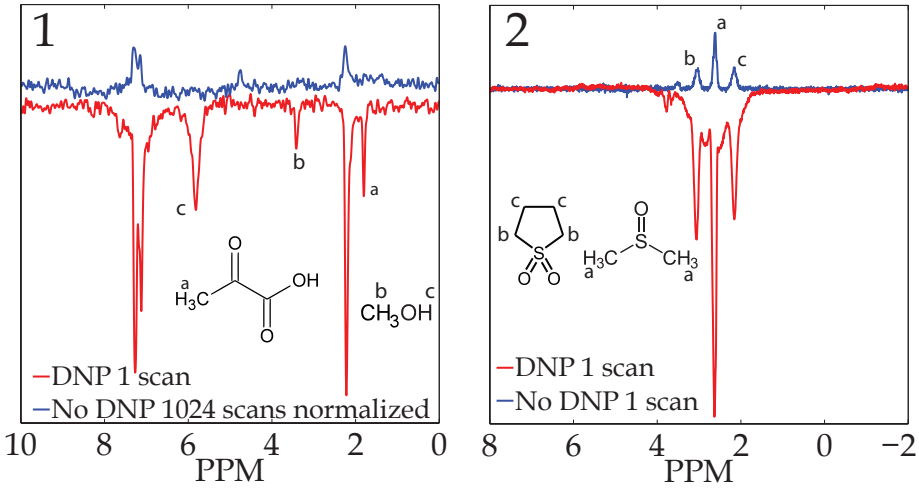

Figure 4.6: 1)The spectrum of 50 mM pyruvic acid dissolved in d8-toluene with 50 mM BDPA and 11 mM MeOD acquired at a tip angle of 10°. The non-DNP spectrum is normalized to the same noise level. The residual protons of hydroxy group of methanol show a broad temperature dependent peak. The peak in the DNP enhanced spectrum at 1.8 ppm is of pyruvic acid. 2)The room temperature and DNP enhanced spectrum of DMSO-sulfolane doped with 20 mM BDPA.

4.4.1 Water polarization in Rapid-melt DNP

To obtain water polarization in the liquid state with rapid-melt DNP, water was dissolved in d8-toluene doped with 50 mM BDPA by adding a surfactant: Triton X-100 (triton). The groups of Griffin and Emsley have previously demonstrated polarization in an aqueous medium for MAS-DNP setup by dissolving hydrophobic radicals using surfactants [101, 102]. In their approach the radicals were encapsulated in the micelles formed by surfactants. The reported concentrations of bi-radicals dissolved in the solutions is ∼10 mM. In our approach rather than dissolving the radical in water we have dissolved water in a radical containing solution of toluene

and surfactant. Water is expected to be encapsulated in reverse micelles formed by the surfactant in toluene. Sample heating was not required during sample preparation. The final solution consisted of d8-toluene (99 % deuterated), triton and D_2O (99.9 % deuterated) in the ratio 9:3:1. A higher radical concentration of 50 mM was obtained in the final solution compared to ∼10mM reported in [101, 102]. As a test molecule l-malic acid was dissolved in D_2O, this D_2O solution was later dissolved in a solution of toluene and triton. Figure 4.7 shows DNP enhanced spectrum of the solution. All the dissolved molecules were polarized by DNP. A DNP enhanced water signal from this sample was observed after a prolonged melting time (∼200 ms) because of the slow melting of water. The liquid state T_1 was ∼500 ms and ∼150 ms for water and Triton X-100 respectively. The relatively long longitudinal relaxation time of water indicates formation of reverse micelles where water is not in contact with free radical spins. The polarization of water may buildup through spin diffusion from the proton chains of the surfactant.

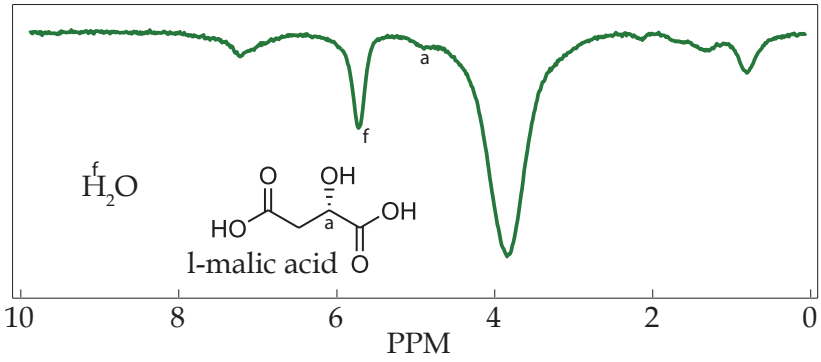

Figure 4.7: DNP enhanced spectrum of d8-toluene (99 % deuterated), Triton X-100 and D_2O (99.9 % deuterated) in the ratio 9:3:1, with 50 mM BDPA. 3 M l-malic acid was dissolved in D_2O before addition of other solvents. Peaks between 0 to 3 ppm are from Triton X-100. Peaks at around 7 ppm are expected from toluene and Triton X-100. The spectrum was recorded in a single scan with 10 seconds of microwave irraditaion at 25.5 W.

4.4.2 Towards water soluble BDPA derivative

An attempt was made to synthesize water-soluble BDPA-like radicals [89, 103] to obtain hyperpolarized signals in the liquid state for water-soluble samples. The stability and the concentration for most of the synthesized molecules were not optimal to perform DNP experiments. Table 4.3 gives an overview of the synthesized radicals. The target concentration in Table 4.3 is the expected concentration if all the molecules are oxidized and no impurities are present in the synthesized compounds.

Table 4.3: Summary of BDPA-like radicals prepared for rapid-melt DNP.

Structure	Reference	Solvent	Stability	Free radical concentration (mM)	
				Target	Measured (EPR)
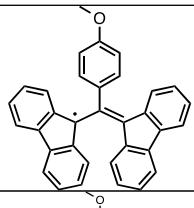	MeO BDPA	Toluene	low	5	2
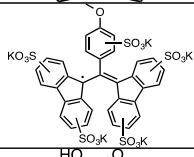	SA MeO BDPA	H_2O	High	5	~5
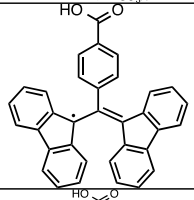	COOH BDPA	H_2O	low	5	0.1
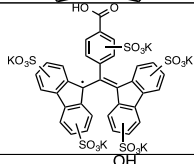	SA COOH BDPA	H_2O	low	5	0.1
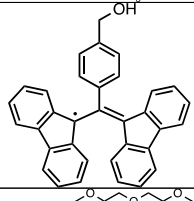	BA BDPA	Methanol/ Ethanol	low	25	13
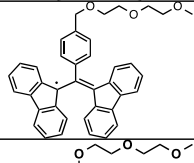	DEG B BDPA	Methanol	low	25	12.5
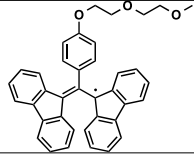	DEG BDPA	Toluene	low	20	0.7

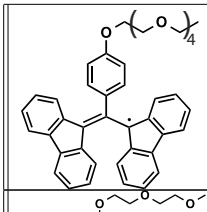	TEG BDPA	Methanol	low	15	0
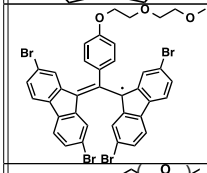	DEG 4Br BDPA	toluene	high	15	15
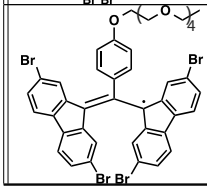	TEG 4Br BDPA	toluene	low	15	10.4

Successful DNP and EPR experiments were performed for the radical di-ethylene glycol 4 bromine BDPA (DEG 4 Br BDPA). The EPR line shape of this radical was similar to the commercial BDPA as shown in Figure 4.8. The enhancement for toluene and deuterated toluene was also found to be similar compared to the commercial BDPA at the same experimental conditions (Figure 4.9). The glycol chain at the molecule has protons which may optimize the spin diffusion. Spin diffusion is the rate limiting step according to the proposed model for Solid Effect DNP in the rapid-melt approach (Chapter 3). Bromine is an electron negative atom which may provide improved water solubility. Although DEG 4 Br BDPA is not readily soluble in water, 20 mM of DEG 4 Br BDPA was successfully dissolved in methanol.

The radical SA MeO BDPA was stable and produced at the target concentration. Rapid-melt DNP experiment with this radical were not completed due to precipitation of the radical after several freeze and thaw cycles.

4.5 Conclusions

We have hyperpolarized different types of molecular species to examine the general applicability of rapid-melt DNP. DNP enhanced signals of all the sample constituents (solvent, co-solvent, solute) have been observed. Solvents with lower latent heat of melting and lower specific heat are optimal for the setup. The fast melting transition of toluene and chloroform and slow paramagnetic relaxation induced by BDPA

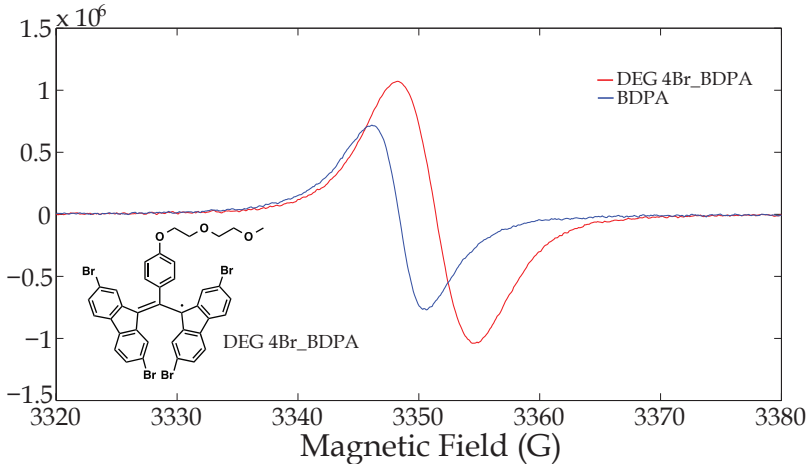

Figure 4.8: The EPR spectrum of commercial BDPA and the homemade DEG 4Br BDPA at room temperature. The concentration of DEG 4Br BDPA was expected to be 25 mM, which was also confirmed by the signal intensity in the EPR spectrum. The g-factor of DEG 4Br BDPA was found to be 2.003.

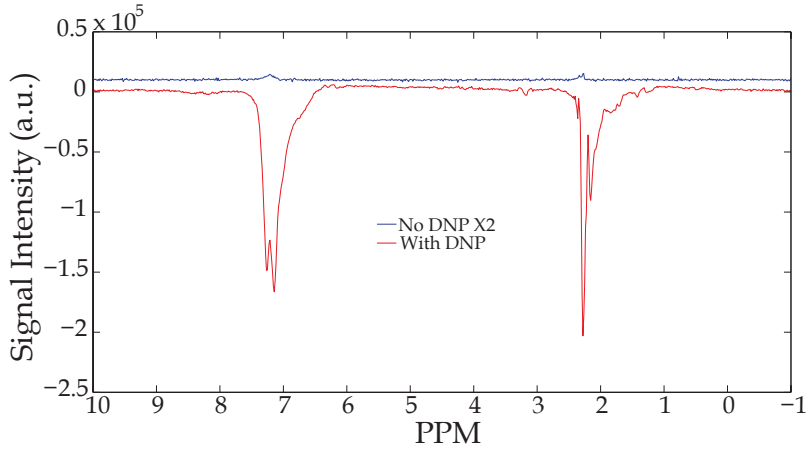

Figure 4.9: Spectrum of toluene with and without DNP for sample doped with 50 mM DEG 4Br BDPA. The enhancement is similar to commercial BDPA in similar conditions. The enhancement at lower proton concentration is also similar to commercial BDPA. The peak near the methyl peak of toluene indicates some impurity.

limits the relaxation losses during melting resulting in high polarization observed in the liquid state. Toluene or chloroform with or without co-solvent can be used to hyperpolarize different molecular species using BDPA. The hyperpolarized spectra of different molecular species like lipids, amino acids, alcohols, vitamins, steroid hormones and small metabolites have been acquired. The enhancement factors observed are smaller than previously reported in Chapter 2 for d8-toluene without

addition of solute. This decrease in the enhancement factor of toluene can result from the combination of two factors: 1) Addition of the solute leads to a higher proton concentration in the sample. Enhancements were found to be strongly depend on the proton concentration. 2) The delay between the shuttling and NMR measurement is longer than for previous experiments. From an application point-of-view all the peaks in hyperpolarized spectra are well above the noise level. The synthesized BDPA derivatives to achieve water solubility are still under development and more work is required to make these radicals stable and water soluble. We have successfully demonstrated the generic nature of rapid-melt DNP at lower magnetic fields. However, for real-life applications the same method should be tested at higher magnetic fields.

Chapter 5

2D NMR with rapid-melt DNP

Abstract

In the recently introduced rapid-melt DNP method, the sample remains intact between the cycles of DNP in the solid state and signal acquisition in the liquid state. This presents the possibility of multidimensional NMR experiments with hyperpolarization. 2D TOCSY (total correlation spectroscopy) experiments were performed to examine the feasibility of multidimensional DNP-NMR in the rapid-melt DNP setup. A proof of principle was established for a rather high proton concentration sample. 2D TOCSY spectra are successfully acquired for 1 nano mole of ethyl pyruvate. A better signal to noise ratio has been obtained in the DNP experiments w.r.t the reference spectrum acquired after massive signal averaging. Spectral resolution of the DNP and non-DNP spectra is found to be similar in the current state of the setup.

5.1 Introduction

NMR is a wide spread technique having applications in many fields including physics, chemistry and biology. NMR is regularly used to analyze the products of chemical synthesis, molecular structure and dynamics. The information in NMR is obtained from the NMR spectrum. A one dimensional NMR spectrum is obtained by Fourier transformation of the free induction decay of spin magnetization along one time axis. In 1971 Jeener came up with the idea of multidimensional NMR [104], which was further developed by Ernst and co-workers [6]. In multidimensional NMR the evolution of NMR signal is observed along more than one time axis. Multidimensional NMR provides information about the correlation of different atoms in a molecule based on some interaction (mainly J-coupling and dipolar) between the atoms which can not be obtained through 1D NMR. 2D NMR is a widely used analysis technique. The reason of 2D NMR being so powerful lies in the vast information that can be obtained. Atoms (same or of different species) connected through chemical bonds can be identified through COSY [6], TOCSY [105], HETCOR [106] experiments while atoms (same or different species) close in space can be distinguished through NOESY [107], HOESY [108] experiments. The non invasive and quantitative nature of NMR makes it an obvious choice for organic chemistry, analytical chemistry, structural biology etcetera [109].

Although NMR is very useful it is relatively mass/concentration insensitive. DNP is used to ameliorate the problem of low sensitivity of NMR. The field of DNP is enjoying a great deal of development over the last few years. Many approaches have been developed to obtain DNP enhanced spectra in the liquid state. The only available DNP mechanism in the liquid state is based on the Overhauser effect. The Overhauser effect is a cross relaxation mechanism and depends on the correlation time of the nuclear and electron spins. The Overhauser effect is effective if $\omega_e\tau < 1$, where τ is the correlation time and ω_e is the Larmor frequency of the electron. For an effective Overhauser effect at higher magnetic fields, the mobilities of molecules have to be fast enough to provide dipolar correlation times in the picosecond timescale. The Overhauser effect is usually utilized for small molecules at low magnetic fields [50]. Other approaches to obtain DNP enhanced spectra in the solution state include a phase change step from solid to liquid either via dissolution or melting. Dissolution DNP [54] is fundamentally a "single shot" experiment due to the change of sample composition during the dissolution step, hence multidimensional NMR experiments are difficult to implement for this method. Even for hyperpolarized samples the duration permitted to observe the hyperpolarized signal is inherently limited by the T_1 of the measured spins. This limitation restricts the

observation of hyperpolarized spins to a few scans. Despite this limitation multidimensional NMR on spins hyperpolarized via dissolution DNP has been performed. Frydman has developed ultrafast 2D methods to be used with dissolution DNP. In this method pulsed field gradients are used to encode different parts of a sample with coherences needed for the 2D spectrum [58]. Hilty and co-workers used low-power off-resonance radio frequency irradiation for differential scaling of scalar coupling to encode a second chemical shift dimension to obtain two-dimensional chemical shift correlations for hyperpolarized samples [59]. The same group later demonstrated sequential 2D experiments using variable flip angles [60]. Griffin and co-workers performed solid state DNP and liquid state NMR in the same spectrometer through melting of the solid sample by CO_2 laser irradiation in a MAS-DNP setup [72]. They later recorded a $^{13}C—^{13}C$ correlation 2D spectrum in the same fashion [73]. Recently, Yoon and co-workers presented the possibility to use the microwave energy from the gyrotron to melt the sample to acquire the NMR spectrum in the liquid state [74]. In principle this method can be used to acquire 2D spectra of hyperpolarized samples in the liquid state.

Although all the above methods have successfully demonstrated 2D NMR of hyperpolarized molecules in the liquid state, they have their own drawbacks. The ultrafast 2D methods depend on the spatial encoding of the coherences, hence are not robust against the fluid motions in the sample tube that may be induced by the violent flow of dissolution. The ultrafast 2D methods are generally hard to implement compared to traditional sequential methods. The resolution in the off-resonance decoupling method is limited and signals of different resonances overlap for larger molecules [60]. The sequential 2D experiments with variable flip angle are again limited by the relaxation time of the targeted spin. In the recently presented rapid-melt DNP method the sample remains unaltered during the DNP in the solid state and the measurement in the liquid state. The melting process is completely reversible, which presents the possibility of performing multidimensional NMR without any special requirements [83]. Here, we have recorded the 2D TOCSY spectrum for $^{1}H—^{1}H$ correlation in the traditional sequential manner. First we will describe the DNP-2D experiment. Then the results of 2D TOCSY are given. We have also investigated the possibilities to implement methods to correct for unstable DNP enhancement.

5.2 Total correlation spectroscopy

Protons are undoubtedly the most commonly studied nuclei in the field of high-resolution liquid-state NMR due to their high natural abundance and the information content of the resulting spectra. Homonuclear proton correlation experiments are an indispensable tool to investigate structural and dynamical features of molecules in biology and organic chemistry, particularly proteins [110]. DNP enhanced homonuclear proton correlation experiments can easily be performed in rapid-melt DNP, which may not be possible for other DNP methods.

Two-dimensional NMR experiments are generally composed of four steps, preparation, evolution, mixing and acquisition [111]. During the preparation the desired spin state is prepared from the equilibrium state of the spin system. The evolution period is an incremental delay during which the spin system evolves under free precession or applied radio frequency (rf) fields. Spins transfer polarization during mixing, which can be used to obtain correlations between different nuclei. During acquisition the phase or amplitude modulated free induction decay (FID) is recorded.

Total correlation spectroscopy (TOCSY) or HOHAHA (homonuclear Hartmann-Hahn) spectroscopy is a widely used pulse sequence to investigate the correlation of nuclei of the same isotopes that are connected through chemical bonds in a molecule [105]. As the name suggests TOCSY provides the correlation of all the spins in a scalar coupled spin system by attaining a Hartmann-Hahn condition. The Hartmann-Hahn condition is satisfied when two different spins have the same precession frequency (no chemical shift difference) in their respective rotating frames [112]. The Hartmann-Hahn condition is obtained by the application of radio frequency (rf) fields. The effect of the rf field is to lock the spins at an effective field lower than the principal magnetic field (B_0). As the spins experience an effective lower field, the coupling term of the Hamiltonian becomes dominant and coherence transfer occurs through scalar coupling.

The Hamiltonian for two coupled spins i and j can be written as Equation 5.1

$$\mathcal{H} = \sum_i -\omega_i I_{iz} + 2\pi \sum_{i \neq j} J_{ij} I_i \cdot I_j \tag{5.1}$$

The first part of the Hamiltonian is the chemical shift part and the second part is the scalar coupling part. This Hamiltonian can be reduced to Equation 5.2 if the homonuclear Hartmann-Hahn condition is satisfied

$$\mathcal{H} = 2\pi \sum_{i \neq j} J_{ij} I_i \cdot I_j \tag{5.2}$$

The Hamiltonian in Equation 5.2 has only a scalar coupling part. In TOCSY, an rf field is applied during the mixing time which locks the spins in the transverse plane. Now the spins are only subject to the effective Hamiltonian given in Equation 5.2 beacuse of the spin lock imposed by the rf field. During the mixing time polarization is transferred among all the spins of a coupled spin system through scalar coupling. Several special pulse sequences (MLEV-17, MLEV-16, DIPSI, DIPSI-2rc) are reported for the rf field to reduce the Hamiltonian from Equation 5.1 to Equation 5.2. These pulse sequences mainly differ in the effective band width of the spin lock. These pulse sequences transfer in-phase magnetization between the spins via the Hamiltonian given in Equation 5.2.

The TOCSY pulse sequence employed in the current experiments is shown in Figure 5.1. The preparation step consists of a 90° pulse. The evolution is an incremental delay t_1 decided by the spectral width of the F_1 dimension (indirect dimension). The second 90°pulse prepares the magnetization for mixing. Mixing consists of many soft pulses distributed evenly on every phase (x, $\bar{x}$, y, $\bar{y}$) which spin locks the spin system allowing a redistribution of the polarization. Finally the last 90° pulse converts the longitudinal polarization to detectable transverse magnetization for acquisition. The signal was acquired in States-TPPI mode with a 4 step phase cycle to avoid the axial signals in the middle of the spectrum [113].

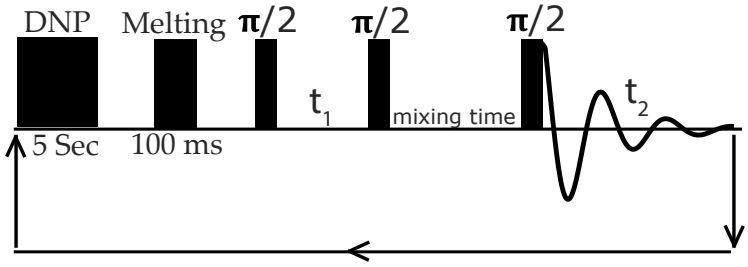

Figure 5.1: Experimental scheme to acquire hyperpolarized TOCSY NMR in the liquid state. First DNP is performed at 77K by irradiating the sample with 94.850 GHz microwaves. The hyperpolarized sample is shuttled to a region of warm nitrogen gas flow for melting. Finally the sample is shuttled to the stripline for NMR acquisition. The TOCSY pulse sequence consisted of three $\pi/2$ pulses. The first pulse positions the magnetization in the transverse plane. The second pulse moves the polarization to longitudinal plane after the incremental delay t_1. In the mixing time, many long pulses are applied at a lower power to get the correlation between all the nearby protons.

5.3 Results and discussion

As a test molecule ethyl pyruvate was dissolved in toluene (50/50 volume) doped with 50 mM BDPA to establish the proof of principle for 2D NMR using rapid-melt DNP. Figure 5.2 shows the 2D TOCSY spectra with and without DNP. Both spectra were recorded using 64 increments in the indirect dimension, with a 4 step phase cycle in the States TPPI mode. The observed enhancements are 5 and 3 respectively for toluene and pyruvate peaks for this sample. The reason for this moderate enhancement is the long delay of 200 ms for melting and stabilization before the acquisition of the NMR spectrum. Also the enhancement is small because of high proton concentration in the sample. As discussed in Chapter 3, the enhancement of the bulk protons decreases at higher proton concentration in the sample. Here, we are only interested in the comparison of 2D spectra acquired with and without DNP and not in the DNP enhancement itself. The spectrum shows that there is no loss of resolution in the 2D spectrum acquired with DNP. The correlation between the CH_3 and CH_2 groups of ethyl pyruvate can clearly be seen as the cross peaks in the spectrum. Truncation artifacts are visible in both spectra at the base of the high intensity peaks because only 64 points were taken in $F1$ and the FID has not decayed completely.

Figure 5.3 shows the 2D TOCSY spectra with and without DNP for a 20 mM (1 nano mole) ethyl pyruvate sample doped in d8-toluene(99 % D atoms) with 50 mM BDPA. The DNP spectrum was acquired in approximately 50 minutes. Each DNP cycle consisted of 5 seconds of microwave irradiation at a frequency of 94.850 GHz and power 25.5 W. The reference spectrum was recorded over night with 160 scans for each increment in the indirect dimension. It is important to note that this experiment not only demonstrates the capability of the setup to acquire 2D spectra but also the stability of NMR and DNP during the experiment to obtain clear cross peaks.

TOCSY spectra of hexanal and l-ascorbic acid are shown in Figure 5.4. The sample consisted of 20 mM hexanal dissolved in d-8 toluene (99 % deuterated) doped with 50 mM BDPA. The cross peaks for hexanal protons are clearly visible in Figure 5.4. 50 mM l-ascorbic acid was dissolved in d8-toluene and d-methanol doped with 50 mM BDPA. The cross peaks can be seen around 4 ppm for the protons of ascorbic acid. In both the spectra the intensity of the cross peaks was lower than the noise level of the solvent peaks. In Figure 5.4 the lower level limit of the contour was set to make cross peaks visible for solute molecules. A higher limit was chosen for the lower level of the contours for the solvent and co-solvent peaks in

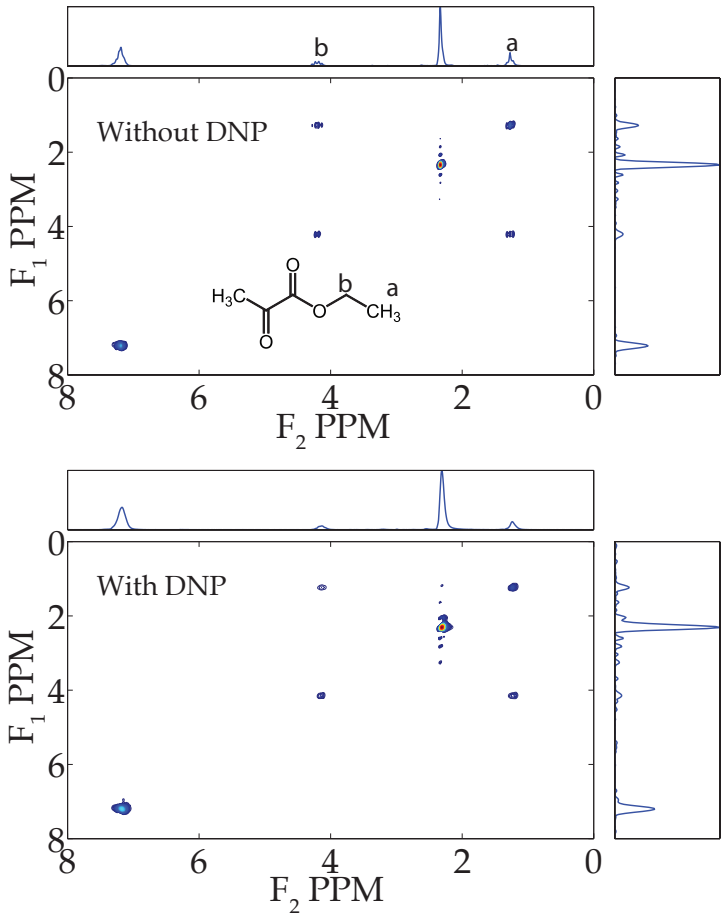

Figure 5.2: TOCSY spectra of ethyl pyruvate dissolved in toluene (50/50 vol %) doped with 50 mM BDPA acquired without (top) and with (bottom) DNP for comparison. The reference spectrum was recorded with the same settings as the DNP spectrum. The DNP spectrum was recorded with 64 increments in the indirect dimension, and 4 scans per increment. Each scan was recorded with irradiation for 3 seconds at 94.850 GHz and 25.5 watts of power. The peak corresponding to the methyl protons of pyruvate coincide with the toluene methyl peak at this concentration. This peak can clearly be seen in Figure 5.3

Figure 5.4 to avoid solvent noise ridges. The reference spectrum for the two samples acquired overnight with massive averaging do not show cross peaks for any molecule because the cross peaks are well below the noise level of the spectrum.

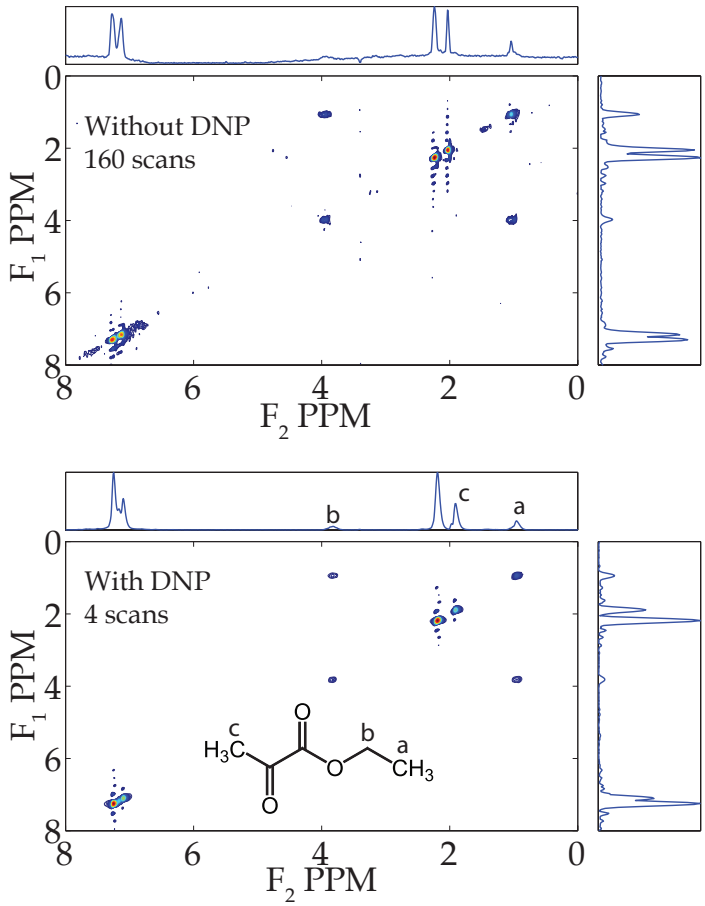

Figure 5.3: The TOCSY spectrum of 1 nano mole of Ethyl pyruvate (20 mM) dissolved in d8-toluene with and without DNP. The top spectrum was acquired in 10 hours without DNP with 160 scans per increment in the indirect dimension. The bottom spectrum was acquired in 1 hour with DNP with a 4 step phase cycle. The cross peaks at 4 ppm and 1 ppm can be seen due to the correlation of methyl protons (a) with aliphatic protons (b) of ethyl pyruvate. The SNR of the DNP enhanced spectrum is much better with respect to the reference spectrum. The resolution is similar in the two experiments.

5.4 t_1 noise in the current setup

Although a proof of principle for hyperpolarized 2D NMR was obtained, t_1 noise occurs and needs further optimization. The origin of t_1 noise is the experimental instability. The main reason of the experimental instability is the temperature variation in the cooling block generated by an unstable cryogen flow. Temperature instabilities in the cooling block result in varying DNP enhancements, hence different starting polarization for different increments of t_1. In addition to the intensity

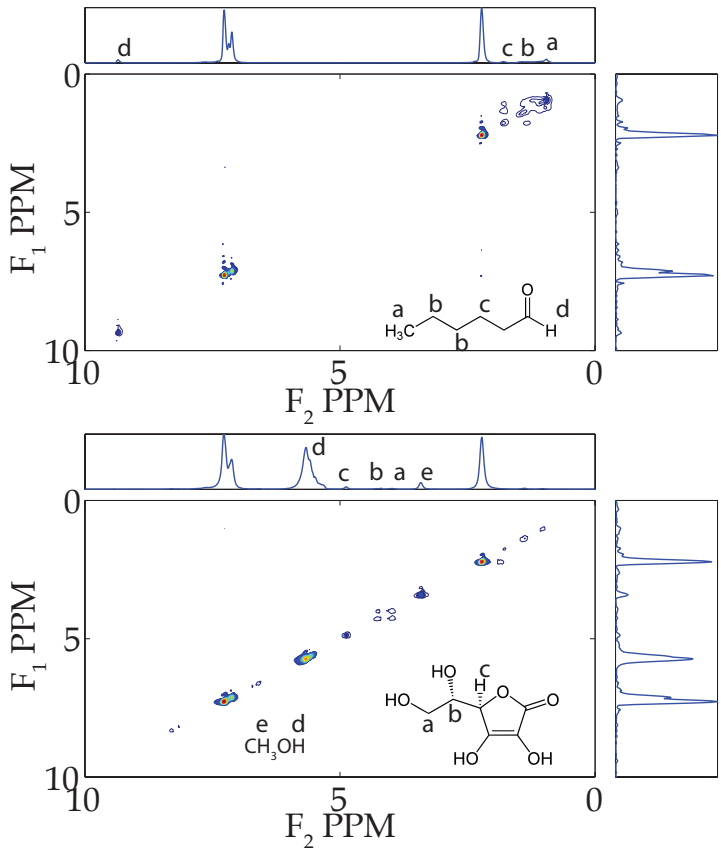

Figure 5.4: Top: DNP-TOCSY spectrum of 20 mM hexanal (1 nano mole) dissolved in d8-toluene doped with 50 mM BDPA. Cross peaks corresponding to the correlated protons in hexanal can be seen between 0 and 2 ppm. Bottom: DNP-TOCSY spectrum of 50 mM l-ascorbic acid dissolved in mixture of d8-toluene and d-methanol doped with 50 mM BDPA. Cross peaks corresponding to the correlated protons in l-ascorbic can be seen at around 4 ppm. In both the experiments the noise level of solvent and co-solvent peaks was higher than the amplitude of the solute peaks. The lower level of contour was chosen to be at a higher limit for solvent and co-solvent peaks to avoid solvent noise ridges.

variations, small variations in the width and the spectral position of peaks are also observed due to the temperature instability. These variations in the intensity, peak position and peak height result in aberrations in the recorded FID as a function of time, which after Fourier transformation shows up in the spectrum as "t_1 noise".

These changes should be fixed by stabilizing the temperature in the cooling block. However, variations in the intensity of the signal can be corrected after quantification of the variation by some internal reference signal. In the present setup solvent peaks can be used as an internal reference to measure the change

in the signal intensity between different scans. A small tip angle pre-pulse can be applied just before the NMR measurement to measure a full NMR spectrum. The pre-pulse spectrum can be acquired with a minimum tip angle to obtain a quantifiable spectrum. Alternatively the intensity can be measured during the 2D pulse sequence. Most of the 2D experiments start with a 90°pulse. A single point acquired just after the first 90°pulse can measure the signal intensity of the whole spectrum. The measurement with the pre-pulse or the first point of FID can be used to normalize the signal for intensity variations.

The intensity of the residual protons of the solvent and co-solvent is much higher than the solute peaks. As the signal intensity is higher for solvent peaks their noise in the F_1 dimension is in the order of the signal intensity of the solute peaks. The peaks corresponding to solute molecules are masked in the noise of solvent peaks at lower contour levels. Solvent suppression techniques can be implemented to avoid high intensity of solvent peaks.

5.5 Conclusions

We have successfully acquired 2D NMR spectra in the liquid state using rapid-melt DNP as a proof of principle of the possibility of hyperpolarized 2D NMR in this setup. The DNP enhanced proton NMR signals in the liquid state can be obtained repeatedly and hence all multidimensional NMR experiments can be performed in the usual sequential manner. High enhancement obtained by DNP enabled the acquisition of a low field 2D TOCSY spectrum for 1 nano mole of molecules in an hour. Although the SNR is sufficient in a single scan after 5 seconds of microwave irradiation a four step phase cycle was used to record the 2D spectrum in the simple traditional sequential manner. Even with the many steps (DNP, sample melting, shuttling) involved in the DNP experiment the resolution in the DNP and non-DNP experiments is found to be similar. TOCSY spectrum of vitamin C has been recorded to demonstrate the generic nature of rapid-melt DNP.

For future applications, the hardware in the current setup needs to be improved. The flow of cryogen is somewhat unstable, leading to unstable temperatures in the cooling block. Temperature instabilities result in variations of enhancement, peak position and peak width. These variations induce noise in the indirect dimension (t_1 noise). The intensity variations can be corrected by normalizing the signal with respect to a reference signal. The resolution is limited in the current state and needs to be improved to perform high-resolution experiments. Solvent suppression can be employed to avoid large peaks of solvent w.r.t. the target molecules.

Chapter 6

Rapid-melt DNP with liquid helium cooling

Abstract

Rapid-melt DNP is a novel approach to perform DNP in the solid state and NMR acquisition in the liquid state. Previously rapid-melt DNP was preformed with liquid nitrogen cooling. Here, rapid-melt DNP is examined at lower temperatures with helium cooling. Helium can be used in gas or liquid form to cool the sample. The use of liquid helium as a coolant produces a proton signal enhancement of up to 2000 times in a single scan. The observed enhancement and the DNP build-up time are in good agreement with previously proposed solid effect in the rapid-melt DNP method.

6.1 Introduction

NMR is a powerful, yet a rather insensitive (in terms of mass-sensitivity) analytical technique. In recent years many DNP methods have been developed to solve the problem of low sensitivity [54, 90, 50]. We presented a novel method called "rapid-melt DNP" to obtain hyperpolarized spins in the liquid state after DNP in the solid state [83]. In Chapters 2 and 4 the details and examples were given of molecules hyperpolarized in the rapid-melt DNP setup. Initially the DNP experiments were performed using readily available and inexpensive liquid nitrogen as a coolant. As demonstrated in Chapter 2, the DNP efficiency is sufficient to establish a proof of principle. Enhancement factors of up to 400 have been obtained in the liquid state, leading to the detection of miniscule amounts (hundreds of picomole) of spins in a single scan, at low field.

Although DNP processes and overall enhancement factors at a liquid nitrogen temperature are adequate, performing DNP at lower temperatures with liquid helium presents the possibility to obtain even higher enhancement levels to lower the limit of detection even further. At a lower temperature the polarization of both the electron and nuclear spins increase, which may provide a higher DNP enhancement as well as a higher Boltzmann enhancement due to the temperature jump. Here, we present preliminary results obtained with rapid-melt DNP at lower temperatures using liquid helium as coolant. We have successfully polarized both the solvent and the solute molecules at lower temperature. In the second section we discuss the experimental details of rapid-melt DNP with liquid helium. The third section contains the results for liquid and cold helium gas cooling of the sample. The model presented in Chapter 3 is used in the fourth section to predict the enhancement at even lower temperatures. The conclusions are summarized in the last section.

6.2 Rapid-melt DNP below 77K

The probe was used in the same setup as with the liquid nitrogen (Chapter 2). None of the parts of the probe were required to be changed or modified, including the cryogen transfer line and the cooling block, for the use of liquid helium. The temperature of the hot gas (to melt the sample) was also kept at 70 °C. The same microwave power and frequency position as in Chapter 2 were used for the following experiments. Experiments were conducted in consecutive steps of DNP, sample melting and NMR measurement as described in Chapter 2. Liquid helium was contained in a 60 liter dewar (Praxair) and was supplied to the probe by applying an

external helium gas pressure. The consumption of helium was around 1.6 l/h. The consumption of liquid helium in MAS-DNP is reported to be 6 l/h when used for cooling and spinning [114] and 1.3 l/h when used only for cooling [115]. In dissolution DNP every dissolution step consumes up to 2 liters of liquid helium.

Besides liquid helium, cold helium gas can also be used for cooling the sample in the current setup. The use of a gas phase cryogen may lead to higher cooling stability. Cold helium gas was transferred to the probe using a concentric tube with a closed bottom and opening at the top for helium gas to enter (Figure 6.1). In this setup helium gas is cooled by passing it through the concentric tube which is in contact with the liquid helium. The liquid helium consumption was less than 1 l/h for this setting.

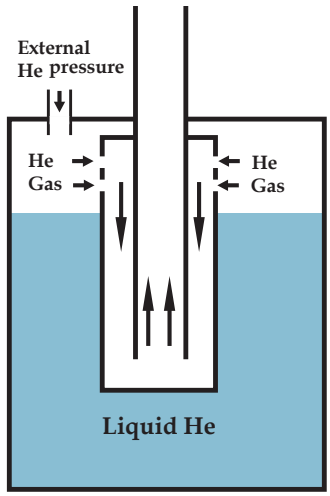

Figure 6.1: Schematic diagram of the modified end of the siphon for creating cold helium gas as a coolant in rapid-melt DNP.

6.3 Results and discussion

6.3.1 Rapid-melt DNP with liquid helium cooling

The liquid helium cooling resulted in higher enhancements of up to ~2000, as shown Figure 6.2. Although poor thermal stability limits the accuracy of the measured DNP build-up time, the estimated time constant is under 20 seconds. A typical build-up curve at lower temperature is shown in Figure 6.3. The polarization build-up time is 12±6 seconds. The time required to melt the sample at lower tem-

perature was found to be similar to the liquid nitrogen temperature. The specific heat of toluene is very low at cryogenic temperatures, hence the duration of the melting transition is governed by the latent heat of the melting process and the specific heat in the liquid state.

The temperature in the cooling block was calculated from the Boltzmann enhancement, due to the temperature jump from cold temperature to the room temperature. The signal intensity at the cold temperature was measured by fitting the Boltzmann buildup curve at low temperature. The Boltzmann build-up curve was measured by keeping the sample in the cooling block without microwaves for variable delays and measuring the NMR intensity after melting the sample. The Boltzmann enhancement obtained from the ratio of the cold temperature intensity to the room temperature reference intensity was found to be 6-7 times, implying the temperature in the cooling block to be ∼40-50 K. As the total enhancement is ∼2000 and the temperature jump provides a gain of 6-7 times, the enhancement due to DNP is expected to be around 250-300. The total enhancement in the case of liquid nitrogen as coolant was ∼400. The gain from the temperature jump in this case was a factor 4 so the DNP enhancement should be around 100. This means that the enhancements from both the temperature jump and the DNP are higher at lower temperatures w.r.t. liquid nitrogen cooling.

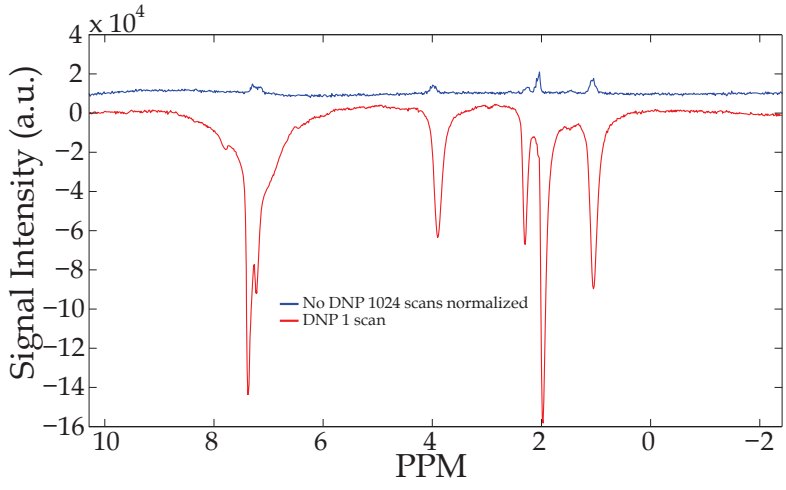

Figure 6.2: The DNP enhancement with liquid helium as cryogen for d8-toluene doped with ethyl pyruvate and BDPA, 50 mM each. The reference spectrum (1024 scans) is normalized by $\sqrt{1024}$ to compare the spectra at the same noise level. The peaks at 7.2 and 2.1 ppm are from aromatic and methyl protons of toluene. The peaks at 1, 2 and 4 ppm are of the ethyl pyruvate protons.

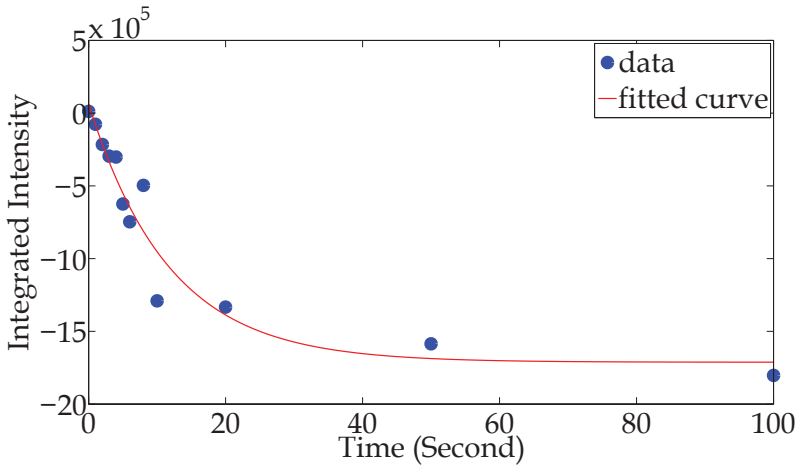

Figure 6.3: The intensity of DNP enhanced signal versus microwave irradiation time of residual methyl protons of d8-toluene doped with 50 mM BDPA for microwave irradiation at 94.850 GHz and 25.5 W with liquid helium cooling. The DNP build-up time is measured to be 12±6 seconds.

6.3.2 Cooling with helium gas

Helium gas as coolant provides a total enhancement of ∼230 for protons of toluene. This is moderately better than the total enhancement (∼200) with liquid nitrogen cooling under similar non-optimal experimental conditions. The DNP build-up time constant in this case is found to be around 5 seconds, which is also similar to the liquid nitrogen cooling results.

Although the enhancement is similar for liquid nitrogen and cold helium gas, cooling with cold helium gas renders a more stable enhancement and spectral position of peaks w.r.t. liquid coolant because of the same phase of coolant through out the transfer from dewar to the probe. Boiling of liquid coolant is avoided in the case of cooling by cold gas. The relative displacement of the pyruvate peak was ±1 Hz during successive measurements. Relative peak displacement of up to 10 Hz has been observed in the case of cooling with a liquid cryogen. The enhancement for cooling with gas is found to be relatively stable with a standard deviation w.r.t. the mean of the intensity of the DNP enhanced signal of 4 %. The intensity of the DNP enhanced signal is observed to change by up to 50 % in case of sample cooling by liquid cryogens. Figure 6.4 shows a DNP enhanced 2D TOCSY spectrum acquired with cold helium gas cooling for a sample of 50 mM ethyl-pyruvate (2.5 nano mol) dissolved in d8-toluene (99.6 %) doped with 50 mM BDPA. The spectrum was recorded in the same fashion as described in Chapter 4. The same experimental settings were used as for Figure 5.3.

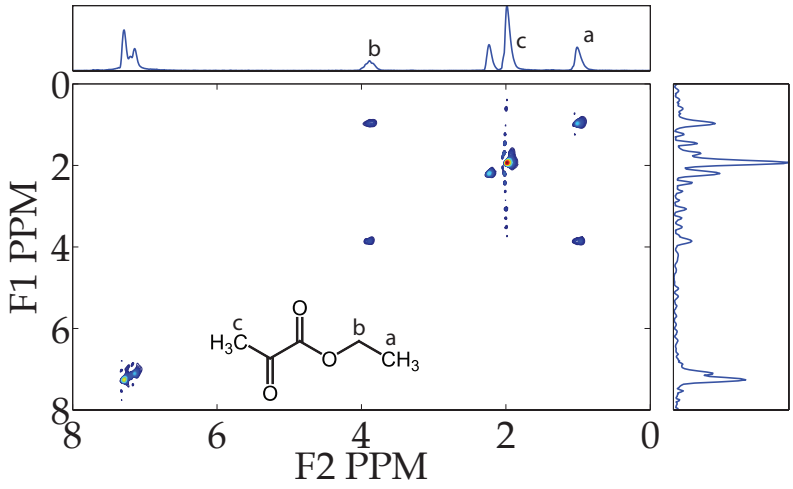

Figure 6.4: DNP enhanced 2D TOCSY spectrum of 50 mM ethyl-pyruvate dissolved in d8-toluene (99.6 %) doped with 50mM BDPA recorded with helium gas cooling. The spectrum was acquired in 1 hour with a 4-step phase cycle and 5 seconds of microwave irradiation. The cross peaks at 4 ppm and 1 ppm can be seen due to the correlation of methyl protons (a) with aliphatic protons (b) of ethyl pyruvate.

6.4 Rapid-melt Solid Effect DNP below 77 K

In Chapter 3, we introduced the rapid-melt Solid Effect model to understand the enhancements observed in our rapid-melt DNP setup with BDPA radicals. The same model can be used at lower temperatures. In Figure 6.5 we have reproduced the total enhancement, including the Boltzmann enhancement, and the build-up time as a function of temperature for a sample of 99 % d8-toluene doped with 50 mM BDPA for a complete solution of the differential Equations 3.6,3.7 and 3.8. The number of bulk protons (N_b) and core protons (N_c) will remain the same at lower temperatures. The main temperature dependent parameters in the differential equations are the longitudinal relaxation times of the core protons T_{1c} and the bulk protons T_{1b}. The values of T_{1c} and T_{1b} are taken from the measured values in Figure 3.4 and extrapolated with an inverse power law. The rate of polarization diffusion per bulk proton W_d/N_b is assumed to be 0.05 (s^{-1}) at all the temperatures. The curves in Figure 6.5 are calculated using a microwave power level required for the saturation of the enhancement.

The enhancement increases and the DNP build-up time becomes longer at lower temperatures. At lower temperatures both T_{1b} and T_{1c} become longer, but the assumption that core protons reach equilibrium polarization much faster than bulk protons remains valid. $T_{1c} \gg T_{1e}$ can always be assumed due to fast relaxation of

the electron spin. Under the above assumptions the enhancement of bulk protons (ϵ_b) will be $\epsilon_b = \frac{f_d+\epsilon_c}{f_d+1}$ as given in Equation 3.11. Here ϵ_c is the enhancement of the core protons and f_d is the diffusion leakage factor defined as $f_d = N_b/(T_{1b}W_d)$. The DNP build-up time for bulk protons at high microwave powers can be written as in Equation 3.13 $\tau_b = \frac{f_d T_{1b}}{1+f_d}$. At lower temperatures T_{1b} becomes longer, the diffusion leakage factor f_d will become small if the number of bulk protons (N_b) and the rate constant of the diffusion of polarization (W_d) remains unchanged. As f_d becomes small the polarization of the bulk protons increases towards ϵ_c and the DNP build-up time becomes longer with longer T_{1b}.

The experimental values observed for the enhancement and the build-up time at lower (∼40 K) and higher (∼90 K) temperatures are in good agreement with the theoretical curves given in Figure 6.5.

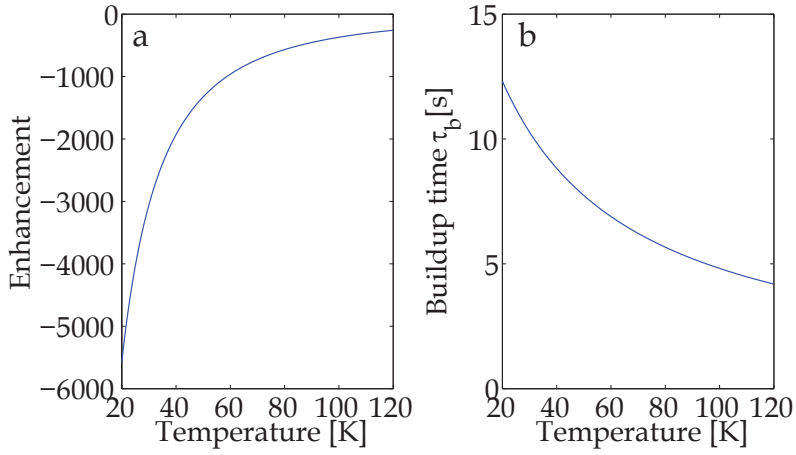

Figure 6.5: Predicted enhancement (a) and DNP build-up time (b) for the protons in a sample of 99 % d8-toluene doped with 50 mM BDPA, as a function of temperature according to the rapid-melt Solid Effect DNP model described in Chapter 3. Parameters used for the Figure are given in the text.

6.5 Conclusions

We have successfully acquired hyperpolarized NMR spectra in the liquid state after DNP at lower temperatures by helium cooling for rapid-melt DNP. For liquid helium cooling the probe can be used without any alteration to the current setup. Proton signal enhancement factors of up to 2000 have been achieved in a single scan. The increase in the enhancement factor w.r.t. liquid nitrogen cooling is due to a combination of a higher temperature jump factor and more efficient DNP at lower

temperatures. The DNP build-up time is only ∼12 seconds. Cold helium gas can also be used as a coolant in the current setup. The use of cold helium gas for cooling results in a stable temperature, therefore it provides better spectral stability. Higher enhancement will reduce the experimental time and can enable the detection of miniscule amounts of spins in the sample. The experimental results are obtained using the Solid Effect in our rapid-melt DNP setup.

The lowest temperature in the cooling block is estimated to be 40-50 K. Improved cryogen flow may provide even lower temperatures at the cooling block hence even higher enhancement factors of up to 6000 in a single scan at 20 K. The spectral stability in both the peak intensity and the peak position may also be improved by a stable liquid coolant flow.

Outlook

Present setup

One of the main advantages of the rapid-melt DNP setup is its modular design. All the three main blocks (cooling/microwave, heating and NMR) can be optimized individually without affecting other parts of the probe.

The main technical problem in the current setup is the temperature instability at the cooling block. The reason for this instability is the evaporation of cryogen during its transfer to the microwave block, which results in unstable cryogen flow. The enhancement, peak position and peak height of NMR signals vary in time due to temperature instabilities. A better isolation of the cryogen transfer line and the implementation of a thermally stabilized evaporator will help in stabilizing the temperature at the cooling block for more reproducible experimental results.

In the present version, the microwave block is a non-resonant cavity. Although the non-resonance mode of operation of the microwave block is ideal for working at different microwave frequencies to examine the frequency dependence of the enhancement and DNP build-up time, it requires higher microwave power for a complete electron saturation. The microwave block can be changed to a resonant cavity for increased microwave B_1 field strengths and decreased microwave heating effects. This would particularly benefit the DNP in the liquid state through the Overhauser effect.

The cooling of the sample is performed by directly spraying the coolant on the sample capillary. The temperature of the coolant can be controlled by addition of a heating element, this might be useful to conduct mechanistic studies at various temperatures.

Instead of hot gas, an IR laser, hot liquid bath, RF heating or any combination of these can be used to shorten the melting duration. If the melting time is shorter than the relaxation time, liquid state DNP signals can be observed even for fast relaxing samples like a water glycerol mixture. Also it will limit the relaxation losses for the slow relaxing samples.

The resolution is not optimal in the current setup and needs to be improved for further applications. The chemical shift dispersion at higher magnetic field is intrinsically better, also an in-situ shim coil in addition to the main shims of the magnet can be employed to improve the resolution of the probe. A tapered stripline in place of the regular stripline can be used to utilize the radio frequency field gradients for various experiments [116].

Rapid-melt DNP at higher magnetic fields and Cross Polarization

Rapid-melt DNP has been successfully demonstrated at 3.4 T. The next step is to explore rapid-melt DNP at more commonly employed magnetic fields in high resolution NMR. The sensitivity and the chemical shift dispersion of NMR is proportional to the strength of the magnetic field B_0, due to a higher polarization and larger Larmor frequency.

Cross polarization (CP) is a routine in solid state NMR to increase the sensitivity of low gamma nuclei by transferring the polarization from proton or any other higher gamma nuclei. In rapid-melt DNP the polarization builds up in the solid state, an additional step of cross polarization from the protons to other low gamma nuclei can thus be employed to enhance the signal of low-gamma nuclei. The T_1 of carbons is much longer than that of protons. In this case, even a nitroxide radical can be used to perform DNP on water and a successive cross polarization step to carbon can store the polarization in a slow-relaxing polarization bath. In the next step melting can be performed to acquire hyperpolarized NMR signals of the low gamma nuclei in the liquid state. For carbons the chemical shift range is much larger than that of protons. This broader range increases the spectral resolution.

At present, observed enhancements are up to 2000 for protons. The enhancement for carbons can be as high as 8000 assuming a perfect CP efficiency. At higher fields the sensitivity of NMR increases, increasing the magnetic field from 3.4 T to 9.4 T will improve the NMR detection sensitivity close to 6 times. This implies that an enhancement approaching 50,000 is in principle possible in a single scan for ^{13}C

in the current setup.

Addition of chromatography

A chromatography instrument can be used to separate or to concentrate different molecules in small sample plugs before hyperpolarization. The different sample plugs separated by buffer plugs can then be transported to the probe in the liquid state, where they can subsequently be examined in the rapid-melt DNP setup after polarization in the solid or the liquid state. Operation in this manner can be used for high throughput screening of small sample volumes. This whole operation can be automated for DNP-NMR measurements.

Examples of solid and liquid state DNP have already been demonstrated in previous Chapters. The possibility of working at higher pressures in the current setup may be particularly useful for liquid state Overhauser DNP by using supercritical solvents for DNP. A preliminary example was already shown in Figure 2.10(b), where supercritical CO_2 was used at 100 bars to perform DNP of toluene protons in the liquid state.

Applications

The main field of application for rapid-melt DNP can be the analysis of low concentration metabolites or natural abundance study of mass limited samples. Rapid-melt DNP can be used as a high throughput NMR analytical tool as the experimental times are in the seconds regime. In the current hyperpolarization approaches, signal enhancement with NMR detection in the liquid state is mainly carried out by dissolution DNP, Overhauser DNP, and para-hydrogen induced polarization (PHIP). As already discussed, the main applications of dissolution DNP are metabolic imaging [61, 117] and the study of metabolic pathways [118, 119]. Other uses of dissolution DNP include biomolecular NMR [63, 64], the study of biological assays [65, 66] and the detection of low concentration reaction intermediates [67]. Only a few analytical application have been demonstrated [120]. Overhauser DNP is so far limited to conceptual studies, but nonetheless some interesting application have been reported like hyperpolarized water as an MRI contrast agent [47], and the study of local water dynamics [93]. Overhauser DNP can indeed be very promising for the hyperpolarization of small molecules if fast molecular dynamics can be realized [53]. The approach of hyperpolarization with reversible exchange of para-hydrogen is called SABRE [25]. In SABRE, not only the requirement of unsaturated compounds

is eliminated, signal averaging is also possible. Detection of compounds with concentrations less than 1 μM have been reported through SABRE [121]. SABRE is 2D NMR compatible and 2D NMR trace analysis has been demonstrated [122]. SABRE is mainly observed for hetrocyclic organic compounds [123]. SABRE is a powerful hyperpolarization technique but it is restricted in application to selected molecules. This selectivity can however be used as an advantage for selective hyperpolarization of molecules [124]. The absence of metal catalyst for solvents like water is the main drawback of this method.

Rapid-melt DNP does not suffer from most of the above drawbacks and can be used as a generic method for hyperpolarization. Rapid-melt DNP can also be quite useful in the studies of the DNP mechanisms themselves. The main reason for this is the tuneability of klystron microwave amplifiers for various microwave frequencies and powers. The sample can be polarized in the solid state or the liquid state. The duration of steps of sample cooling, microwave irradiation and sample melting can be varied to examine the dependence on various parameters like relaxation times.

Concluding remarks

We have examined and successfully demonstrated the possibility of rapid-melt DNP at a magnetic field of 3.4 T to obtain hyperpolarized NMR signals of different molecules. This approach is compatible with all general NMR pulse sequences. All the test molecules have been successfully polarized. There are a few technical improvements required for the current setup to perform real life applications, mainly temperature stabilization, resolution and water soluble BDPA-like radicals to minimize relaxation losses. These technical issues can be mended in the near future, requiring relatively small efforts.

Rapid-melt DNP is a generic method based on a dedicated probe design to achieve DNP, sample melting and NMR in the same magnet and can be implemented at the contemporary high resolution NMR magnetic fields with relative ease. The requirement of another magnet for a Gyrotron or as a polarizer is avoided and the method can be implemented on an existing magnet. The probe design is modular so all the different parts of the probe can be manufactured and optimized separately. The different parts of the probe are relatively simple in design e.g. cryogenics, sample shuttling, sample melting. Steps towards rapid-melt DNP at 400 MHz (9.4 T) are already underway. The microwave source, an extended interaction oscillator (EIO), is already in place for generating microwaves at 263 GHz. Cross polarization to low gamma nuclei is the obvious next step to exploit the generic

nature of rapid-melt DNP for various experiments. The operational costs (cryogens, chemicals) for rapid-melt DNP are limited due to miniaturization of DNP, sample melting and NMR parts. Hyphenation of chromatography with rapid-melt DNP can be used for high throughput analytic purposes. Very low concentration samples can be concentrated by chromatography in small volume samples for DNP.

In the end we can say that rapid-melt DNP is a viable approach for generic DNP-NMR experiments. Experiments at low-field have demonstrated the potential of this method, which shall be further explored at higher magnetic fields.

Summary

Nuclear magnetic resonance (NMR) is a spectroscopic technique which is used in physics, medicine and chemistry. The main applications of NMR include determination of molecular structure and composition, mixture and trace analysis, quality control and quantitative analysis. Although NMR is widely used it is rather insensitive due to inherently low nuclear spin polarization. The polarization of electron spins at similar experimental conditions is 660 times higher than that of protons. Dynamic nuclear polarization (DNP) is a process through which the sensitivity of NMR can be enhanced by transferring polarization from the electrons to the nuclei.

In this thesis we describe a novel method called rapid-melt DNP which is generic and very easy to implement. Rapid-melt DNP benefits from the efficient hyperpolarization in the solid state and from high sensitivity liquid-state NMR on a stripline chip. In this method a microfluidic sample is polarized at liquid nitrogen temperature and afterwards melted by warm nitrogen gas and finally measured in the liquid state. The main advantages of rapid-melt DNP are the possibility of signal averaging, hyperpolarized spectra of fast relaxing nuclei in the liquid state, easy translation to other magnetic fields and less demanding hardware.

Chapter 1 gives an introduction to the field of DNP NMR. The problem of sensitivity in NMR and an overview of approaches to overcome this problem are mentioned. The known DNP mechanisms in the liquid state and the solid state are briefly summarized. Details of the contemporary DNP methods mainly to obtain DNP enhanced spectra in the liquid state are introduced. At the end a qualitative description of rapid-melt DNP is presented.

Chapter 2 contains the full technical details of the rapid-melt DNP setup. Details of different parts of the probe namely the shuttling mechanism, cryogenics, microwaves, sample melting and NMR are described. Typical time constants are

5-6 seconds for DNP buildup and tens to hundreds of milliseconds for sample melting. DNP results of non-polar solvents (toluene) show that enhancements of up to 400 are possible in the liquid state with BDPA free radicals. An enhancement factor of ∼500 has been observed in the solid state for polar solvents (water), but fast relaxation induced by the TEMPOL free radicals annihilates the polarization during melting. Hyperpolarization of caffeine and methyl pyruvate was demonstrated as a proof of concept in the liquid state.

Chapter 3 is dedicated to mechanistic studies of the rapid-melt DNP method. All the known DNP mechanisms are observed in the current setup. The Solid Effect DNP mechanism was studied in detail for a BDPA toluene solution and also for a TEMPOL water solution. DNP enhancement and build-up time for several proton concentrations in the toluene sample were recorded as a function of the microwave power. The results obtained were explained through a simplified spin diffusion model.

We have summarized the DNP results obtained for different molecules in **Chapter 4**. After the proof of principle and mechanistic studies various molecules like lipids, amino acids, alcohols, vitamins, steroid hormones and small metabolites were examined for DNP efficiency in the rapid-melt DNP setup. All the tested molecules were successfully hyperpolarized. Polarization of water in the liquid state was achieved by adding a surfactant to a solution of BDPA and toluene to dissolve the water. BDPA-like water-soluble radicals were also attempted to be synthesized, to limit the relaxation losses during melting transition. Further research is required to obtain radicals with the desired properties.

One of the main advantages of rapid-melt DNP is its compatibility with generic NMR experiments with signal averaging or 2D NMR. We explored the possibility of 2D NMR in the rapid-melt DNP setup in **Chapter 5**. DNP enhanced 2D TOCSY spectra were successfully acquired for a few model compounds. Technical problems such as temperature instabilities during DNP and limited resolution of the current probe design restrict its application, but this can be remedied with some technical improvements.

After successful demonstration of rapid-melt DNP at liquid nitrogen temperature it was tested at even lower temperatures with liquid helium cooling. Preliminary results of rapid-melt DNP at lower temperatures are presented in **Chapter 6**. A higher enhancement factor of up to 2000 was observed in a single scan for a typical toluene sample doped with BDPA. Cold vapor of helium gas could also be used for DNP in the current setup. The use of cold helium gas results in more stable experimental conditions. Higher enhancement factors and longer build-up times

are consistent with the calculations based on the Solid Effect model described in **Chapter 3**.

Samenvatting

Kernspinresonantie (NMR) is een spectroscopische techniek die wordt gebruikt in de natuurkunde, chemie en geneeskunde. De voornaamste toepassingen van NMR omvatten de bepaling van moleculaire structuren en samenstellingen, mengsel- en sporenanalyse, kwaliteitscontrole en kwantitatieve analyse. Hoewel NMR breed wordt toegepast, is het nogal ongevoelig als gevolg van een inherent lage kernspinpolarisatie. De polarisatie van elektronspins is bij vergelijkbare experimentele condities 660 keer hoger dan die van protonen. Dynamische kernpolarisatie (DNP) is een proces waarmee de gevoeligheid van NMR verhoogd kan worden door polarisatie over te dragen van de elektronen naar de kernen.

In dit proefschrift beschrijven wij een nieuwe methode, getiteld 'snelle-smelt DNP', die generiek en makkelijk te implementeren is. Snelle-smelt DNP profiteert van de efficiënte hyperpolarisatie in de vaste stof en van de hoge gevoeligheid van vloeistof NMR op een stripline chip. In deze methode wordt een microfluïde monster bij de temperatuur van vloeibare stikstof gepolariseerd, vervolgens door warm stikstofgas gesmolten en ten slotte in de vloeistoffase gemeten. De grote voordelen van snelle-smelt DNP zijn de mogelijkheden tot signaalmiddeling, het meten van gehyperpolariseerde spectra van snel relaxerende moleculen in de vloeistoffase, een gemakkelijke vertaling naar andere magneetvelden en lagere hardware-eisen.

Hoofdstuk 1 geeft een inleiding tot het werkveld DNP NMR. Het probleem van de gevoeligheid van NMR en reeds bestaande methodes om dit probleem te overkomen worden besproken. Een korte omschrijving van de bekende DNP mechanismes in zowel vloeistof als vast stof wordt gegeven. Details van de hedendaagse DNP methodes om DNP-versterkte spectra in de vloeistoffase te verkrijgen worden vervolgens geïntroduceerd. Ten slotte wordt een kwalitatieve beschrijving van snelle-smelt DNP gepresenteerd.

Hoofdstuk 2 geeft een volledige technische beschrijving van de snelle-smelt DNP opstelling. Details van de verschillende onderdelen van de probe, te weten het shuttlemechanisme, de cryogene koeling, de microgolven, de monstersmelter en de NMR detector worden beschreven. Typische tijdsconstanten zijn 5-6 seconden voor DNP signaalversterking in de vaste stof en tientallen tot honderden milliseconden voor het smelten van het monster. DNP resultaten voor apolaire oplosmiddelen (tolueen) met daarin het vrije radicaal BDPA laten zien dat signaalversterkingen van een factor 400 mogelijk zijn in de vloeistoffase. Een versterking van ∼500 is waargenomen in de vaste stof voor polaire oplosmiddelen (water), maar de snelle relaxatie door de vrije radicalen van TEMPOL doet tijdens het smelten de verhoogde polarisatie teniet. Hyperpolariseren van cafeïne en methylpyruvaat in de vloeistoffase is gedemonstreerd als proof-of-concept.

Hoofdstuk 3 is toegewijd aan mechanistische studies van de snelle-smelt DNP techniek. Alle bekende DNP mechanismes zijn in de huidige opstelling waargenomen. Het 'Solid Effect DNP' mechanisme is in detail bestudeerd voor een oplossing van BDPA in tolueen en ook voor TEMPOL in water. DNP signaalversterkingen en opbouwtijden voor verschillende protonconcentraties in het tolueenmonster zijn opgenomen als functie van de sterkte van de microgolven. De verkregen resultaten kunnen worden verklaard door middel van een versimpeld spindiffusiemodel.

De DNP resultaten die verkregen zijn voor verschillende moleculen zijn samengevat in **Hoofdstuk 4**. Na de proof-of-principle metingen en de mechanistische studies zijn verschillende moleculen zoals vetzuren, aminozuren, alcoholen, vitamines, steroïden en kleine metabolieten onderzocht voor hun DNP efficiëntie in de snelle-smelt DNP opstelling. Alle geteste moleculen konden succesvol worden gehyperpolariseerd. Polarisatie van water in de vloeistoffase kon worden bereikt door een emulgator toe te voegen aan een oplossing van BDPA en tolueen, zodat water kon worden opgelost. Er is geprobeerd om BDPA-achtige wateroplosbare radicalen te synthetiseren om zo de relaxatieverliezen gedurende de smeltovergang te minimaliseren. Er is echter nog meer onderzoek nodig om radicalen met de gewenste eigenschappen te synthetiseren.

Een van de grote voordelen van snelle-smelt DNP is de compatibiliteit met generieke NMR experimenten waarbij meerdere metingen worden gedaan, bijvoorbeeld voor signaalmiddeling of 2D NMR. We hebben de mogelijkheden van 2D NMR in de snelle-smelt DNP opstelling onderzocht in **Hoofdstuk 5**. DNP-versterkte 2D TOCSY spectra zijn succesvol opgenomen voor een aantal testmoleculen. Technische problemen, zoals instabiliteit van de temperatuur gedurende het DNP proces en een beperkte resolutie van het huidige probe ontwerp, verhinderen op dit mo-

ment verdere toepassing, maar dit kan verholpen worden met enkele technische verbeteringen.

Na een succesvolle demonstratie van snelle-smelt DNP bij vloeibare stikstoftemperaturen, is het ook getest bij nog lagere temperaturen die bereikt worden door te koelen met vloeibare helium. Voorlopige resultaten van snelle smelt-DNP bij deze lage temperaturen worden gepresenteerd in **Hoofdstuk 6**. Een hogere signaalversterking, een factor 2000, werd gehaald in één enkele scan voor een doorsnee tolueenmonster met BDPA. In de huidige opstellingen kan ook koud heliumgas voor het DNP proces gebruikt worden. Het voordeel hiervan is stabielere experimentele condities. De hogere signaalversterkingen en langere opbouwtijden zijn in overeenstemming met de berekeningen die gebaseerd zijn op het 'Solid Effect' model dat in **Hoofdstuk 3** is beschreven.

Acknowledgments

It is my great pleasure to express my gratitude to all the people who helped and supported me during my PhD to make this thesis possible. First and foremost, I owe my deepest gratitude to my supervisors Prof. Dr. Arno Kentgens and Dr. Jan van Bentum for accepting me into this prestigious group to pursue a PhD under their esteemed guidance. I would also like to particularly thank Dr. Jan van Bentum for his continuous guidance, patience, support, and for giving me the intellectual freedom during my term. I am also very grateful to both for their scientific advice, many insightful discussions, and suggestions. I would like to thank my committee members for finding time in their busy schedules for my manuscript.

Every result described in this thesis was accomplished with the help and support of fellow lab-mates and collaborators. I thank Gerrit for patiently fixing the probe and making new parts throughout the project. I want to extend my heart-full thanks to James for his help in the beginning of the project, his insights were instrumental for the completion of this thesis. I am also grateful to Vincent for helping me with the 2D experiments and suggestions for the test molecules. Thanks to Alberto and Dr. Martin Feiters for putting lots of efforts to make optimal free-radicals for Rapid-melt DNP. I am thankful to Michael and Gijs for helping me with instruments and concepts in the beginning of my PhD. I would also like to extend my gratitude to all the colleagues Marian, Hans Heus, Nan, Niels, Martijn, Indrek, Tatiana, Lavinia, Wanling, Ernst, Marco, Vinod, Walter, Frank, Aafke, Ruud, Anna-jo, Sander, Hans Janssen, Jan van Os, Piotr, and Jan Schoonboord at department for the friendly and welcoming environment.

I was lucky to have found friends in my colleagues. I enjoyed the humorous and intellectual company of my fellow lab mates during our many social activities and Friday evening borrels. Thanks to Koen my neighbour for showing me the Dutch way and helping with the culture shock in the initial days. Many thanks to Ole for

being a helpful friend, you and Malve were very supportive company for me and my wife. Thanks to Bas for many interesting conversations and for amazing puzzle times. A special thanks to Merijn for being helpful and a wonderful sports partner. I would also like to particularly thank Swapneel, we were the two Indian guys in the same boat, we helped each other and I will forever remember those times. Thanks to Fleur and Wouter for being great friends and always ready to support in times of need.

I had a great work life balance thanks to my friends outside work Sonny, Lokesh, Aravind, Aishwarya, Swathi, Chandan, Ashim, Raj, Shaji, Amit, Sami, Daniel, Vladimir, and Eduardo. Thanks to Suruchi, Suhas, Prasenjeet and Azhar for the countless gatherings and Indian dinners which became a routine and helped me feel at home. Thanks to my Indian friends Rahul, Kriti, Venkat, Swathi, Jani, and Kuntal for playing badminton on the weekends. Also, thanks to Kiran, Ashutosh, Chirojyoti, Kshiti, Ann and Payaswini. A special thanks to my long time friend Anuj More for being a constant support and guidance. I would also like to express my gratitude to my mentors Dr. T.S. Mahesh and Dr. T.G. Ajithkumar for their teachings which triggered my interest in NMR.

The PhD journey for me was special because of my marriage to my lovely wife Anshika, she has been a true support during my thesis writing days. I also want to thank my family, my grandparents for their blessings and wise words. The constant push from my parents helped me during tough days and big thanks to my siblings for being just a call away.

List of publications

- **M. Sharma**, G. Janssen, J. Leggett, A. Kentgens, and P. van Bentum, "Rapid-melt dynamic nuclear polarization," Journal of Magnetic Resonance, vol. 258, pp. 40 - 48, 2015.
- P. van Bentum, **M. Sharma**, S. van Meerten, and A. Kentgens, "Solid effect dnp in a rapid-melt setup," Journal of Magnetic Resonance, vol. 263, pp. 126 - 135, 2016.
- P. van Bentum, S. van Meerten, **M. Sharma**, and A. Kentgens, "Perspectives on DNP-enhanced NMR spectroscopy in solutions,"Journal of Magnetic Resonance, vol. 264, pp. 59 - 67, 2016.
- **M. Sharma**, V. Breukels, A. Kentgens, and P. van Bentum, "Applications and DNP 2D NMR in rapid-melt DNP", in preparation.

References

[1] G. E. Uhlenbeck and S. Goudsmit, “Ersetzung der hypothese vom unmechanischen zwang durch eine forderung bezüglich des inneren verhaltens jedes einzelnen elektrons,” *Die Naturwissenschaften*, vol. 13, no. 47, pp. 953–954, 1925.

[2] I. I. Rabi, J. R. Zacharias, S. Millman, and P. Kusch, “A new method of measuring nuclear magnetic moment,” *Phys. Rev.*, vol. 53, pp. 318–318, Feb 1938.

[3] F. Bloch, W. W. Hansen, and M. Packard, “Nuclear induction,” *Phys. Rev.*, vol. 69, pp. 127–127, Feb 1946.

[4] E. M. Purcell, H. C. Torrey, and R. V. Pound, “Resonance absorption by nuclear magnetic moments in a solid,” *Phys. Rev.*, vol. 69, pp. 37–38, Jan 1946.

[5] R. R. Ernst and W. A. Anderson, “Application of fourier transform spectroscopy to magnetic resonance,” *Review of Scientific Instruments*, vol. 37, no. 1, pp. 93–102, 1966.

[6] W. P. Aue, E. Bartholdi, and R. R. Ernst, “Two-dimensional spectroscopy. application to nuclear magnetic resonance,” *The Journal of Chemical Physics*, vol. 64, no. 5, pp. 2229–2246, 1976.

[7] K. Wüthrich, *NMR in structural biology: a collection of papers by Kurt Wüthrich*, vol. 5. World Scientific, 1995.

[8] P. Mansfield, “Multi-planar image formation using nmr spin echoes,” *Journal of Physics C: Solid State Physics*, vol. 10, no. 3, p. L55, 1977.

[9] P. LAUTERBUR, “Image formation by induced local interactions: Examples employing nuclear magnetic resonance,” *Nature*, vol. 242, no. 190, p. 191, 1973.

[10] C. D. Jeffries, “Dynamic orientation of nuclei,” *Annual Review of Nuclear Science*, vol. 14, no. 1, pp. 101–134, 1964.

[11] M. H. Levitt, *Spin dynamics: basics of nuclear magnetic resonance*. John Wiley & Sons, 2001.

[12] A. W. Overhauser, “Polarization of nuclei in metals,” *Phys. Rev.*, vol. 92, pp. 411–415, Oct 1953.

[13] T. R. Carver and C. P. Slichter, “Polarization of nuclear spins in metals,” *Phys. Rev.*, vol. 92, pp. 212–213, Oct 1953.

[14] T. R. Carver and C. P. Slichter, “Experimental verification of the overhauser nuclear polarization effect,” *Phys. Rev.*, vol. 102, pp. 975–980, May 1956.

[15] A. Abragam, “Overhauser effect in nonmetals,” *Phys. Rev.*, vol. 98, pp. 1729–1735, Jun 1955.

[16] C. D. Jeffries, “Polarization of nuclei by resonance saturation in paramagnetic crystals,” *Phys. Rev.*, vol. 106, pp. 164–165, Apr 1957.

[17] C. F. Hwang and D. A. Hill, “New effect in dynamic polarization,” *Phys. Rev. Lett.*, vol. 18, pp. 110–112, Jan 1967.

[18] C. F. Hwang and D. A. Hill, “Phenomenological model for the new effect in dynamic polarization,” *Phys. Rev. Lett.*, vol. 19, pp. 1011–1014, Oct 1967.

[19] A. Abragam and M. Goldman, “Nuclear magnetism: Order and disorder,” 1982.

[20] M. Goldman, *Spin temperature and nuclear magnetic resonance in solids*. Clarendon Press Oxford, 1970.

[21] T. V. Can, M. A. Caporini, F. Mentink-Vigier, B. Corzilius, J. J. Walish, M. Rosay, W. E. Maas, M. Baldus, S. Vega, T. M. Swager, and R. G. Griffin, “Overhauser effects in insulating solids,” *The Journal of Chemical Physics*, vol. 141, no. 6, 2014.

[22] M. L. Hirsch, N. Kalechofsky, A. Belzer, M. Rosay, and J. G. Kempf, “Brute-force hyperpolarization for nmr and mri,” *Journal of the American Chemical Society*, vol. 137, no. 26, pp. 8428–8434, 2015. PMID: 26098752.

[23] C. R. Bowers and D. P. Weitekamp, “Transformation of symmetrization order to nuclear-spin magnetization by chemical reaction and nuclear magnetic resonance,” *Physical Review Letters*, vol. 57, no. 21, p. 2645, 1986.

[24] C. R. Bowers and D. P. Weitekamp, “Parahydrogen and synthesis allow dramatically enhanced nuclear alignment,” *Journal of the American Chemical Society*, vol. 109, no. 18, pp. 5541–5542, 1987.

[25] R. W. Adams, J. A. Aguilar, K. D. Atkinson, M. J. Cowley, P. I. P. Elliott, S. B. Duckett, G. G. R. Green, I. G. Khazal, J. López-Serrano, and D. C. Williamson, “Reversible interactions with para-hydrogen enhance nmr sensitivity by polarization transfer,” *Science*, vol. 323, no. 5922, pp. 1708–1711, 2009.

[26] U. L. Günther, *Dynamic Nuclear Hyperpolarization in Liquids*, pp. 23–69. Berlin, Heidelberg: Springer Berlin Heidelberg, 2013.

[27] M. Albert, G. Cates, B. Driehuys, W. Happer, B. Saam, C. Springer, and A. Wishnia, “Biological magnetic resonance imaging using laser-polarized 129xe,” 1994.

[28] A. Bifone, Y.-Q. Song, R. Seydoux, R. Taylor, B. Goodson, T. Pietrass, T. Budinger, G. Navon, and A. Pines, “Nmr of laser-polarized xenon in humanâĂĽblood,” *Proceedings of the National Academy of Sciences*, vol. 93, no. 23, pp. 12932–12936, 1996.

[29] C. Witte and L. Schröder, “Nmr of hyperpolarised probes,” *NMR in Biomedicine*, vol. 26, no. 7, pp. 788–802, 2013.

[30] C. Ludwig, M. Saunders, I. Marin-Montesinos, and U. L. Günther, “Quantum rotor induced hyperpolarization,” *Proceedings of the National Academy of Sciences*, vol. 107, no. 24, pp. 10799–10803, 2010.

[31] J. Haupt, “A new effect of dynamic polarization in a solid obtained by rapid change of temperature,” *Physics Letters A*, vol. 38, no. 6, pp. 389 – 390, 1972.

[32] M. Bennati, I. Tkach, and M.-T. Turke, “Dynamic nuclear polarization in liquids,” in *Electron Paramagnetic Resonance: Volume 22*, vol. 22, pp. 155–182, The Royal Society of Chemistry, 2011.

[33] M. D. Lingwood and S. Han, “Chapter 3 - solution-state dynamic nuclear polarization,” vol. 73 of *Annual Reports on NMR Spectroscopy*, pp. 83 – 126, Academic Press, 2011.

[34] T. Maly, G. T. Debelouchina, V. S. Bajaj, K.-N. Hu, C.-G. Joo, M. L. Mak-Jurkauskas, J. R. Sirigiri, P. C. A. van der Wel, J. Herzfeld, R. J. Temkin, and R. G. Griffin, “Dynamic nuclear polarization at high magnetic fields,” *The Journal of Chemical Physics*, vol. 128, no. 5, 2008.

[35] A. Henstra, P. Dirksen, and W. Wenckebach, “Enhanced dynamic nuclear polarization by the integrated solid effect,” *Physics Letters A*, vol. 134, no. 2, pp. 134 – 136, 1988.

[36] C. T. Farrar, D. A. Hall, G. J. Gerfen, S. J. Inati, and R. G. Griffin, “Mechanism of dynamic nuclear polarization in high magnetic fields,” *The Journal of Chemical Physics*, vol. 114, no. 11, pp. 4922–4933, 2001.

[37] J. Heckmann, C. Hess, W. Meyer, E. Radtke, G. Reicherz, and M. Schiemann, “Recent progress in the dynamic nuclear polarization of solid deuterated butanol targets,” *Applied Magnetic Resonance*, vol. 34, no. 3, pp. 461–473, 2008.

[38] V. Bajaj, C. Farrar, M. Hornstein, I. Mastovsky, J. Vieregg, J. Bryant, B. Eléna, K. Kreischer, R. Temkin, and R. Griffin, “Dynamic nuclear polarization at 9 t using a novel 250 ghz gyrotron microwave source,” *Journal of Magnetic Resonance*, vol. 160, no. 2, pp. 85 – 90, 2003.

[39] V. S. Bajaj, M. K. Hornstein, K. E. Kreischer, J. R. Sirigiri, P. P. Woskov, M. L. Mak-Jurkauskas, J. Herzfeld, R. J. Temkin, and R. G. Griffin, “250 ghz cw gyrotron oscillator for dynamic nuclear polarization in biological solid state nmr,” *Journal of Magnetic Resonance*, vol. 189, no. 2, pp. 251 – 279, 2007.

[40] Ü. Akbey and H. Oschkinat, “Structural biology applications of solid state mas dnp nmr,” *Journal of Magnetic Resonance*, vol. 269, pp. 213 – 224, 2016.

[41] A. Lesage, M. Lelli, D. Gajan, M. A. Caporini, V. Vitzthum, P. Miéville, J. Alauzun, A. Roussey, C. Thieuleux, A. Mehdi, G. Bodenhausen, C. Coperet, and L. Emsley, “Surface enhanced nmr spectroscopy by dynamic nuclear polarization,” *Journal of the American Chemical Society*, vol. 132, no. 44, pp. 15459–15461, 2010. PMID: 20831165.

[42] H. Takahashi, S. Hediger, and G. De Paepe, “Matrix-free dynamic nuclear polarization enables solid-state nmr ^{13}C-^{13}C correlation spectroscopy of proteins at natural isotopic abundance,” *Chem. Commun.*, vol. 49, pp. 9479–9481, 2013.

[43] M. Kaplan, A. Cukkemane, G. C. van Zundert, S. Narasimhan, M. Daniëls, D. Mance, G. Waksman, A. M. Bonvin, R. Fronzes, G. E. Folkers, *et al.*, “Probing a cell-embedded megadalton protein complex by dnp-supported solid-state nmr,” *Nature methods*, vol. 12, no. 7, pp. 649–652, 2015.

[44] M. Reese, D. Lennartz, T. Marquardsen, P. Höfer, A. Tavernier, P. Carl, T. Schippmann, M. Bennati, T. Carlomagno, F. Engelke, and C. Griesinger,

"Construction of a liquid-state nmr dnp shuttle spectrometer: First experimental results and evaluation of optimal performance characteristics," *Applied Magnetic Resonance*, vol. 34, no. 3, p. 301, 2008.

[45] S. Stevenson and H. C. Dorn, "^{13}C dynamic nuclear polarization: A detector for continuous-flow, online chromatography," *Analytical Chemistry*, vol. 66, no. 19, pp. 2993–2999, 1994.

[46] S. Stevenson, T. Glass, and H. C. Dorn, "^{13}C dynamic nuclear polarization: an alternative detector for recycled-flow nmr experiments," *Analytical Chemistry*, vol. 70, no. 13, pp. 2623–2628, 1998. PMID: 21644781.

[47] M. D. Lingwood, T. A. Siaw, N. Sailasuta, B. D. Ross, P. Bhattacharya, and S. Han, "Continuous flow overhauser dynamic nuclear polarization of water in the fringe field of a clinical magnetic resonance imaging system for authentic image contrast," *Journal of Magnetic Resonance*, vol. 205, no. 2, pp. 247 – 254, 2010.

[48] A. Krahn, P. Lottmann, T. Marquardsen, A. Tavernier, M.-T. Turke, M. Reese, A. Leonov, M. Bennati, P. Hoefer, F. Engelke, and C. Griesinger, "Shuttle dnp spectrometer with a two-center magnet," *Phys. Chem. Chem. Phys.*, vol. 12, pp. 5830–5840, 2010.

[49] V. Denysenkov, M. J. Prandolini, M. Gafurov, D. Sezer, B. Endeward, and T. F. Prisner, "Liquid state dnp using a 260 ghz high power gyrotron," *Phys. Chem. Chem. Phys.*, vol. 12, pp. 5786–5790, 2010.

[50] P. J. M. van Bentum, G. H. A. van der Heijden, J. A. Villanueva-Garibay, and A. P. M. Kentgens, "Quantitative analysis of high field liquid state dynamic nuclear polarization," *Phys. Chem. Chem. Phys.*, vol. 13, pp. 17831–17840, 2011.

[51] G. van der Heijden, A. Kentgens, and P. van Bentum, "Liquid state dynamic nuclear polarization of ethanol at 3.4 t (95 ghz)," *Physical Chemistry Chemical Physics*, vol. 16, no. 18, pp. 8493–8502, 2014.

[52] E. V. Kryukov, M. E. Newton, K. J. Pike, D. R. Bolton, R. M. Kowalczyk, A. P. Howes, M. E. Smith, and R. Dupree, "Dnp enhanced nmr using a high-power 94 ghz microwave source: a study of the tempol radical in toluene," *Phys. Chem. Chem. Phys.*, vol. 12, pp. 5757–5765, 2010.

[53] S. van Meerten, M. Tayler, A. Kentgens, and P. van Bentum, "Towards overhauser dnp in supercritical co2," *Journal of Magnetic Resonance*, vol. 267, pp. 30 – 36, 2016.

[54] J. H. Ardenkjær-Larsen, B. Fridlund, A. Gram, G. Hansson, L. Hansson, M. H. Lerche, R. Servin, M. Thaning, and K. Golman, "Increase in signal-to-noise ratio of > 10,000 times in liquid-state nmr," *Proceedings of the National Academy of Sciences*, vol. 100, no. 18, pp. 10158–10163, 2003.

[55] P. Miéville, S. Jannin, and G. Bodenhausen, "Relaxometry of insensitive nuclei: Optimizing dissolution dynamic nuclear polarization," *Journal of Magnetic Resonance*, vol. 210, no. 1, pp. 137 – 140, 2011.

[56] J. Leggett, R. Hunter, J. Granwehr, R. Panek, A. J. Perez-Linde, A. J. Horsewill, J. McMaster, G. Smith, and W. Kockenberger, "A dedicated spectrometer for dissolution dnp nmr spectroscopy," *Phys. Chem. Chem. Phys.*, vol. 12, pp. 5883–5892, 2010.

[57] S. Jannin, A. Bornet, S. Colombo, and G. Bodenhausen, "Low-temperature cross polarization in view of enhancing dissolution dynamic nuclear polarization in nmr," *Chemical Physics Letters*, vol. 517, no. 4-6, pp. 234 – 236, 2011.

[58] L. Frydman and D. Blazina, "Ultrafast two-dimensional nuclear magnetic resonance spectroscopy of hyperpolarized solutions," *Nature physics*, vol. 3, no. 6, pp. 415–419, 2007.

[59] S. Bowen, H. Zeng, and C. Hilty, "Chemical shift correlations from hyperpolarized nmr by off-resonance decoupling," *Analytical chemistry*, vol. 80, no. 15, pp. 5794–5798, 2008.

[60] H. Zeng, S. Bowen, and C. Hilty, "Sequentially acquired two-dimensional nmr spectra from hyperpolarized sample," *Journal of Magnetic Resonance*, vol. 199, no. 2, pp. 159–165, 2009.

[61] S. J. Nelson, D. Vigneron, J. Kurhanewicz, A. Chen, R. Bok, and R. Hurd, "Dnp-hyperpolarized ^{13}C magnetic resonance metabolic imaging for cancer applications," *Applied Magnetic Resonance*, vol. 34, no. 3, pp. 533–544, 2008.

[62] F. Jähnig, G. Kwiatkowski, and M. Ernst, "Conceptual and instrumental progress in dissolution dnp," *Journal of Magnetic Resonance*, vol. 264, pp. 22 – 29, 2016. Hyperpolarized NMR Comes of Age.

[63] M. Ragavan, H.-Y. Chen, G. Sekar, and C. Hilty, "Solution nmr of polypeptides hyperpolarized by dynamic nuclear polarization," *Analytical chemistry*, vol. 83, no. 15, pp. 6054–6059, 2011.

[64] T. Harris, O. Szekely, and L. Frydman, "On the potential of hyperpolarized water in biomolecular nmr studies," *The Journal of Physical Chemistry B*, vol. 118, no. 12, pp. 3281–3290, 2014.

[65] M. H. Lerche, S. Meier, P. R. Jensen, S.-O. Hustvedt, M. Karlsson, J. Ø. Duus, and J. H. Ardenkjær-Larsen, "Quantitative dynamic nuclear polarization-nmr on blood plasma for assays of drug metabolism," *NMR in Biomedicine*, vol. 24, no. 1, pp. 96–103, 2011.

[66] S. Meier, P. R. Jensen, M. Karlsson, and M. H. Lerche, "Hyperpolarized nmr probes for biological assays," *Sensors*, vol. 14, no. 1, pp. 1576–1597, 2014.

[67] P. R. Jensen, S. Meier, J. H. Ardenkjær-Larsen, J. O. Duus, M. Karlsson, and M. H. Lerche, "Detection of low-populated reaction intermediates with hyperpolarized nmr," *Chem. Commun.*, pp. 5168–5170, 2009.

[68] H.-Y. Chen, M. Ragavan, and C. Hilty, "Protein folding studied by dissolution dynamic nuclear polarization," *Angewandte Chemie International Edition*, vol. 52, no. 35, pp. 9192–9195, 2013.

[69] R. Buratto, A. Bornet, J. Milani, D. Mammoli, B. Vuichoud, N. Salvi, M. Singh, A. Laguerre, S. Passemard, S. Gerber-Lemaire, S. Jannin, and G. Bodenhausen, "Drug screening boosted by hyperpolarized long-lived states in nmr," *ChemMedChem*, vol. 9, no. 11, pp. 2509–2515, 2014.

[70] J. H. Ardenkjær-Larsen, "On the present and future of dissolution-dnp," *Journal of Magnetic Resonance*, vol. 264, pp. 3 – 12, 2016. Hyperpolarized NMR Comes of Age.

[71] J. H. Ardenkjær-Larsen, A. M. Leach, N. Clarke, J. Urbahn, D. Anderson, and T. W. Skloss, "Dynamic nuclear polarization polarizer for sterile use intent," *NMR in Biomedicine*, vol. 24, no. 8, pp. 927–932, 2011.

[72] C.-G. Joo, K.-N. Hu, J. A. Bryant, , and R. G. Griffin, "In situ temperature jump high-frequency dynamic nuclear polarization experiments: Enhanced sensitivity in liquid-state nmr spectroscopy," *Journal of the American Chemical Society*, vol. 128, no. 29, pp. 9428–9432, 2006. PMID: 16848479.

[73] C.-G. Joo, A. Casey, C. J. Turner, and R. G. Griffin, "In situ temperature-jump dynamic nuclear polarization: Enhanced sensitivity in two dimensional 13c 13c correlation spectroscopy in solution," *Journal of the American Chemical Society*, vol. 131, no. 1, pp. 12–13, 2009. PMID: 18942782.

[74] D. Yoon, M. Soundararajan, C. Caspers, F. Braunmueller, J. Genoud, S. Alberti, and J.-P. Ansermet, "500-fold enhancement of in situ 13 c liquid state nmr using gyrotron-driven temperature-jump dnp," *Journal of Magnetic Resonance*, vol. 270, pp. 142–146, 2016.

[75] F. Kurdzesau, B. van den Brandt, A. Comment, P. Hautle, S. Jannin, J. J. van der Klink, and J. A. Konter, "Dynamic nuclear polarization of small labelled molecules in frozen water-alcohol solutions," *Journal of Physics D: Applied Physics*, vol. 41, no. 15, p. 155506, 2008.

[76] P. Miéville, S. Jannin, L. Helm, and G. Bodenhausen, "Nmr of insensitive nuclei enhanced by dynamic nuclear polarization," *Chimia-International Journal for Chemistry*, vol. 65, no. 4, p. 260, 2011.

[77] D. Hoult and R. Richards, "The signal-to-noise ratio of the nuclear magnetic resonance experiment," *Journal of Magnetic Resonance (1969)*, vol. 24, no. 1, pp. 71 – 85, 1976.

[78] P. van Bentum, J. Janssen, A. Kentgens, J. Bart, and J. Gardeniers, "Stripline probes for nuclear magnetic resonance," *Journal of Magnetic Resonance*, vol. 189, no. 1, pp. 104 – 113, 2007.

[79] R. R. Ernst, "Measurement and control of magnetic field homogeneity," *Review of Scientific Instruments*, vol. 39, no. 7, pp. 998–1012, 1968.

[80] J. D. van Beek, "matnmr: A flexible toolbox for processing, analyzing and visualizing magnetic resonance data in matlab®," *Journal of Magnetic Resonance*, vol. 187, no. 1, pp. 19 – 26, 2007.

[81] A. P. M. Kentgens and P. J. M. Van Bentum, "Rapid cycle dynamic nuclear polarization magnetic resonance apparatus," Dec. 21 2012. US Patent App. 14/368,011.

[82] J. Bart, A. J. Kolkman, A. J. O. de Vries, K. Koch, P. J. Nieuwland, H. J. W. G. Janssen, J. P. J. M. van Bentum, K. A. M. Ampt, F. P. J. T. Rutjes, S. S. Wijmenga, H. J. G. E. Gardeniers, and A. P. M. Kentgens, "A microfluidic high-resolution nmr flow probe," *Journal of the American Chemical Society*, vol. 131, no. 14, pp. 5014–5015, 2009. PMID: 19320484.

[83] M. Sharma, G. Janssen, J. Leggett, A. Kentgens, and P. van Bentum, "Rapid-melt dynamic nuclear polarization," *Journal of Magnetic Resonance*, vol. 258, pp. 40 – 48, 2015.

[84] A. Abragam and W. Proctor, "A novel method of dynamic polarization of atomic nuclei in solids," *CR Acad. Sci*, vol. 246, p. 2253, 1959.

[85] E. Erb, J.-L. Motchane, and J. Uebersfeld, "Effet de polarisation nucleaire dans les liquides et les gaz adsorbes sur les charbons," *COMPTES RENDUS HEBDOMADAIRES DES SEANCES DE L ACADEMIE DES SCIENCES*, vol. 246, no. 14, pp. 2121–2123, 1958.

[86] A. Abragam and M. Borghini, "Chapter viii dynamic polarization of nuclear targets," vol. 4 of *Progress in Low Temperature Physics*, pp. 384 – 449, Elsevier, 1964.

[87] D. S. Wollan, "Dynamic nuclear polarization with an inhomogeneously broadened esr line. i. theory," *Phys. Rev. B*, vol. 13, pp. 3671–3685, May 1976.

[88] A. A. Smith, B. Corzilius, A. B. Barnes, T. Maly, and R. G. Griffin, "Solid effect dynamic nuclear polarization and polarization pathways," *The Journal of Chemical Physics*, vol. 136, no. 1, 2012.

[89] O. Haze, B. Corzilius, A. A. Smith, R. G. Griffin, and T. M. Swager, "Water-soluble narrow-line radicals for dynamic nuclear polarization," *Journal of the American Chemical Society*, vol. 134, no. 35, pp. 14287–14290, 2012. PMID: 22917088.

[90] M. Rosay, L. Tometich, S. Pawsey, R. Bader, R. Schauwecker, M. Blank, P. M. Borchard, S. R. Cauffman, K. L. Felch, R. T. Weber, R. J. Temkin, R. G. Griffin, and W. E. Maas, "Solid-state dynamic nuclear polarization at 263 ghz: spectrometer design and experimental results," *Phys. Chem. Chem. Phys.*, vol. 12, pp. 5850–5860, 2010.

[91] J. H. Lee, Y. Okuno, and S. Cavagnero, "Sensitivity enhancement in solution nmr: Emerging ideas and new frontiers," *Journal of Magnetic Resonance*, vol. 241, pp. 18 – 31, 2014. A special JMR Perspectives issue: Foresights in Biomolecular Solution-State NMR Spectroscopy - From Spin Gymnastics to Structure and Dynamics.

[92] Q. Z. Ni, E. Daviso, T. V. Can, E. Markhasin, S. K. Jawla, T. M. Swager, R. J. Temkin, J. Herzfeld, and R. G. Griffin, "High frequency dynamic nuclear polarization," *Accounts of Chemical Research*, vol. 46, no. 9, pp. 1933–1941, 2013. PMID: 23597038.

[93] B. D. Armstrong and S. Han, "Overhauser dynamic nuclear polarization to study local water dynamics," *Journal of the American Chemical Society*, vol. 131, no. 13, pp. 4641–4647, 2009. PMID: 19290661.

[94] C. Sauvée, M. Rosay, G. Casano, F. Aussenac, R. T. Weber, O. Ouari, and P. Tordo, "Highly efficient, water-soluble polarizing agents for dynamic nuclear polarization at high frequency," *Angewandte Chemie International Edition*, vol. 52, no. 41, pp. 10858–10861, 2013.

[95] C. Sauvée, G. Casano, S. Abel, A. Rockenbauer, D. Akhmetzyanov, H. Karoui, D. Siri, F. Aussenac, W. Maas, R. T. Weber, T. Prisner, M. Rosay, P. Tordo, and

O. Ouari, “Tailoring of polarizing agents in the bturea series for cross-effect dynamic nuclear polarization in aqueous media,” *Chemistry - A European Journal*, vol. 22, no. 16, pp. 5598–5606, 2016.

[96] A. Henstra and W. Wenckebach, “Dynamic nuclear polarisation via the integrated solid effect i: theory,” *Molecular Physics*, vol. 112, no. 13, pp. 1761–1772, 2014.

[97] A. Henstra, T.-S. Lin, J. Schmidt, and W. Wenckebach, “High dynamic nuclear polarization at room temperature,” *Chemical Physics Letters*, vol. 165, no. 1, pp. 6 – 10, 1990.

[98] H. E. Gottlieb, V. Kotlyar, and A. Nudelman, “Nmr chemical shifts of common laboratory solvents as trace impurities,” *The Journal of organic chemistry*, vol. 62, no. 21, pp. 7512–7515, 1997.

[99] P. van Bentum, M. Sharma, S. van Meerten, and A. Kentgens, “Solid effect dnp in a rapid-melt setup,” *Journal of Magnetic Resonance*, vol. 263, pp. 126 – 135, 2016.

[100] P. Severino, S. C. Pinho, E. B. Souto, and M. H. Santana, “Polymorphism, crystallinity and hydrophilic-lipophilic balance of stearic acid and stearic acid-capric/caprylic triglyceride matrices for production of stable nanoparticles,” *Colloids and Surfaces B: Biointerfaces*, vol. 86, no. 1, pp. 125 – 130, 2011.

[101] M. K. Kiesewetter, V. K. Michaelis, J. J. Walish, R. G. Griffin, and T. M. Swager, “High field dynamic nuclear polarization nmr with surfactant sheltered biradicals,” *The Journal of Physical Chemistry B*, vol. 118, no. 7, pp. 1825–1830, 2014. PMID: 24506193.

[102] M. Lelli, A. J. Rossini, G. Casano, O. Ouari, P. Tordo, A. Lesage, and L. Emsley, “Hydrophobic radicals embedded in neutral surfactants for dynamic nuclear polarization of aqueous environments at 9.4 tesla,” *Chem. Commun.*, vol. 50, pp. 10198–10201, 2014.

[103] J. L. Munoz-Gomez, E. Monteagudo, V. Lloveras, T. Parella, J. Veciana, and J. Vidal-Gancedo, “A benzyl alcohol derivative of the bdpa radical for fast dissolution dynamic nuclear polarization nmr spectroscopy,” *Org. Biomol. Chem.*, vol. 13, pp. 2689–2693, 2015.

[104] J. Jeener, “Two-dimensional fourier transform nmr.” Ampere International Summer School II,Basko Polje, Yugoslavia, 1971.

[105] L. Braunschweiler and R. Ernst, "Coherence transfer by isotropic mixing: Application to proton correlation spectroscopy," *Journal of Magnetic Resonance (1969)*, vol. 53, no. 3, pp. 521 – 528, 1983.

[106] A. Bax and S. Grzesiek, "Methodological advances in protein nmr," *Accounts of Chemical Research*, vol. 26, no. 4, pp. 131–138, 1993.

[107] S. Macura and R. Ernst, "Elucidation of cross relaxation in liquids by two-dimensional n.m.r. spectroscopy," *Molecular Physics*, vol. 41, no. 1, pp. 95–117, 1980.

[108] C. Yu and G. C. Levy, "Two-dimensional heteronuclear noe (hoesy) experiments: investigation of dipolar interactions between heteronuclei and nearby protons," *Journal of the American Chemical Society*, vol. 106, no. 22, pp. 6533–6537, 1984.

[109] P. Giraudeau and L. Frydman, "Ultrafast 2d nmr: an emerging tool in analytical spectroscopy," *Annual Review of Analytical Chemistry*, vol. 7, pp. 129–161, 2014.

[110] A. Bax, "Two-dimensional nmr and protein structure," *Annual review of biochemistry*, vol. 58, no. 1, pp. 223–256, 1989.

[111] J. CAVANAGH, W. J. FAIRBROTHER, A. G. P. III, M. RANCE, and N. J. SKELTON, *Protein NMR Spectroscopy (Second Edition)*. Burlington: Academic Press, second edition ed., 2007.

[112] S. R. Hartmann and E. L. Hahn, "Nuclear double resonance in the rotating frame," *Phys. Rev.*, vol. 128, pp. 2042–2053, Dec 1962.

[113] D. Marion, M. Ikura, R. Tschudin, and A. Bax, "Rapid recording of 2d nmr spectra without phase cycling. application to the study of hydrogen exchange in proteins," *J. Magn. Reson*, vol. 85, no. 2, pp. 393–399, 1989.

[114] K. Thurber and R. Tycko, "Low-temperature dynamic nuclear polarization with helium-cooled samples and nitrogen-driven magic-angle spinning," *Journal of Magnetic Resonance*, vol. 264, pp. 99–106, 2016.

[115] Y. Matsuki, K. Ueda, T. Idehara, R. Ikeda, I. Ogawa, S. Nakamura, M. Toda, T. Anai, and T. Fujiwara, "Helium-cooling and-spinning dynamic nuclear polarization for sensitivity-enhanced solid-state nmr at 14t and 30k," *Journal of Magnetic Resonance*, vol. 225, pp. 1–9, 2012.

[116] D. Canet, "Radiofrequency field gradient experiments," *Progress in Nuclear Magnetic Resonance Spectroscopy*, vol. 30, no. 1, pp. 101 – 135, 1997.

[117] S. J. Nelson, J. Kurhanewicz, D. B. Vigneron, P. E. Z. Larson, A. L. Harzstark, M. Ferrone, M. van Criekinge, J. W. Chang, R. Bok, I. Park, G. Reed, L. Carvajal, E. J. Small, P. Munster, V. K. Weinberg, J. H. Ardenkjær-Larsen, A. P. Chen, R. E. Hurd, L.-I. Odegardstuen, F. J. Robb, J. Tropp, and J. A. Murray, "Metabolic imaging of patients with prostate cancer using hyperpolarized [1-13c]pyruvate," *Science Translational Medicine*, vol. 5, no. 198, pp. 198ra108–198ra108, 2013.

[118] M. A. Schroeder, L. E. Cochlin, L. C. Heather, K. Clarke, G. K. Radda, and D. J. Tyler, "In vivo assessment of pyruvate dehydrogenase flux in the heart using hyperpolarized carbon-13 magnetic resonance," *Proceedings of the National Academy of Sciences*, vol. 105, no. 33, pp. 12051–12056, 2008.

[119] S. Meier, M. Karlsson, P. R. Jensen, M. H. Lerche, and J. O. Duus, "Metabolic pathway visualization in living yeast by dnp-nmr," *Mol. BioSyst.*, vol. 7, pp. 2834–2836, 2011.

[120] J.-N. Dumez, J. Milani, B. Vuichoud, A. Bornet, J. Lalande-Martin, I. Tea, M. Yon, M. Maucourt, C. Deborde, A. Moing, L. Frydman, G. Bodenhausen, S. Jannin, and P. Giraudeau, "Hyperpolarized nmr of plant and cancer cell extracts at natural abundance," *Analyst*, vol. 140, pp. 5860–5863, 2015.

[121] N. Eshuis, N. Hermkens, B. J. A. van Weerdenburg, M. C. Feiters, F. P. J. T. Rutjes, S. S. Wijmenga, and M. Tessari, "Toward nanomolar detection by nmr through sabre hyperpolarization," *Journal of the American Chemical Society*, vol. 136, no. 7, pp. 2695–2698, 2014. PMID: 24475903.

[122] N. Eshuis, R. L. E. G. Aspers, B. J. A. van Weerdenburg, M. C. Feiters, F. P. J. T. Rutjes, S. S. Wijmenga, and M. Tessari, "2d nmr trace analysis by continuous hyperpolarization at high magnetic field," *Angewandte Chemie International Edition*, vol. 54, no. 48, pp. 14527–14530, 2015.

[123] J.-N. Dumez, "Perspectives on hyperpolarised solution-state magnetic resonance in chemistry," *Magnetic Resonance in Chemistry*, vol. 55, no. 1, pp. 38–46, 2017. MRC-16-0094.R1.

[124] N. K. J. Hermkens, N. Eshuis, B. J. A. van Weerdenburg, M. C. Feiters, F. P. J. T. Rutjes, S. S. Wijmenga, and M. Tessari, "Nmr-based chemosensing via p-h2 hyperpolarization: Application to natural extracts," *Analytical Chemistry*, vol. 88, no. 6, pp. 3406–3412, 2016. PMID: 26901632.

Curriculum Vitae

Manvendra Sharma was born on 13th December 1987 in Kota, India. He got admission in Indian Institute of Science Education and Research (IISER) Pune, India for a dual Bachelors-Masters degree in 2007. At IISER, he studied basic sciences in the first two years after which he opted for Physics as his major. For his master thesis "Contextuality of quantum states: Theoretical Analysis and Experimental Investigations" he worked under the supervision of Dr. T.S. Mahesh. In 2102, he moved to Nijmegen, the Netherlands where he worked under the guidance of Prof. Dr. Arno Kentgens and Dr. Jan van Bentum to pursue a PhD in the field of microfluidic DNP-NMR. In June 2017, he joined the group of Prof. Dr. Marcel Utz as a Senior Research Assistant at the University of Southampton, the United Kingdom.